UPPSALA
UNIVERSITET

Digital Comprehensive Summaries of Uppsala Dissertations from the Faculty of Science and Technology 1827

The Electrochemistry of $LiNi_{0.5-x}Mn_{1.5+x}O_{4-\delta}$ in Li-ion Batteries

Structure, Side-reactions and Cross-talk

BURAK AKTEKIN

ACTA
UNIVERSITATIS
UPSALIENSIS
UPPSALA
2019

ISSN 1651-6214
ISBN 978-91-513-0698-8
urn:nbn:se:uu:diva-389848

Dissertation presented at Uppsala University to be publicly examined in Häggsalen, Ångströmlaboratoriet, Lägerhyddsvägen 1, Uppsala, Friday, 13 September 2019 at 09:15 for the degree of Doctor of Philosophy. The examination will be conducted in English. Faculty examiner: Professor Christian Masquelier (Université de Picardie Jules Verne).

Abstract

Aktekin, B. 2019. The Electrochemistry of $LiNi_{0.5-x}Mn_{1.5+x}O_{4-\delta}$ in Li-ion Batteries. *Structure, Side-reactions and Cross-talk*. *Digital Comprehensive Summaries of Uppsala Dissertations from the Faculty of Science and Technology* 1827. 84 pp. Uppsala: Acta Universitatis Upsaliensis. ISBN 978-91-513-0698-8.

The use of Li-ion batteries in portable electronic products is today widespread and on-going research is extensively dedicated to improve their performance and energy density for use in electric vehicles. The largest contribution to the overall cell weight comes from the positive electrode material, and improvements regarding this component thereby render a high potential for the development of these types of batteries. A promising candidate is $LiNi_{0.5}Mn_{1.5}O_4$ (LMNO), which offers both high power capability and energy density. However, the instability of conventional electrolytes at the high operating potential (~4.7 V vs. Li^+/Li) associated with this electrode material currently prevents its use in commercial applications.

This thesis work aims to investigate practical approaches which have the potential of overcoming issues related to fast degradation of LNMO-based batteries. This, in turn, necessitates a comprehensive understanding of degradation mechanisms. First, the effect of a well-known electrolyte additive, fluoroethylene carbonate is investigated in LNMO-$Li_4Ti_5O_{12}$ (LTO) cells with a focus on the positive electrode. Relatively poor cycling performance is found with 5 wt% additive while 1 wt% additive does not show a significant difference as compared to additive-free electrolytes. Second, a more fundamental study is performed to understand the effect of capacity fading mechanisms contributing to overall cell failure in high-voltage based full-cells. Electrochemical characterization of LNMO-LTO cells in different configurations show how important the electrode interactions (cross-talk) can be for the overall cell behaviour. Unexpectedly fast capacity fading at elevated temperatures is found to originate from a high sensitivity of LTO to cross-talk.

Third, in situ studies of LNMO are conducted with neutron diffraction and electron microscopy. These show that the oxygen release is not directly related to cation disordering. Moreover, microstructural changes upon heating are observed. These findings suggest new sample preparation strategies, which allow the control of cation disorder without oxygen loss. Following this guidance, ordered and disordered samples with the same oxygen content are prepared. The negative effect of ordering on electrochemical performance is investigated and changes in bulk electronic structure following cycling are found in ordered samples, accompanied by thick surface films on surface and rock-salt phase domains near surface.

Keywords: LNMO, High-voltage spinel, FEC, Cross-talk, Cation ordering, Oxygen deficiency, Anionic redox

Burak Aktekin, Department of Chemistry - Ångström, Structural Chemistry, Box 538, Uppsala University, SE-751 21 Uppsala, Sweden.

ISSN 1651-6214
ISBN 978-91-513-0698-8
urn:nbn:se:uu:diva-389848 (http://urn.kb.se/resolve?urn=urn:nbn:se:uu:diva-389848)

To my parents

List of Papers

This thesis is based on the following papers, which are referred to in the text by their Roman numerals.

I Aktekin, B., Younesi, R., Zipprich, W., Tengstedt, C., Brandell, D., Edström, K. (2017). The Effect of the Fluoroethylene Carbonate Additive in $LiNi_{0.5}Mn_{1.5}O_4$ - $Li_4Ti_5O_{12}$ Lithium-Ion Cells, *Journal of the Electrochemical Society, 164 (4), A942-A948.*

II Aktekin, B., Lacey, M.J., Nordh, T., Younesi, R., Tengstedt, C., Zipprich, W., Brandell, D., Edström, K. (2018). Understanding the capacity loss in LNMO-LTO lithium-ion cells at ambient and elevated temperatures, *The Journal of Physical Chemistry C, 122 (21), 11234-11248.*

III Aktekin, B., Valvo, M., Smith, R.I., Sørby, M., Marzano, F.L., Zipprich, W., Brandell, D., Edström, K., Brant, W. (2019). Cation Ordering and Oxygen Release in $LiNi_{0.5-x}Mn_{1.5+x}O_{4-y}$ (LNMO): In Situ Neutron Diffraction and Performance in Li Ion Full Cells, *ACS Applied Energy Materials, 2, 3323-3335.*

IV Massel, F., Aktekin, B., Liu, Y.S., Guo, J.H., Younesi, R., Brandell, D., Hahlin, M., Duda, L.C. (2019). The role of anionic processes in $Li_{1-x}Ni_{0.44}Mn_{1.56}O_4$ studied by resonant inelastic X-ray scattering, *In manuscript.*

V Aktekin, B., Massel, F., Ahmadi, M., Valvo, M., Hahlin, M., Zipprich, W., Marzano, F.L., Duda, L.C., Younesi, R., Edström, K., Brandell, D. (2019). How Mn/Ni ordering controls electrochemical performance in high-voltage spinel $LiNi_{0.44}Mn_{1.56}O_4$ (LNMO) with fixed oxygen content, *In manuscript.*

Reprints were made with permission from the respective publishers. Disclaimer: Part of this thesis is based on licentiate thesis entitled *High voltage positive electrodes for lithium-ion batteries: $LiNi_{0.5}Mn_{1.5}O_4$*, (Burak Aktekin, Uppsala University, 2017).

My Contribution to the Papers

I Performed all experiments (electrode fabrication, battery assembly, electrochemical tests) and carried out the surface characterization including measurements and data processing. Wrote the whole manuscript with feedback provided from co-authors, took part in all discussions.

II Performed all experiments and carried out the surface characterization including all measurements (SEM, XPS, HAXPES, XANES). Performed most of the data processing. Wrote the whole manuscript (except the LTO surface characterization part) with feedback provided from co-authors, took part in all discussions.

III Performed the in situ experiment and Raman analysis with other authors. Performed all other experiments except ex situ ND. Performed all data processing and wrote the entire manuscript with feedback provided from co-authors, took part in all discussions.

IV Performed sample preparation, half cell assembly, electrochemical cycling and sample preparation for XAS/RIXS measurements. Wrote the related experimental details, took part in general discussions and gave feedback on the manuscript.

V Performed all experiments except XAS/RIXS and TEM measurements. Performed all data processing (except XAS/RIXS part) and wrote the entire manuscript (except XAS/RIXS part) with feedback provided from co-authors, took part in all discussions.

Contents

Abbreviations

3-D	Three-dimensional
BoP	Beginning of charge
CCD	Charged coupled device
CE	Coulombic efficiency
CEI	Cathode electrolyte interface
CMC	Carboxymethyl cellulose
CV	Constant voltage
DEC	Diethyl carbonate
DMC	Dimethyl carbonate
DMMP	Dimethylmethylphosphonate
EC	Ethylene carbonate
EDS	Energy dispersive spectroscopy
EELS	Electron energy loss spectroscopy
EMC	Ethyl methyl carbonate
EoC	End of charge
EoD	End of discharge
EoP	End of plateau
FEC	Fluoroethylene carbonate
FFT	Fast Fourier Transform
FIB	Focused ion beam
HAADF	High-angle annular dark-field
HAXPES	Hard X-ray photoelectron spectroscopy
HFiP	Tris(hexafluoro-iso-propyl)phosphate
HFP	Hexafluoropropylene
HOMO	Highest occupied molecular orbital
ICI	Intermittent current interruption
ICP-OES	Inductively coupled plasma optical emission spectrometry
IMFP	Inelastic mean free path
LAGP	$Li_{1+x}Al_xGe_{2-x}(PO_4)_3$
LATP	$Li_{1.5}Al_{0.5}Ti_{1.5}(PO_4)_3$
LIB	Lithium-ion battery
LiBOB	Lithium bis(oxalato)borate
LIPON	Lithium phosphorus oxynitride
LiTf	Lithium trifluoromethanesulfonate
LiTFSI	Lithium bis(trifluoromethanesulfonyl)imide
LMO	$LiMn_2O_{4-x}$

LNMO	$LiNi_{0.5-x}Mn_{1.5+x}O_{4-\delta}$
LTO	Lithium titanate oxide
NASICON	Sodium (Na) super ionic conductor
NCA	$LiNi_xAl_yCo_zO_2$ (x+y+z=1)
ND	Neutron diffraction
NMC	$LiNi_xMn_yCo_zO_2$ (x+y+z=1)
NMP	N-Methyl-2-pyrrolidone
OCV	Open circuit voltage
PAN	Polyacrylonitrile
PEC	Polyethylene carbonate
PECA	Poly(ethyl α-cyanoacrylate)
PEO	Polyethylene oxide
PFY	Partial fluorescence yield
PI	Polyimide
PMC	Propylmethyl carbonate
PMCA	Poly(methylethyl α–cyanoacrylate)
PPC	Poly(propylene carbonate)
PTFE	Polytetrafluoroethylene
PVA	Poly(vinyl alcohol)
PVdF	Polyvinylidene difluoride
RIXS	Resonant inelastic X-ray scattering
RT	Room temperature
RTIL	Room temperature ionic liquid
SAED	Selected area electron diffraction
SEI	Solid electrolyte interphase
SEM	Scanning electron spectroscopy
SOC	State of charge
SPE	Solid polymer electrolyte
STEM	Scanning transmission electron microscopy
TEM	Transmission electron microscopy
TEY	Total electron yield
TFY	Total fluorescence yield
TGA	Thermal gravimetric analysis
TMdis	Transition metal disordered
TMord	Transition metal ordered
TMSP	tris(trimethylsilyl)phosphate
TOF	Time of flight
VC	Vinylene carbonate
XANES	X-ray absorption near edge spectroscopy
XAS	X-ray absorption spectroscopy
XPS	X-ray photoelectron spectroscopy
XRD	X-ray diffraction

1. Introduction

1.1. Lithium-Ion Batteries

The use of Li-ion batteries in portable electronic products – i.e. cell phones, notebooks, etc. – is today widespread and on-going research is extensively dedicated to improve their performances. As a substitute to fossil fuels, future state of the art lithium-based batteries can power the next generation of electric vehicles in a sustainable manner, if the energy stored in such batteries is provided by renewable energy sources. A conventional Li-ion cell used today contains a graphite negative electrode, a lithium metal oxide positive electrode, e.g. $LiCoO_2$, and a lithium salt such as $LiPF_6$ in a mixture of organic solvents as electrolyte [1]. A simple Li-ion cell is shown in *Figure 1*. In its discharged state, the cell is in thermodynamical equilibrium and the positive electrode is in the lithiated state while the negative electrode is in the delithiated state. During charging, lithium ions are removed from the positive electrode and intercalated into the negative electrode structure, which is thermodynamically less favorable. Therefore, external work is required while electrons are transferred from positive to the negative electrode through an external circuit.

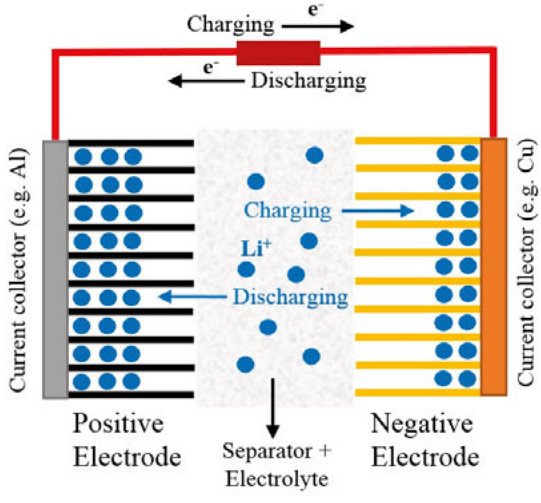

Figure 1. Schematic view of a Li-ion cell during charging and discharging.

At the end of charging, all lithium ions are hosted in negative electrode. During discharging, the lithium ions will spontaneously leave the negative electrode and intercalate into the positive electrode. The transport of lithium ions occurs in an ionically conductive medium which is normally a porous separator soaked in liquid electrolyte. As this medium is electronically insulating, electron transfer is forced via an external electrical connection which allows the use of electrical energy for any desired purpose. During discharge (i.e. galvanic cell operation), the negative electrode acts as anode since it is the electrode where electrons are emitted, while the positive electrode acts as cathode (electrons are accepted). It is common to use the term 'anode' instead of negative electrode and similarly 'cathode' for positive electrode, irrespective of charge or discharge. This convention will also be used in the following parts of the thesis.

Since the Li-ion batteries entered the commercial market in the early 1990s [2], graphite and other carbon based materials have primarily been the choice of anode (negative electrode). Alternative anode materials have been proposed [1,3], such as Li-Si, Li-Sn, Sn-Co-C alloys; TiO_2, $Li_4Ti_5O_{12}$ oxides; Cu_6Sn_5, InSb and Cu_2Sb intermetallics; as well as conversion-type materials of oxides, fluorides, sulphides, nitrides, phosphides and hydrides [4]. As electrolyte, liquid organic carbonate solutions are used in most systems today. The widely used lithium salt $LiFP_6$ is dissolved in a solvent mixture of for example ethylene carbonate (EC) and dimethyl carbonate (DMC), where the latter can be substituted by diethyl carbonate (DEC), ethylmethyl carbonate (EMC) and propylmethyl carbonate (PMC) without much significant performance change. Lithium salts such as $LiClO_4$, $LiAsF_6$, $LiBF_4$, LiTf and LiTFSI have also been used, but $LiPF_6$ has been the choice of lithium salt in commercial cells due to its overall performance regarding ionic conductivity, dissociation constant and thermal-chemical stability [5].

For the cathode, $LiCoO_2$ and similar layered oxides have largely been used in commercial batteries. However, other types of materials are required as a result of cobalt's high cost and toxicity [6]. Alternative layered oxides are attractive due to their reduced Co content, reduced cost and increased capacity, e.g. $LiNi_{1/3}Co_{1/3}Mn_{1/3}O_2$, $LiNi_{0.5}Co_{0.2}Mn_{0.3}O_2$ and $LiNi_{0.8}Co_{0.15}Al_{0.05}O_2$ [7]. Such compounds are usually abbreviated as NMC and NCA with the general formula $LiNi_xMn_yCo_zO_2$ and $LiNi_xAl_yCo_zO_2$ (x+y+z=1), respectively. While the theoretical capacity is high for such cathodes, the practical capacities are lower than that, e.g. about 160 mAh/g for $LiNi_{1/3}Co_{1/3}Mn_{1/3}O_2$, since full Li extraction is avoided during cycling as irreversible phase transformations otherwise takes place in low lithiation states [8,9]. While substitution of Co with other transition metal elements generates the NMC type materials, substitution of Li into the transition metal layers is also possible. In Li-rich layered oxides such as Li-rich NMC, Li is hosted in transition metal layers in addition to the van der Waals gap in the layered structure [10]. High capacities around 250 mAh/g are thereby achieved due to anionic oxygen redox activity observed

along with the transition metal redox activity [7]. The main problems for these type of materials are low initial coulombic efficiency, poor rate capability and structural instabilities observed during cycling [11].

An alternative class of materials is olivine-type phosphate cathodes, e.g. $LiFePO_4$ (3.4 V vs. Li^+/Li). This material has been extensively studied and has a theoretical charge capacity of 170 mAh/g. It is an inexpensive and environmentally friendly cathode material, but it suffers from slow ionic and electronic kinetics, which necessitate further modifications [12] that eventually increase its final cost. A third group of cathodes is spinel type materials such as $LiMnO_4$ with operational voltages 4.0-4.2 V vs. Li^+/Li and 148 mAh/g charge capacity. The 3-D lithium pathways available in the crystal structure allows fast lithium diffusion and makes this type of electrodes suitable for high power applications. However, its moderate energy density as well as fast capacity fading – especially observed at elevated temperature – constitute the main problems for this type of cathode materials [13], [14].

1.2. High Voltage Spinel Cathodes: $LiNi_{0.5}Mn_{1.5}O_4$

As approximately 50 % of the total cell weight is due to the cathode material, improvements of the cathode plays an important role when batteries with higher energy densities are desired [2]. Cathode materials operating at higher voltages improve the energy density, since the energy is determined by the product of charge capacity and the operating voltage. Therefore, one approach for such an improvement would be to use cathodes with a high voltage plateau. Having a spinel crystal structure, $LiNi_{0.5}Mn_{1.5}O_4$ (LNMO) is a promising cathode with a theoretical capacity of 147 mAh/g and an operating voltage around 4.7 V (vs. Li^+/Li). The high voltage plateau is due to the active Ni^{2+}/Ni^{4+} redox couple, and increases the theoretical energy density to 690 Wh/kg for the active material [6]. The spinel crystal structure allows excellent rate capability, and with the moderately high energy density obtained from its high voltage plateau, this material is regarded as a promising cathode material for high power applications (e.g. electric vehicles) [2].

However, the gain in terms of energy comes at the price of parasitic reactions. The anodic stability is determined by the highest occupied molecular orbital (HOMO) of the conventional electrolytes ($LiPF_6$ in organic carbonates), and starts to become a problem at voltages above 4.3 V (vs. Li^+/Li) [7]. Undesired interfacial side reactions as well as accompanied transition metal dissolution from the spinel structure causes rapid capacity fading in LNMO-based cells, especially at elevated temperatures [15], [7]. The synthesis conditions of LNMO also affect material properties, which in turn affect the electrochemical performance in Li-ion full and half cells. These material properties will be discussed in following sub-sections.

1.2.1. Crystal Structure

The $LiNi_{0.5}Mn_{1.5}O_4$ can be categorized into two different structures, *F*d-3*m* and $P4_332$, which are both spinel structures but differ from each other depending on Mn/Ni ordering (see *Figure 2*), which is usually associated with oxygen deficiency. In the face-centered cubic structure (*F*d-3*m*), the lithium atoms occupy the 8a sites while manganese together with nickel atoms are randomly positioned at 16d sites. Oxygen is located at the 32e positions. In the case of the simple cubic ($P4_332$) structure, lithium atoms are at 8c sites, manganese at 12d and nickel at 4a sites, while oxygen atoms occupy 24e and 8c sites [16]. These definitions are based on bulk average structure of LNMO and Mn/Ni ordering may still exist locally in the disordered phase [17].

As seen in *Figure 2*, both structures are very similar except the arrangement of Mn and Ni atoms. In literature, $P4_332$ phase is usually referred to as 'ordered LNMO' and *F*d-3*m* as 'disordered LNMO'. In order to obtain ordered samples, the synthesized powders are usually annealed at 700 °C and then slowly cooled while this temperature is above 750 °C (followed by fast cooling) for disordered samples [18–22].

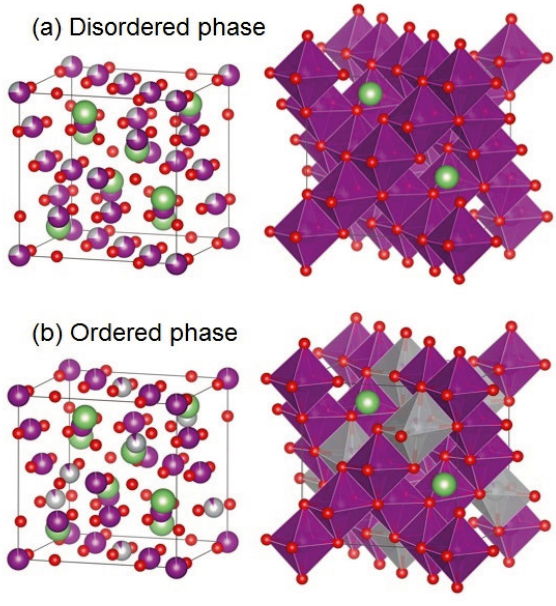

Figure 2. Schematic drawings for (a) spinel F*d*-3*m* and (b) spinel $P4_332$ space group. The spheres represent oxygen (red), Mn (purple), Ni (grey) and Li (green).

The ideal $LiNi_{0.5}Mn_{1.5}O_4$ structure includes only Mn^{4+} so that the active redox couple simply becomes Ni^{2+}/Ni^{4+}, which is responsible for the plateau around 4.7 V (vs. Li^+/Li). During synthesis, however, the high calcination temperature may result in oxygen release from the structure and reduction of Mn^{4+} to

Mn^{3+}. This results in another plateau around 4.0-4.1 V (vs. Li^+/Li) which decreases the energy density [23]. While ordered samples possess a single plateau around 4.7 V (vs. Li^+/Li), disordered samples possess both plateaus (i.e. also the second at low voltage). A majority of the studies show that disordered $LiNi_{0.5}Mn_{1.5}O_4$ shows better kinetics (and thus better power capability) and cyclability [23]. However, superior performance of cells with ordered LNMO powders as compared to disordered powders has also been reported [24].

In literature, the terminology of 'ordered' and 'disordered' is not well defined [25] due to insufficient characterization of ordering and other material properties that change during sample preparation. High temperature annealed samples which show the presence of a low voltage plateau due to Mn^{3+} are usually characterized with X-ray diffraction (XRD) and identified with the *F*d-3*m* space group. However, Mn and Ni have very similar X-ray scattering powers which makes the characterization of ordering very difficult by this technique. Additionally, due to different synthesis and heat treatment routes, samples can have different degrees of ordering, e.g. partial ordering [23], and it is not possible to determine the degree of ordering with XRD. It is also clear that particle size and geometry, concentration of crystal defects, oxygen stoichiometry, impurity phase concentrations, etc., can also be affected by the synthesis routes. These can, in turn, affect the electrochemical performance and might have a larger influence on performance compared to the effect of cation ordering itself.

During charging of LNMO, Li ions leave the structure and this causes phase transformations. For ordered LNMO, two phase transformations occur between $LiNi_{0.5}Mn_{1.5}O_4$ and $Li_{0.5}Ni_{0.5}Mn_{1.5}O_4$ and then between $Li_{0.5}Ni_{0.5}Mn_{1.5}O_4$ and $Ni_{0.5}Mn_{1.5}O_4$, involving three cubic phases [19,25–27]. However, disordered LNMO shows an additional solid-solution region at the beginning of charging [25]. In the computational work of Lee and Persson [28], it is suggested that cation disordering itself could be responsible for this observed solid solution behaviour in high lithiation states. Therefore, cation disordering in 'disordered LNMO' can be beneficial for cycling stability since single phase transformations are advantageous in cycling stability due to reduced strain and kinetic barriers.

1.2.2. Effect of Oxygen Release

During heating of LNMO (under air), oxygen release first starts at temperatures near 700 °C and becomes more noticeable at 730 °C [29]. Further increase of temperature makes the oxygen release more severe and phase transformations start to take place. At temperatures above 750-780 °C, the transition from spinel to rock-salt phase starts to occur [30], [22]. If the sample is

slowly cooled below 700 °C, the powders will have sufficient time to eliminate the rock salt phase, otherwise some rock salt phase domains risk being trapped in the structure due to fast cooling [31].

A possible consequence of oxygen release is formation of oxygen vacancies [30]. This would disrupt the charge balance and as a result, some of the Mn^{4+} in the structure would be reduced to Mn^{3+}. As the rock-salt phase is formed following significant oxygen release, this can also introduce some Mn^{3+} into the spinel structure. Several compositions have been reported for the rock-salt phase such as NiO [22], $Li_xNi_{1-x}O$ [32], $Li_{1/3}Mn_{1/2}Ni_{1/6}O$ [30] and $(Li_xMn_{0.66}Ni_{0.34})_yO$ [33]. If the rock-salt phase has a lower Mn/Ni ratio than the starting spinel phase, then the ratio of Mn/Ni would be higher in the spinel after rock-salt phase formation. This could also introduce Mn^{3+} into the structure without any oxygen vacancy requirement [33].

Kunduraci et al. [34] reported that Mn^{3+} present in the disordered phase would be responsible for the improvement of electrochemical performance in the disordered phase, since it would increase the electronic conductivity. Electron hopping between Mn^{3+} and Mn^{4+} was predicted as the reason for the higher electronic conduction in the disordered spinel. The disordered structure has 2.5 orders of magnitude higher values of conductivity compared to ordered phase. One problem with the disordered phase is the accompanying Ni-rich rock salt phase formation, which is electrochemically inactive. It also increases the Mn^{3+} content and reduces energy density further [23]. The explanation to the increase in electronic conductivity by the Mn^{3+}/Mn^{4+} couple, as proposed by Kunduraci et al., has on the other hand been debated by Ma et al. with the argument that Mn^{3+} is consumed already at the beginning of charging, and that it is not well-known if the electronic conductivity is rate limiting in the cell [34,35]. Recent studies have shown that improvement in conductivity is only limited to high lithiation states, while the conductivities of both phases are similar when the whole range of cycling is considered [26,36]. Since the exact reasons behind the performance improvement are unclear, there is no well recognised method for optimum sample preparation. Nevertheless, use of partially ordered samples have been suggested, as it could possess the respective advantages of both structures; i.e., higher capacity due to ordering and better cycle life and rate capability due to disordering [23,37].

1.2.3. Particle Size and Morphology

It is reasonable to expect that an extensively increased specific surface of the electrode powders (e.g. by smaller particle size) would lead to worse battery performance, considering that undesired reactions take place on the electrode surface. Therefore, there is a conflict between the positive effect of small particle sizes (shorter diffusion length) and the negative effect of high surface area (thus more side reactions) when using nano-sized electrode powders [38].

Moreover, during lithiation and delithiation, the electrode integrity can be lost due to particle cracking, or passivation layers can be continuously damaged. For nano-scale powders, the volume expansion occurring during cell reactions is usually less problematic as strain is more conveniently accommodated for nano-scaled electrode materials [3]. In the case of $LiNi_{0.5}Mn_{1.5}O_4$, micron-sized powders may show good kinetics and good cycle life at the same time [38], [35]. However, there have been studies reporting advantages of nano-scaling. Shaju et al. for example reported that nano-sized LNMO (50 nm particles) could still yield 80 mAh/g capacity at a very high rate of 40 C after 300 cycles [39].

Zhang et al. [40] synthesized LNMO porous nanorods in dimensions around 100-400 nm in diameter and >10 μm in length. As a comparison, another cathode was prepared from LNMO powders with particle sizes around 2 μm. At 1 C and 20 C rates, the nanorods showed 140 and 109 mAh/g capacities while the micron sized sample showed 120 and 80 mAh/g, respectively. The capacity retentions after 500 cycles were 91 % for the nanorods and 77 % for the bulk samples. The better performance was attributed to the stability of the cathode electrolyte interphase (CEI) layer formed, as the geometry of the nanorods would facilitate a strain relaxation along this layer during cycling.

Another factor affecting the performance is related to the crystal planes on the surfaces of electrodes, since different planes may have different reactivity and lead to different degree of surface film formation. Chemelewski et al. [41] synthesized cubic, spherical, octahedral and truncated powders to study these effects of morphology. A set of powders were further annealed at 700 °C. It was proposed that the effects of the degree of cation ordering and presence of rock salt phase were not profound. Cubic as well as octahedral powders on the other hand outperformed truncated and spherical powders in terms of cyclability, indicating that the surface planes play an important role for performance. Cubic and octahedral powder facets were identified with {112},{111} and {111} planes, respectively [41]. The possession of facile Li-ion transport pathways, better passivation against electrolyte side-reactions and transition metal dissolution have been suggested for {111} facets [42]. However, there have also been reports indicating better characteristics of {001} facets over {111} facets since truncated octahedron shaped powders with both facets have been reported to outperform octahedron shaped powders with only {111} facets [43].

It should be noted in this context that the evaluation of electrochemical performance is not straightforward since changes regarding surface elemental distribution, surface morphology, crystallinity, impurity phases, etc., can also be induced during synthesis to yield powders with different facets [7]. Additional comparisons of power capabilities and cycling stabilities between different studies are likewise hard due to different electrode qualities and mass loadings applied in most experiments.

1.3. Failure of High Voltage Cathode Based Cells

It was mentioned earlier that the electrochemical stability of conventional organic carbonate based electrolytes is problematic at voltages above 4.3 V (vs. Li^+/Li) [7]. Therefore, electrolyte oxidation occurring at high voltages can cause loss of cyclable lithium of the cathode or can increase the internal resistance due to accumulation of side-reaction products on different cell components. At the anode side, electrolyte reduction normally happen at low voltages (below ca. 1 V vs. Li^+/Li). For graphite for instance, electrolyte reduction starts at 0.8 V (vs. Li^+/Li) before lithium intercalation (around 0.2 V vs. Li^+/Li), but fortunately the formation of a passivating film (i.e. the SEI) – that is ionically conductive but electronically insulating – prevents further electrolyte reduction [44]. However, as the focus of this thesis is on the high voltage cathode, only cathode related failure mechanisms will be discussed in this section.

In composite electrodes, the active material is not only in contact with the electrolyte, but also with the current collector (aluminium for the cathode), conductive additive (e.g. carbon black) and binders (e.g. PVdF). The degradation of these components might cause active material loss or impedance rise. Here, the active mass loss is usually caused by isolation of active powders. This can be due to electronic contact loss after particle cracking, carbon black degradation and electrode delamination, etc., or due to ionic contact loss as a result of pore clogging. Another reason for active mass loss might be degradation of the active material itself. For example, the dissolution of transition metals from the structure [45] can reduce the amount of active particles.

In optimized LNMO electrodes, the electrode integrity remains relatively intact as the volume expansion of LNMO during lithiation and delithiation (around 7%) is moderate [46] and binders such as PVdF [47] has acceptable anodic stability. Carbon based conductive additives (e.g. carbon black) have been reported to show some reactivity at high potentials [48],[49] and Al current collectors have been shown to dissolve to some extent [50], but it is unlikely that these are the main reasons for the fast capacity decay of LNMO-based cells. The common picture in literature is that the two main causes of failure for this material are undesired electrolyte oxidation and transition metal dissolution.

Another characteristic of this material is its significantly faster capacity fade when tested in full cells compared to half cells. This can be explained by the cyclable lithium loss in a full cell. Interactions between the cathode and the anode also play an important role for this behaviour [51]. Being considered the major problems for LNMO-based cells, the impact of electrolyte oxidation and metal dissolution, as well as the reasons of cyclable lithium loss in a full cell, are further discussed in the following sections. Recently, near-surface structural changes following charging have been reported for LNMO [52], and is therefore discussed in a separate section at the end.

1.3.1. Electrolyte Oxidation on the Cathode

A standard electrolyte used in Li-ion batteries consists of $LiPF_6$ salt dissolved in a mixture of organic carbonate solvents (EC, DEC, DMC, EMC, etc.). The anodic stability of the anion in the salt (PF_6^-) is an important factor in determining the oxidation potential of electrolytes [53] and different anions in the same solvent might result in different oxidation potentials of the electrolyte [54]. A proposed mechanism of anion oxidation is given as follows [5]:

$$PF_6^- \rightarrow PF_6^\bullet + e^- \quad (1.1)$$
$$PF_6^\bullet \rightarrow PF_5 + F^\bullet \quad (1.2)$$

After the last step (1.2), HF can be formed since solvent molecules or water impurities in the electrolyte can serve as the proton source for a hydrogen abstraction reaction [5]. The resulting HF will cause further problems such as metal dissolution and will be discussed in the following section. For the salt anion, a quantitative determination of the intrinsic oxidation potential is problematic due to interfering solvent oxidation and counter-ion effects [55]. Additionally, even though the calculated oxidation potentials of the solvents are relatively high (e.g. 6.95 V vs. Li^+/Li for EC) [56], solvent oxidation reactions can start at lower voltages as a result of nucleophilic attacks of surface oxygen atoms in the cathode materials [57], and it is likely that anion and solvent oxidation are interconnected. For example, oxidation of the solvent/anion complexes at lower voltages, accompanied with H-abstraction from the solvent molecules and F-abstraction from the anions, has been suggested [58]. In one study, Borodin et al. calculated the intrinsic PF_6^- oxidation stability limit to be 8.7 eV and the intrinsic EC stability limit to 7.1 eV, however, the oxidation stability limit of the PF_6^-/EC complex was only 6.15 eV [58].

As electrolyte oxidation occurs, oxidized products will form (gases, soluble and solid species) accompanied by electron transfer to the cathode. Electrolyte depletion and build-up of reaction products in different parts of the cell will likely cause further problems in the cell [59]. The formation of a surface film on LNMO, consisting of LiF, C-F, P-F_x species and organic compounds such as polyethers, can increase the electrode impedance [60]. X-ray photoelectron spectroscopy (XPS) analysis of LNMO surfaces has indicated presence of organic species, including lithium alkoxides (ROLi), lithium alkyl carbonates ($ROCO_2Li$) and polyethylene carbonate (PEC) [61].

Formation (and further decomposition) of the radical cation $EC^{\bullet+}$ (formed after a one-electron oxidation reaction of EC) might yield CO_2, CO and various radical cations [62]. The highly reactive radical cations can participate in further side reactions in different parts of the cells. If it reacts with the counter electrode, it can be reduced to the original solvent species or be involved in other reactions [59]. Metzger et al. showed that reduction of protic species (on the NMC cathode surface) could cause H_2 evolution on graphite [63]. This is

an example of electrode interactions (so called 'cross-talk') which will be discussed further in following sections.

1.3.2. Transition Metal Dissolution

The dissolution of Mn from the spinel $LiMn_2O_4$ cathode material is well-known and is believed to be initiated by a disproportion reaction on the cathode surface (1.3) [64]:

$$2\ Mn^{3+} \rightarrow Mn^{4+} + Mn^{2+} \quad (1.3)$$

It has been suggested that Mn^{2+} ions are dissolved into the acid-medium while Mn^{4+} ions stay in the active material. The acid attack by HF (generated after electrolyte oxidation) as well as structural instabilities accelerate the dissolution process [64]. For instance, increasing amounts of proton concentration in the electrolyte as a result of electrolyte oxidation has been shown to promote more Mn dissolution [65]. In the case of the Ni substituted spinel oxide $LiNi_{0.5}Mn_{1.5}O_4$ studied here, metal dissolution of Mn and Ni has similarly been observed [6]. Aurbach et al. suggested that the LNMO would transform to λ-MnO_2 at elevated temperatures [60]:

$$4\ LiNi_{0.5}Mn_{1.5}O_4 + 8\ H^+ \rightarrow$$
$$2\ \lambda\text{-}MnO_2 + Mn^{2+} + Ni^{2+} + 4\ Li^+ + 4\ H_2O + 2\ Ni_{0.5}Mn_{1.5}O_4 \quad (1.4)$$

As mentioned earlier, for the ideal stoichiometry of LNMO, all Mn ions are expected to be in the +IV state, however, it is common to observe some Mn^{3+} in the structure due to oxygen deficiency and impurity phases formed during synthesis [6] and this can cause the Mn dissolution via disproportion reaction. However, even though there is some Mn^{3+} present in the structure, it should be transformed to Mn^{4+} after charging. It has been shown that metal dissolution is more severe in the charged state (i.e. delithiated LNMO; only Mn^{4+} present) [45], and it is therefore suggested that the presence of Mn^{3+} in the structure is not necessary for metal dissolution. If the consequences of transition metal dissolution are considered, a decrease in the active cathode mass loss is expected as seen in reaction (1.4). An increase in cell resistance can be caused by the erosion of active material as this would damage the existing electrical network in the cathode. Deposition of dissolved ions in the form of MnF_2, NiF_2 and LiF on the cathode could similarly increase the electrode impedance [45]. Apart from these mechanisms, migration of dissolved transition metal ions to the anode can cause further side reactions, especially in full-cells [51] and possible outcomes of this interaction are also explained in the next section.

1.3.3. Cross-talk Between Positive and Negative Electrodes

Electrode interactions occurring between the positive (cathode) and the negative electrode (anode) inside an electrochemical cell is usually referred to as 'cross-talk'. Such interactions can occur via migration of electrolyte oxidation products from the cathode to the anode. Dedryvere et al. observed with XPS that both inorganic (LiF, phosphates) and organic species were present on LTO electrodes after cycling in LNMO-LTO cells [66]. Presence of organic species on the anode can be due to migration/diffusion of organic cations/organic species originating from the cathode [66,67]. It is a possibility that such reacted species can also shuttle back to the positive electrode [68].

Migration of transition metals dissolved from the cathode to the anode is another example of cross-talk which has been extensively studied in $LiMn_2O_4$ (LMO) based cells [64]. In LNMO-graphite cells, this type of cross-talk is believed to cause damages to the existing SEI layer on graphite [51]. Incorporation of transition metals on the anode surface can induce pores and increase the electronic conductivity of the SEI layer [69], facilitate electrolyte reduction by coordination to solvent molecules [70] or reducing reduction barriers via an electrocatalytic mechanism [71].

Recently, some studies focusing on a different kind of cross-talk have been reported: interaction of gas products in systems such as LNMO-graphite [72] and NMC-graphite [63],[73],[74]. Electrolyte oxidation at high cathode voltages would yield gases such as CO_2 [75]. On the anode side, C_2H_4, CO and H_2 might evolve at potentials below 1 V (Li^+/Li) [63]. Xiong et al. suggested that CO_2 evolving from delithiated NMC stored at 60 °C would be consumed by graphite [74]. The reduction of CO_2 to species such as lithium oxalate or lithium carbonate would decrease the lithium inventory in the anode, and back-migration of the former product can also cause a shuttle mechanism [68]. Apart from gas consuming reactions, gases would also evolve as a result of cross-talk. Metzger et al. showed that H_2 evolution on a graphite surface is caused by reduction of protic species that were formed continuously by electrolyte oxidation (on NMC) [63].

As seen in literature, different types of electrode interactions may exist in high voltage cathode based full cells. It is possible that these interactions are connected in some way as these problems have the same origin, i.e. electrolyte oxidation. It is thus important to identify the exact roles of the different interactions when studying the capacity fade of high voltage cathode based full cells. It should also be noted that a reverse cross-talk can also happen, i.e. originating from the negative electrode. It was shown that the choice of negative electrode can affect the surface film composition and its thickness on NMC positive electrodes. Thicker films which are richer in organic species have been observed when the counter electrode is Li as compared to graphite and LTO [76].

1.3.4. Electrochemical Behaviour in Full-Cells

It has already been stated that side reactions occurring at high voltages and accompanied transition metal dissolution from the active material cause a variety of problems in LNMO-based cells and result in capacity fading. Unfortunately, the capacity fading of cells is considerably faster when LNMO is cycled in full-cells as compared to half-cells. Especially at elevated temperatures (e.g. 55 °C), this capacity fading becomes quite dramatic [18]. It should be noted that the lithium metal anode provides an unlimited lithium source in a half cell while the amount of lithium inventory in a full cell is limited and determined by the initial cathode capacity. Therefore, faster capacity fade observed in full cells can be explained with severe oxidative decomposition of electrolyte and (in relation to this) consumption of the limited lithium inventory in the cell [77]. This explanation needs elaboration, as it can be somewhat misleading. A decrease in lithium inventory is usually expected by reductive side reactions occurring on anode. In fact, oxidative side reactions on the cathode are expected to increase the amount of lithium inventory in a full cell. In order to make these expected behaviors more clear, a simple example is demonstrated below in *Figure 3*.

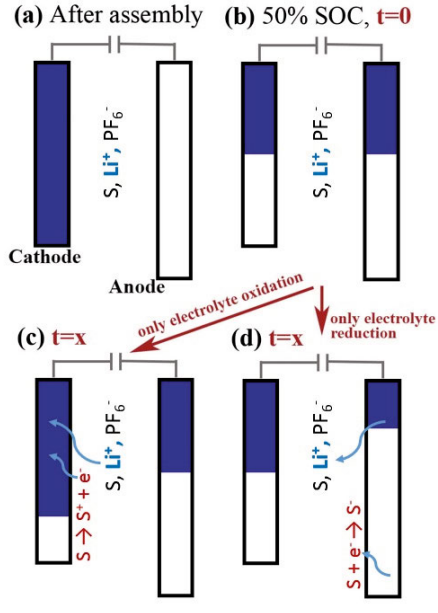

Figure 3. Schematic representation of cathode limited full-cells just after cell assembly (a) and after being charged to 50 % SOC (b). If this cell (b) is calendar aged for sufficient time, the amount of charge in anode and cathode would be similar to (c) if only electrolyte oxidation has occurred, or (d) in case of only electrolyte reduction.

In this simple example, a cathode limited full-cell is first charged to 50 % SOC and then left at OCV state for calendar aging. During this period, electrolyte oxidation can occur on the cathode and reduction on the anode. If only 'electrolyte oxidation' occurs as shown in *Figure 3c*, the surface reactions will generate positively charged decomposition products and electrons. The electrons are accepted by the cathode, but will be accompanied by intercalation of lithium ions available in the electrolyte back into the cathode in order to remain charge neutrality. This will result in a gradual increase of the lithium inventory in the cathode as the electrolyte oxidation proceeds. If another possibility is considered (*Figure 3d)* so that only electrolyte reduction on the anode occurs, then the side reactions would involve electrons provided by the anode accompanied with Li de-intercalation, causing a decrease in the lithium inventory. After calendar aging, if these cells are discharged, in the case of electrolyte oxidation, only a part of the charge (Li) in the anode can be transferred back into cathode, while some will remain in anode. On the other hand, for electrolyte reduction, all charge could return to the cathode while the anode will be completely in the delithiated state after discharge.

After this demonstration, it can be concluded that the oxidative reactions could cause 'cyclable lithium loss' via an *increase* in 'lithium inventory'. On the other hand, in the case of reductive reactions, cyclable lithium loss could originate from a *decrease* in 'lithium inventory'. In the light of this information, it should be clear why explaining the capacity fade in LNMO based cells with a correlation between electrolyte oxidation and lithium inventory loss might be misleading. Studies of LNMO-graphite cells have shown that the capacity fading originates from a decrease in lithium inventory [51]. Therefore, reductive processes should be responsible for the capacity fading. As suggested [51], migration of dissolved transition metal ions from the cathode to the anode could cause reduction of these ions to their metallic states, causing some lithium loss. Additionally, deposition of these ions could damage the passivating SEI layer on graphite and therefore result in continuous electrolyte reduction.

It could thus be understood that the direct cause of cyclable lithium loss is largely related to the instability of non-passivated graphite surfaces towards electrolyte reduction. However, when LNMO electrodes instead have been coupled to LTO, similarly the decrease of lithium inventory was found to be responsible for the capacity fade [67]. This is interesting, since LTO has a high operating voltage (1.55 V vs. Li^+/Li) and is known for its stability in electrolyte. Therefore, it does not require an SEI for protection and 'SEI damage' should not be a problem in contrast to graphite. Thereby, it is seen that electrode interactions (or cross-talk) exists in LNMO based full-cells, and has a significant role in determining cell life-time [66],[67]. This cross-talk between the electrodes is likely not limited only to the migration of dissolved metal ions.

1.3.5. Surface Structural Reconstruction

It is known that spinel cathodes are more prone to instability issues in their delithiated (charged) state [52,78]. Also, in some recent studies, near-surface structural reconstruction has been reported for delithiated spinels such as $LiMn_2O_4$ [79] and LNMO [52]. As evidenced with STEM-HAADF imaging, 'Mn_3O_4-like' or 'rock-salt like' phases can form in near-surface regions which are likely accompanied with oxygen release and TM dissolution from the lattice [52]. Formation of rock-salt phases occurs via migration of transition metal ions to the empty octahedral sites. Similar surface reconstruction during charging are known to occur in layered oxide electrodes, and spinel electrodes are considered to have a more robust structure and being less prone to near surface phase changes [7]. As these recent studies indicate, however, near surface changes do occur to some degree when LNMO is charged to its delithiated state, and more research is necessary to understand how this reconstruction layer grows over cycling and how it affects the electrochemical performance. Similarly, oxygen release during cycling has been little considered for LNMO (as compared to layered oxides) [80], but observations of rock-salt like phases indicate that oxygen release also takes place during cycling. To what degree this oxygen release occur and its effect on electrochemical performance should also be a subject of future studies.

1.4. Approaches to Increase Calendar and Cycle Life

From the description formulated above, it is seen that one major problem for LNMO-based cells is related to the high voltage instability of the electrolyte. These problems decrease the calendar and cycle life of batteries, i.e. the storage and usage time that the battery can deliver at least 80 % of its initial capacity, respectively. Therefore, the search for alternative novel electrolyte systems that are stable at high voltages (i.e. with high anodic stability) would be an ideal solution. Sulfone-based solvents, ionic liquids and dinitrile solvents have high anodic electrolyte stability, but have on the other hand disadvantages such as high intrinsic viscosity and severe reductive decomposition at low voltages (e.g. at the graphite anode) [77]. Ionic liquid electrolytes compatible with graphite have been reported [81] and such electrolytes have been tested with LNMO. For example, the room temperature ionic liquid (RTIL) based electrolyte LiTFSI/pyrrolidinium bis(trifluoromethane-sulfonyl)imide have been suggested to improve high temperature cycling stability [82].

The use of solid ceramic or glassy electrolytes has also been reported with LNMO (thin film) half cells and showed good cycling stability, for example when using lithium phosphorus oxynitride (Lipon) [83]. In more realistic solid state cells (e.g. not thin film based), contact problems at the electrode-electrolyte interface result in high cell resistance. Nasicon-type materials are also

good candidates due to their high voltage stability. All solid state batteries with $Li_{1+x}Al_xGe_{2-x}(PO_4)_3$ electrolyte (LAGP) have been reported in LNMO-Li half cells, but high interfacial resistance was observed between LNMO and LAGP [84]. For $Li_{1.5}Al_{0.5}Ti_{1.5}(PO_4)_3$ electrolytes (LATP), formation of insulating phases are also expected during the preparation of composite electrodes [85]. Even though these are promising materials in terms of anodic stability and safety aspects, preparation of composite electrodes and ensuring a good contact at the interface are problematic, and practical applications of such battery systems therefore seem less realistic in the near future.

Solid polymer electrolytes (SPEs) are also interesting as they offer advantages for electric vehicle applications which necessitate more strict safety requirements as well as suitability for elevated temperature operation. However, drawbacks in ionic conductivity and interfacial functionality exist [1,86]. In the case of LNMO, possessing a high anodic stability is crucial for the SPE material. The well-known polyethylene oxide (PEO) based electrolytes are known to be unstable at moderately high potentials (> 4 V vs. Li^+/Li) [87] and are therefore not compatible with the LNMO surface. Alternative host materials are polycarbonates, polyesters, polynitriles, polyalcohols, polyamines, etc. [86], which have still not been thoroughly tested with LNMO material.

In the short-term perspective, solutions regarding existing electrolyte systems are likely more feasible. In a first approach, carbonate based solvents can be substituted with their relatively more stable counterparts, such as FEC instead of EC [88]. Another approach would be to accomplish protection of the cathode surface against electrolyte oxidation (and acidic attack) via surface passivation. External coatings for the active material before electrode fabrication, or in situ coating in the cell via electrolyte additives, can constitute possible solutions. As examples of the former approach, some improvements have been reported by coating cathodes with mildly oxidized graphene [89] or GaF_3 which would also enhance the conductivity [90]. Other examples of coating materials include ZnO, Li_3PO_4, Zn, Au, Ag, SiO_2, Bi_2O_3, Al_2O_3, ZrP_2O_7, ZrO, $LiCoO_2$, $LiAlO_2$, $FePO_4$, $AlPO_4$ and $LiFePO_4$ [6], [91], [92]. Solid state inorganic electrolytes have also been aimed for coating purposes (as thin films) between the LNMO and the conventional liquid electrolyte. For instance, LATP modified LNMO powders were used in a standard electrolyte and some improvements in the electrochemical performance were reported [93,94].

The use of polymers together with standard electrolytes have also been reported in several studies. For instance, poly(methylethyl α–cyanoacrylate) (PMCA) with lithium bis(oxalate)borate (LiBOB) were casted on nonwoven polytetrafluoroethylene (PTFE) and the resultant composite was saturated with liquid electrolyte (PC + 1 M LiBOB) to form a gel polymer electrolyte [95]. In a similar study, poly(propylene carbonate) (PPC) was casted on a cellulose membrane which was saturated with liquid electrolyte [96]. In–situ polymerization was also applied to coat LNMO powders with poly(ethyl α-cyanoacrylate) (PECA) [97].

Gel–polymer electrolytes have been applied on LNMO electrodes, for example, poly(vinylidene fluoride-co-hexafluoropropene) (PVdF–HFP) polymers prepared with a standard electrolyte was tested in half cells and some improvements were observed [98]. Poly(methyl methacrylate–acrylonitrile–ethyl acrylate) terpolymer [99] or poly(methyl methacrylate–butyl acrylate–acrylonitrile–styrene) [100] based gel–polymer electrolytes have also been tested in half cells. In the work by Panero et al., a gel–polymer electrolyte consisting poly(acrylonitrile) (PAN) saturated with 1 M $LiPF_6$ in PC was used [101]. In another study, a coating strategy was applied on LNMO using polyimide (PI) with a thickness around 10 nm (achieved by thermal imidization of polyamic acid) [102].

Polymers can also be used as binders. For instance, an acrylonitrile–grafted poly(vinyl alcohol) (PAN-g PVA) copolymer was used as binder for LNMO [103]. In this work, the motivation for using branched copolymers was the oxidation resistance of PAN and the high adhesive strength of PVA. These branched copolymer was reported to provide better coverage of LNMO surface. Among several alternatives, one particularly promising strategy would be the employment of nitrile groups (e.g. polynitriles). Being a strong electron withdrawing group [104], higher anodic stability and therefore higher oxidation resistance is expected for polynitriles, which also possess Li ion coordinating abilities.

Yet another approach is the use of additives to form passivating surface layers. This would be the most preferred solution due to its practical feasibility. A number of electrolyte additives have been reported in recent years for this purpose [105], including LiBOB [106], succinic anhydride [107], HFiP [108], DMMP [109], TMSP [110], thiophene [111], etc. These approaches have focused directly on the cathode stability. As mentioned in above, however, cross-talk also exists in LNMO-based full cells and plays an important role in capacity fade. To this end, some studies have aimed to mitigate the negative effects of electrolyte decomposition products. For instance, electroactive separators have been proposed [112], targeting the protection of the negative electrode from dissolved metal ions from the positive electrode by scavenging them during passage. For this purpose, Leitner et al. studied a separator containing lithiated LTO ($Li_{4+x}Ti_5O_{12}$) in LNMO/graphite cells [112].

As a completely different approach, some enhancements can be made via slight changes in stoichiometry or with doping of other elements into the active material since such modifications can affect the crystal structure and electronic properties as well as the surface characteristics. For instance, Fe substituted LNMO, or more specifically $LiMn_{1.5}Ni_{0.42}Fe_{0.08}O_4$, was reported to provide stabilization of the cation disordered structure with Fe enrichment on the surface, thereby leading to formation of thin CEI layers and thus a low polarization resistance [113]. Improvements with Cr and Ru doped LNMO have also been reported [114]. With near surface (2-4 nm) Ti doping, it is possible to increase cycling performance and reduce transition metal dissolution [115].

It was also reported that in TiO_2 surface modified LNMO particles, Ti can diffuse into LNMO surface and cause phase transitions from spinel to rock-salt and rock-salt-like phases, which was suggested to mitigate transition metal dissolution and electrolyte oxidation [116]. These results also indicate that inorganic coatings on LNMO might affect electrochemical performance not only due to the stabilization provided by the coating, but also near-surface changes that can occur by diffusion of elements in the coating material into the LNMO particles.

Finally, it should be noted that even though some improvements have been obtained, none of these approaches mentioned in this section deliver the cycling stability demanded by the practical applications (especially for elevated temperature) and more research is clearly necessary with each of these mentioned approaches to solve the issues related to this otherwise promising cathode material.

2. Scope of the Thesis

In this thesis, the spinel high voltage cathode material $LiNi_{0.5-x}Mn_{1.5+x}O_{4-\delta}$ (LNMO) has been studied with a focus on understanding its degradation mechanisms in Li-ion battery cells and exploring the different approaches aiming to improve its electrochemical performance.

The first part of this thesis (*Paper I*) focuses on fluoroethylene carbonate (FEC) which is a well-known electrolyte additive that has been used in other lithium-ion cell chemistries. Its effect on high voltage cathodes is not clear in literature and for that reason the primary focus was to understand if this additive has a beneficial effect on LNMO – rather than on the counter electrode. Observations from this study not only answered this question, but at the same time brought several new questions for understanding the capacity fading mechanisms in high voltage cathode based full cells, e.g. understanding the electrode interactions and unexpectedly fast capacity fading at elevated temperature. This naturally led to the *Paper II*, which aims to develop a comprehensive understanding of capacity fading mechanisms, and the results from this study constitutes the second part of the thesis.

It is well-known that the synthesis conditions affect the rate of performance degradation in LNMO-based cells since changes in material properties are induced during synthesis such as cation ordering and oxygen content. With the aim of exploring such changes, in situ studies of ordered LNMO have been conducted via ND (*Paper III)* and TEM, respectively. These studies showed that the oxygen release is not directly related to cation ordering. Also, local microstructural changes upon heating were observed. These findings thereby suggested new sample preparation strategies which allow obtaining cation disordering in oxygen non-deficient samples.

In *Paper IV*, the changes in electronic structure were analysed at different state of charges via RIXS and XAS techniques. Considerable contributions from oxygen redox activity is found during charge compensation on delithiation. In *Paper V*, ordered and disordered samples with the same oxygen content were prepared via a novel strategy. The negative effect of ordering on electrochemical performance was investigated in terms of surface, near-surface and bulk electronic structural changes via a range of characterization techniques: XPS, XAS, RIXS and TEM.

3. Experimental Methods

A variety of experimental techniques have been utilized in this work. Details of materials and electrode preparation, cell assembly and their electrochemical testing are described briefly in this section, together with materials characterization techniques. For further details, the reader is referred to the appended papers.

3.1. Materials

Commercial powders of LNMO were used directly, or heat treated either under oxygen or air atmosphere. Alumina crucibles were used for sample treatment. In order to obtain conventional disordered samples, powders were heated to 800 °C in a quartz tube furnace under air atmosphere. After 12 hours of annealing at this temperature, the crucibles were removed quickly from the furnace and water cooled to RT. For conventional ordered samples, the atmosphere was pure oxygen and the annealing temperature was 600 °C, while the samples were cooled slowly in the furnace to RT. In order to obtain ordered and disordered samples with the same oxygen content, both samples were first heated to 760 °C in 6 hours, then cooled to 500 °C and heated back to 760 °C, and finally cooled to 710 °C. After two hours annealing at this temperature, the samples were cooled to RT in two different ways. In order to obtain disordered samples, the alumina crucible was taken rapidly from the furnace and powders were quenched to RT. For the ordered sample, sample was cooled slowly to RT in furnace.

To fabricate composite electrodes, a mixture of LNMO powders (90 wt%) with carbon black (5 wt%) and PVdF-HFP binder (5 wt%, PVdF-HFP) in NMP was ball-milled for 2 hours. The slurry was casted on bare aluminum foil so that the active electrode had a thickness around 50 μm. The electrode was calendared slowly (one pass) and the final average porosity was estimated to 40-50 %. The active mass loading was around 10.6 mg/cm^2 (or 1.56 mAh/cm^2). For high rate applications, electrodes were put between 22 mm diameter stainless steel discs with polished surfaces and then pressed till the pressure on electrode was 160 MPa. Commercial LTO electrodes (from Leclanché) were used as counter electrodes. LTO electrodes had a capacity around 1.7 mAh/cm^2 and resulting full cells therefore were then limited by the LNMO electrode. 1 M $LiPF_6$ dissolved in EC and DEC with 1:1 volume ratio

was used as electrolyte with polypropylene (Celgard) separators. As current connectors, aluminum foil was used for LNMO and copper was used for LTO electrodes, while nickel was used for lithium. The lithium foil was 125 µm thick and had a diameter of 26 mm.

3.2. Electrochemical Testing

LNMO-LTO cells were prepared using 2 cm diameter electrodes. 1 layer (*Paper I*) or 2 layers (*Paper II, III, V*) of separator were used (4 × 4 cm^2 area). In order ensure homogeneous pressure distribution, current connectors having 2 cm diameter circular tips were used. The electrolyte volume was 80 µl (*Paper I*) or 120 µl (*Paper II, III, V*).

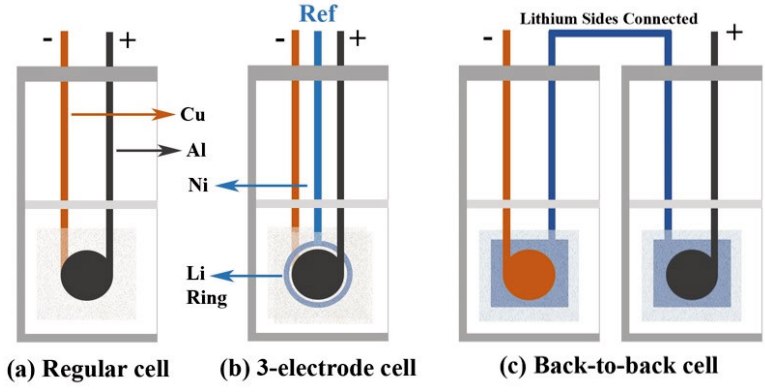

Figure 4. Schematic representation of different type of pouch cells used.

Regular pouch cells used in this study are shown in *Figure 4a*. Apart from regular cells (2-electrode), also three electrode cells (*Figure 4b*) have been used. In those cells, concentric lithium rings were punched with an inner diameter of 2.2 cm and outer diameter of 2.6 cm. These rings were carefully placed between LNMO and LTO so that it faced the separators on both sides. A third type of cells, called back-to-back cells, have also been tested with the aim to check electrochemical performance in cases where no cross-talk is allowed between LNMO and LTO electrodes. In these cells (*Figure 4c*), one LTO half cell was connected to another LNMO half cell through their lithium sides. Then, these two cells were handled as one full-cell. The LNMO side was connected to the working electrode and the lithium side to reference electrode, while the LTO side was connected to the counter electrode terminal of the cycling equipment. Additionally, a modified back-to-back cell was constructed to investigate the cell behaviour when interactions by gas products were possible, but not any interactions through the electrolyte. For this, a large lithium sheet around 4.5 × 4.5 cm was placed between the electrodes and two

sheets of separator were placed on both sides of the lithium, but with a smaller area.

Full cells were galvanostatically cycled between 1.5 V and 3.5 V at different rates according to the calculated capacity of LNMO. Before starting the cycling, a waiting time (10 hours) was applied. A Novonix HPC (High Precision Charger) system (30 and 55 °C) and a Digatron BTS-600 system (24 °C – 25 ˚C) were used. Internal resistance measurements were made in three electrode and back to back cells. Here, galvanostatic cycling was combined with an intermittent current interruption (ICI) resistance determination method [117], using a Bio-Logic VMP2 instrument. The calculation of cell resistance was made using the Ohmic voltage drop during interruptions.

3.3. Materials Characterization

3.3.1. Sample Preparation

After the cycling of LNMO-LTO and LNMO-Li cells, they were carefully opened in a glove-box (argon atmosphere). After separation of electrodes from the separator, they were rinsed with DMC three times (*Paper I*, 0.5 ml each time) or 3-5 times (*Paper II, IV and V,* 4-5 droplets each time) and left for drying. This was applied to remove salt residues from the electrode surface. For SEM analysis, small pieces were cut and placed on carbon tapes inserted on aluminium SEM stubs. For XPS, XANES, XAS and RIXS measurements, samples were prepared in a similar way but using copper tape instead. For samples measured at a synchrotron facility, they were inserted into plastic boxes and vacuum sealed into coffee bags (two times) to ensure air-tightness during transport.

3.3.2. Scanning Electron Microscopy

Imaging in a scanning electron microscope (SEM) is done by sending a focused beam of electrons onto a sample surface and subsequently detecting the secondary electrons emitted from this small area where the beam is focused. If this process is repeated step by step to scan a selected area on the sample, it is possible to form a two dimensional image of this area. In this study, the technique was mainly used to observe the morphology of the electrodes before and after cycling. In *Paper I*, an air-tight transfer system was used to insert cycled samples into a SEM chamber. For this purpose, a Zeiss Sigma Series SEM was used. In *Paper II*, airtight glass vials were used for transfer and the samples were exposed to air for 15-20 seconds before being inserted into the SEM chamber of the Zeiss 1550 SEM instrument. Both microscopes were equipped with a field emission gun. In order to increase surface sensitivity of

the imaging, the accelerating voltage was decreased (e.g. to 3 kV). The working distance was kept at 5 mm. When a set of images are presented, each image in the set was scaled to the same magnification using the ImageJ software by calibrating them using scale bars.

3.3.3. X-ray Photoelectron Spectroscopy

This technique uses X-rays to irradiate samples and analyses the kinetic energy of emitted electrons (the photoelectric effect). Since the distance that electrons can travel without any energy loss in a solid is quite limited (depending on inelastic mean free path, IMFP), this technique is very surface sensitive – with a probing depth of only a few nanometers. The kinetic energy of the emitted electrons can be defined using the equation (3.1):

$$E_K = h\nu - E_B - \Phi_s \quad (3.1)$$

In equation (3.1), E_K is the kinetic energy of electron detected, $h\nu$ is the energy of incoming X-ray, E_B is the binding energy of the orbital that the electron is ejected from and Φ_s is the spectrometer work function. Using this equation, it is possible determine E_B using the measured E_K value. The E_B is element specific (and depends on chemical state), and therefore this allows identification and quantification of elements in the surface layer of the materials. In this study, pristine electrodes as well as electrodes after electrochemical cycling have been analyzed using in-house XPS, which is a Phi-5500 instrument with monochromatized Al-Kα radiation (1486.6 eV).

As stated, probing depth depends on IMFP, and it is dependent on the kinetic energy of electrons. If photons with higher energies are used, electrons with higher kinetic energies would be emitted which increases the probing depth of the analysis. The analysis using different photon energies can provide depth profiling in a non-destructive way. It is possible to tune the photon energy in a synchrotron facility in order to change probing depth (and perform depth profiling). For this reason, additional measurements were conducted at the Helmholtz Zentrum Berlin, BESSY KMC-1 beamline, High Kinetic Energy Photoelectron Spectrometer (HIKE) end station using a Scienta R4000 electron analyzer. Photon excitation energies of 2005 and 6015 eV were used. Data calibration was made by linear shifting of the hydrocarbon peak to 285 eV, except for the LTO electrodes in *Paper II* which were calibrated using the Ti 2p peak. Casa XPS and Igor software were used for the analysis of data.

3.3.4. X-ray Absorption Spectroscopy

At a synchrotron facility, it is possible to obtain high energy X-rays which are tunable in energy. Therefore, the energy of the incoming photon hitting the

sample can be changed gradually, while the response of the material is detected (e.g. intensity of X-rays transmitted through the material, the intensity of total fluorescence and the electron yield). This response originates from the excitation of electrons from a core level in an element when the incoming photon energy is sufficiently high. In this way, it is possible to obtain the absorption edge spectrum of different elements. This technique has been proven to be a useful tool to determine the oxidation state of metal ions [118] and has therefore been utilized in *Paper II* for LTO electrodes to identify oxidation state of Ni and Mn deposited on the surface. For this purpose, measurements were done for Mn K-edge and Ni K-edge. Measurements were performed at the beamline BESSY KMC-1 using a Bruker XFlash 4010 fluorescence detector. Au 4f spectra was used for calibration and data analysis was made via Athena software. In *Paper IV and V*, XAS spectra of Mn L-edge, Ni L-edge and O K-edge were measured in the total fluorescence yield (TFY) and total electron yield (TEY) modes to get information on the electronic structure from different probing depths. Here, TFY mode allows a penetration depth of around 100 nm and TEY mode around 10 nm. Measurements were done at the Advanced Light Source of Lawrence Berkeley National Laboratory, beamline 8.0.1. [119] and SPring-8 (Super Photon Ring – 8 GeV) synchrotron radiation facility in Hyōgo Prefecture, Japan.

3.3.5. Resonant Inelastic X-ray Scattering

In resonant inelastic X-ray scattering (RIXS), X-rays are sent to sample and a core hole is created by electron excitation from core level to an unoccupied state around the Fermi level. This core hole decays by electron transfer from the valence band, and as a result X-ray photons are emitted. The energy of such photons are recorded with a spectrometer. In RIXS measurements, the incoming photon energy is tuned to the absorption edge of the interest. For this reason, it is called a resonant technique and requires synchrotron radiation. In order to determine the absorption edge, first an XAS spectrum is measured and the edge energies are determined. In the RIXS process, the energy difference between the incoming and outgoing photons correspond to energy of excitations left in the sample. Since some energy is lost in these excitations, the outgoing photons are said to be ‘inelastically’ scattered. The energy spectrum of inelastically scattered X-rays will give information about the dispersion of excitations in the sample. This spectrum can reveal fingerprints for electronic structure changes which may not be possible to see via XAS spectra. This renders it as a very valuable complementary technique to XAS analysis.

In *Paper IV and V*, RIXS measurements were performed for Ni L-edge and O K-edge in Advanced Light Source of Lawrence Berkeley National Laboratory, beamline 8.0.1 and SPring-8 synchrotron radiation facility in Hyōgo Prefecture, Japan. The same samples were used as described in the XAS section.

3.3.5. Raman Spectroscopy

Raman spectroscopy is based on inelastic scattering of optical light sent to a sample of interest using a monochromatic light source (e.g. a laser). Molecular vibrations in the sample interact with the photons and will cause some of them (indeed only a very small fraction of them) to scatter by gaining or losing energy (inelastically) while most photons are scattered with the same energy (elastically). Photons which are inelastically scattered are recorded with a detector and the Raman spectrum is consequently obtained. Information about the type of bonds and crystal structure can be obtained by analyzing the Raman spectrum. It is, for example, possible to see presence of cation ordering in LNMO (i.e. the Mn/Ni arrangement) using this technique, or to evaluate the degree of ordering qualitatively. Therefore, this technique was used as a complementary technique to neutron diffraction due to its more surface sensitive character (a probing depth of few hundred nanometers) and practical accessibility (Paper III and Paper V). The instrument used was a Raman microscope (Renishaw – inVia) with a laser wavelength of 532 nm. A crystalline Si sample (confirming the reference peak around 520.6 cm^{-1}) was used for calibration. In each acquisition, the measurement time was 20 seconds. Acquisitions were repeated 20 times for better statistics and the nominal power was adjusted to 0.5 mW.

3.3.6. Transmission Electron Microscopy

In transmission electron microscopy (TEM), high energy electrons are used for imaging of very thin samples which are durable under high vacuum. While the basic imaging is similar to an optical light microscope, since electrons with significantly smaller wavelength are used in contrast to visible light, it is possible to reach very high magnifications. In TEM, high energy electrons are projected on the sample coherently using proper magnetic lenses (objective lenses) whereby the electrons interact and pass through it. For this reason, the sample need to be sufficiently thin. After passing the sample, specific lenses are used (intermediate and projection lenses) for the electrons and the sample image is formed on a fluorescent screen (or a CCD camera). With state of the art electron microscopes, it is possible to reach atomic scale resolution and do complementary characterization such as electron diffraction from the areas of interest (selected area electron diffraction, SAED), elemental analysis via energy dispersive spectroscopy (EDS), or analysis of electronic structure via electron energy loss spectroscopy (EELS). In this study, such an electron microscope was used to analyze LNMO samples before and after electrochemical cycling (*Paper V*). For this, some part of the electrodes were scraped off and then dispersed in DMC in the glovebox via ultra-sonication for about 5

minutes. Then, a few drops of the solutions were drop casted onto a molybdenum TEM grid which was transferred to the microscope through a vacuum transfer double-tilt holder.

For in situ TEM experiment, a thin lamella was prepared using a focused ion beam (FIB) technique and this lamella was inserted onto a specific heating stage which allowed the observation of structural and morphological changes in situ during heating up to 600 °C. The microscope was a field-emission FEI Cs-corrected (image corrected) cubed TitanTM microscope operating at 300 kV.

3.3.7. Inductively Coupled Plasma Analysis

In inductively coupled plasma – optical emission spectroscopy (ICP-OES), plasma forming gas (e.g. Ar) is ionized inside a plasma torch surrounded by induction coils. Following ionization, plasma with temperatures as high as 5000-7000 K is formed. The sample to be analysed is sprayed as an aerosol into this high temperature plasma. The sample is atomized at this high temperature, followed by excitation and ionization of atoms present in the sample. At this stage, atoms emit photons and since each element has specific characteristic emission spectrum, it is possible to determine the elements present and their relative concentration by detecting the wavelength and intensity of the emitted photons. In this thesis (*Paper III*), ICP-OES was used for determining the Mn/Ni ratio in the LNMO powders. The instrument used was a PerkinElmer Optima 7300DV spectrometer. LNMO powders were digested in aqua regia, diluted with deionized water and analysed using an internal standard method (scandium) with two point calibration.

3.3.8. Thermal Gravimetric Analysis

In thermal gravimetric analysis (TGA) performed in this thesis (*Paper III and V*), powders were inserted into a Pt pan which was hanged on a very sensitive balance. In the sample chamber, a flow of pure oxygen was maintained. The sample was heated to 780 °C and then cooled back to RT. During this heating/cooling cycle, the weight change of the sample was recorded. This weight change was used to obtain information on oxygen release and recovery of the samples, since no other reactions were expected to cause weight change. The instrument used was a Q500-TGA from TA instruments.

3.3.9. Neutron Diffraction

In diffraction techniques, elastic scattering of radiation (or matter) which have wave character are studied. Following scattering from obstacles in the sample (e.g. atoms), under specific conditions these interactions will lead to constructive interference. As a result, enhanced scattering will be observed in certain

directions while destructive interference will lead to complete or partial cancellation in other directions. Under the conditions giving constructive interference, the scattering of radiation or matter is called diffraction. These conditions require a periodic arrangement of obstacles and constant wavelength parallel beams, and depending on the wavelength and arrangement of these obstacles, constructive interference will occur in certain directions. In *Figure 5*, such a condition is schematically shown. The incoming beam is initially in phase, and for constructive interference they should still be in phase after interaction with the sample. If the interplanar spacing is 'd' and the angle of incoming beam is θ, then the difference between two scattered waves can be written as 2 times dsinθ. If this distance is a multiple of λ, the second wave would still be in phase with the first one and generate constructive interference, i.e. diffraction. This criteria simply leads to Bragg's law as written in equation (3.2):

$$n\lambda = 2d \sin\theta \tag{3.2}$$

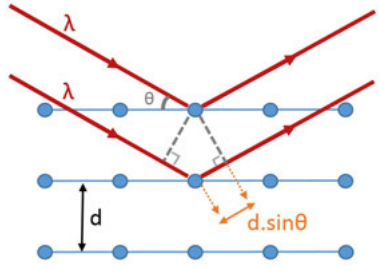

Figure 5. Schematic representation of diffraction from parallel planes separated by an interplanar distance of 'd' and derivation of Bragg's law.

It is possible to determine the crystal structure by analyzing the set of Bragg reflections from different planes (i.e. the diffraction pattern). When X-rays are used for the diffraction, X-rays will be scattered from the electrons around the nuclei. However, the scattering powers of Mn and Ni are quite similar with X-rays, and therefore cation ordering of Mn and Ni in LNMO are almost impossible to detect when X-rays are used for the diffraction. On the other hand, when neutrons are used for the diffraction, superlattice reflections originating from Mn/Ni ordering will easily be seen. This is because neutrons are scattered from nuclei of atoms in the sample instead of the electrons, and the scattering powers of Mn and Ni are then quite different.

As discussed in the introduction, Mn/Ni ordering is known to affect electrochemical performance and the mechanisms behind the improvements from cation disordering are still not well understood. For these reasons, crystal

structure analysis was made using neutron diffraction (ND) in this thesis (*Paper III*). In situ neutron diffraction experiment (during heating under oxygen atmosphere) was performed on the POLARIS medium resolution time-of-flight (TOF) powder diffractometer at the ISIS spallation neutron source, Rutherford Appleton Laboratory, UK [120]. A special stainless steel reaction cell which allows gas flow through the sample was used in the experiment. Pipes used for the gas flow had a coiled shape before the reaction cell so that the gas would reach equilibrium with the furnace temperature before entering the reaction cell. A disordered LNMO sample was used as the starting powder (around 2 grams). 257 patterns were collected in total (5 minutes for each pattern). Sequential Rietveld refinement was performed on those patterns using GSAS [121] with the interface EXPGUI [122] and cation mixing was allowed for the $P4_332$ structure during refinements.

For the ex situ characterization of heat treated LNMO powders, ND was performed using a (1.555 Å) powder neutron diffractometer PUS at the JEEP II reactor, Norway. These measurements were done at room temperature.

4. Results and Discussion

4.1. Fluoroethylene Carbonate as Electrolyte Additive

The function of fluoroethylene carbonate (FEC) in full cells is usually correlated to improvements regarding anode performance (e.g. silicon electrodes) [123,124]. It is important that the additives intended to modify the anode performance should not cause side reactions affecting the cathode in a negative way, and it is therefore sensible to investigate the effect of FEC for high voltage cathode materials. In the case of LNMO, there is no consensus in literature regarding its effect, when used as an additive or co-solvent. FEC has been reported to have negative [125], neutral [126], [107] and positive effects [88] on LNMO. A previous dedicated study focusing on its effect on LNMO (studied in half cells) reported FEC to provide better passivation [127].

It is not easy to correlate the electrochemical behaviour in a cell to an individual electrode, since the additive can affect both electrodes. Additionally, even though half cells are often considered as an 'ideal' cell configuration to get information from only the electrode of interest, this is based on an assumption of a 'stable' lithium negative electrode. This might, however, not be valid, especially at high current rates [128]. It is possible that the impedance rise due to Li metal electrode can cause cell failure and electrolyte additives such as FEC can mitigate this impedance contribution [129,130]. Also, cyclable lithium loss can play an important role when determining cell life time in full cells, but this type of mechanism is not observable in half cells due to the unlimited lithium inventory provided by the lithium metal. Therefore, testing of electrolyte additives in full cells has advantages. For this purpose, the *LNMO-LTO system* was chosen in *Paper I* to study the effect of FEC, as it can be considered a comparatively less complex system due to the high operating anode potential, and can therefore provide useful information regarding the use of this additive on the cathode side. Three electrolytes were tested with FEC concentrations 0, 1 and 5 wt%. The galvanostatic cycling results of the three resulting cells (cycled at C/5 rate - 30 ºC) are shown in *Figure 6*.

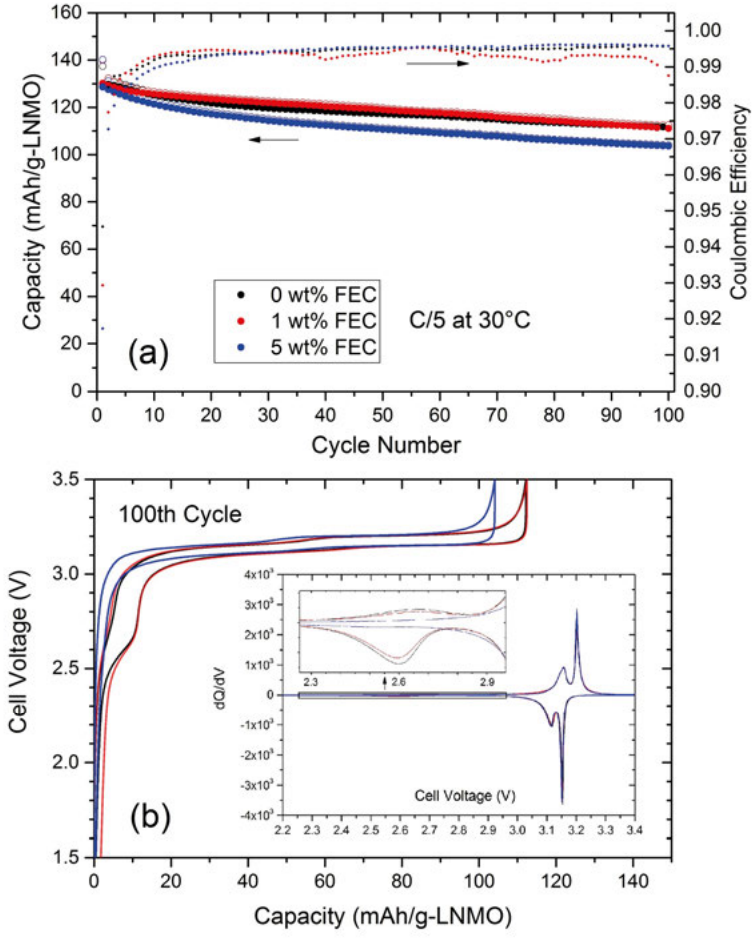

Figure 6. Galvanostatic cycling results of LNMO-LTO cells with 0, 1 and 5 wt% FEC in the electrolyte (a). The voltage curves of those cells during the 100th cycle (b) with the inset showing 'dQ/dV vs. capacity' for the same data. From *Paper I*.

It is seen from *Figure 6a* that the capacity fades noticeably in the cell with high FEC content (5 wt%). The cells with 0 and 1 wt% FEC perform quite similarly over 100 cycles. The coulombic efficiencies start to stabilize and reach a value above 0.99 after ten initial cycles, however, the 5 wt% FEC sample showed a lower efficiency at the beginning. These observations indicate that there is not any significant improvement from FEC, and especially during the initial cycles, the 5 wt% FEC containing electrolyte likely generates more side reactions. Electrolyte oxidation and related transition metal dissolution, migration of side reaction products from cathode to the anode, lithium inventory loss in the full cell and increase of cell resistance are possible reasons for the fading of these cells. In order to get more insight about the capacity difference caused by FEC, the voltage curves during the 100th cycle are

shown in *Figure 6b*. Here, it is seen that the voltage curves are quite similar except for at the beginning of charging. The low voltage plateau around 2.6 V seems to disappear for the FEC containing samples while the rest of the profile is almost identical. For a better visualization, dQ/dV vs. capacity curves are shown in the inset. It is seen that the higher voltage peaks are matching perfectly for all cells, which indicates that they are not subject to kinetic limitations at this rate. Possibly, they have comparable internal resistances and there is no significant electrode degradation. The difference of capacity originates from the absence of the low voltage plateau which indicates that the capacity difference is primarily due to loss in lithium inventory.

4.1.2. Surface Characterization of LNMO

Surface characterization of LNMO electrodes after the 1st and 100th cycles are shown in *Figure 7* for O 1s and C 1s together with pristine electrodes (prior to electrolyte contact), since the main differences in the XPS measurements were observed for these spectra. For the C 1s spectrum, the most intense peak is assigned to carbon black positioned at 284.5 eV while a smaller contribution at 285 eV is due to hydrocarbons. For clarity, all peaks originating from the binder have been colored green. The remaining peaks at 288.3 eV and 286.8 eV correlate to binding energies of C=O and C-O related species, respectively. These are assigned to adsorbed species on the pristine electrode. For the O 1s spectrum, the peak at 529.8 eV is due to metal oxides from LNMO. The other two peaks at higher binding energies were similarly assigned to adsorbed species on the active material surface.

After one cycle, the C 1s spectra of all samples look quite similar except for a shift of the binder related peaks to lower energies (0.4-0.5 eV). In the O 1s spectra, the metal oxide peak intensity at 529.8 eV decreases slightly with increasing amounts of FEC, implying a thicker surface layer. After 100 cycles, with increasing amounts of FEC, carbon black peaks and binder related peaks decrease in intensity. On the other hand, the C-O and C=O related peaks increase in intensity due to deposition of species on the surface. It is easier to see in the O 1s spectra that the C-O related peak increases profoundly with increasing FEC contents. This can originate from the presence of organic ethers such as poly(ethylene oxide), PEO. In all cases, the surface layer formed is seen to be thin, but FEC seems to promote relatively thicker layers.

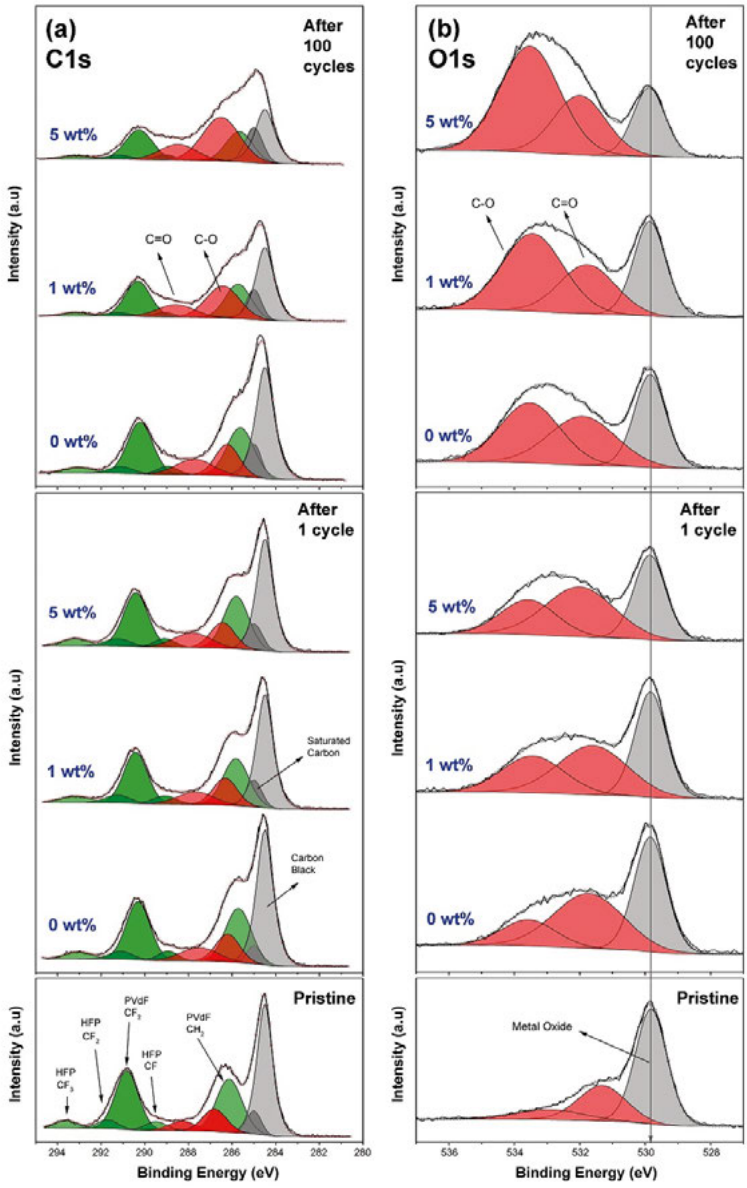

Figure 7. XPS results of LNMO electrodes for C 1s (a) and O 1s (b) after cycling at C/5 rate and 30 °C together with the spectra of pristine electrodes. From *Paper I.*

4.1.3. Effect of Temperature

As a complementary test, a set of LNMO-LTO cells with 0, 1 and 5 wt% FEC were tested at C/5 rate and at room temperature for 100 cycles. These cells were cycled further at 55 ºC for another 100 cycles in order to see if the addition of FEC has any positive effect at the elevated temperature. The results are shown in *Figure 8*. It clearly shows that there is no beneficial effect of the FEC additive at elevated temperature and all cells faded very rapidly, and actually worse for FEC containing cells. This also shows how temperature dramatically changes the fading rate of such full cells which is well beyond the expectation from a simple Arrhenius type behaviour.

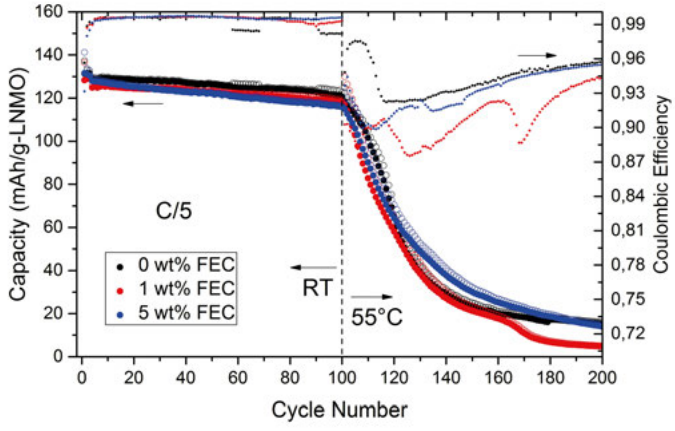

Figure 8. Galvanostatic cycling (C/5 rate) of 0, 1 and 5 wt% FEC added cells at room temperature and subsequently at 55 ºC. From *Paper I.*

4.1.4. Electrode Interactions

In order to investigate if there exists any 'cross-talk' between the LNMO and LTO electrodes and to see how these interactions are affected by the presence of FEC, XPS analysis was also performed on the LTO electrodes. The Mn 2p and Ni 2p spectra of the LTO electrodes were taken from the same full cells used for LNMO surface characterization. It is seen in *Figure 9* that even after 1 cycle (10 hours at OCV and 10 hours of cycling), Mn and Ni peaks are easily observed on the LTO electrodes. The relative intensities of the peaks were similar for all samples irrespective of FEC content in the electrolyte. It is interesting to see that the Mn intensity was approximately the same after 1 and 100 cycles, and its concentration was estimated to be below 1 at%. The relative amount of Ni instead increased slightly with cycling.

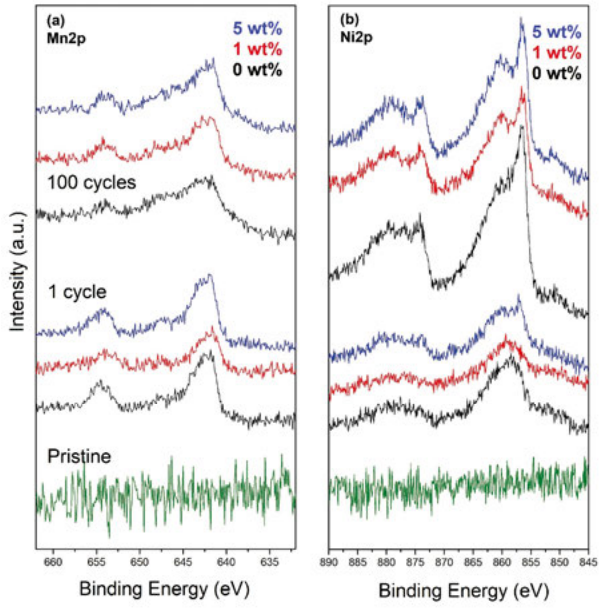

Figure 9. XPS spectra of LTO electrodes for Mn 2p (a) and Ni 2p (b) after 1 and 100 cycles (discharged state) with the spectra of pristine electrodes. From *Paper I*.

4.2. Understanding the Failure Mechanisms

Paper I showed that 5 wt% FEC caused an additional decrease in lithium inventory of the cell, and moreover that deposited metal ions on the anode indicated that there is electrochemical cross-talk which is likely correlated to the observed capacity fading of the cells. Independent of the FEC additive, a rapid fading at elevated temperature could also be observed, which did not seem to follow an Arrhenius-type trend. These observations called for further investigations of the different capacity fading mechanisms occurring in LNMO-LTO full cells.

Therefore, in *Paper II*, the change in internal resistance with respect to LNMO and LTO electrodes during cycling was analyzed, and how the electrode interactions effect the cyclable lithium loss was investigated. This was achieved by employing different electrochemical techniques as well as ex situ characterization of the electrodes. In parallel, the background to the good cycling stability observed at room temperature in LNMO-LTO cells, and the rapid capacity fading present at elevated temperature (55 ºC), were explored.

4.2.1. Performance of LNMO-LTO Cells: RT vs. 55 ºC

As seen in *Figure 10*, the performance of LNMO-LTO full cells cycled at room temperature showed quite stable cycling, while the fading was quite fast at 55 ºC. After 50 cycles, a final cycle at C/20 rate showed very limited improvement in the capacity, indicating that the cell resistance only had a small effect on the capacity. When the first and the 50th cycles are compared, a partial disappearance of the low voltage plateau was visible for the 55 ºC sample. This indicates that there is a decrease in the cyclable lithium amount. The coulombic efficiency reached around 0.997 at the 20th cycle (RT) while it was around 0.98 for the 55 ºC cell. If the final cycle is considered, it is seen that coulombic efficiency is time-dependent. An improvement in cycling performance compared to *Paper I* was observed after increasing the volume in the pouch cell for evolving gases, indicating that the very fast fading at 55 °C is partly due to cell design and evolving gases. However, even after these improvements, the fading rate is still quite rapid.

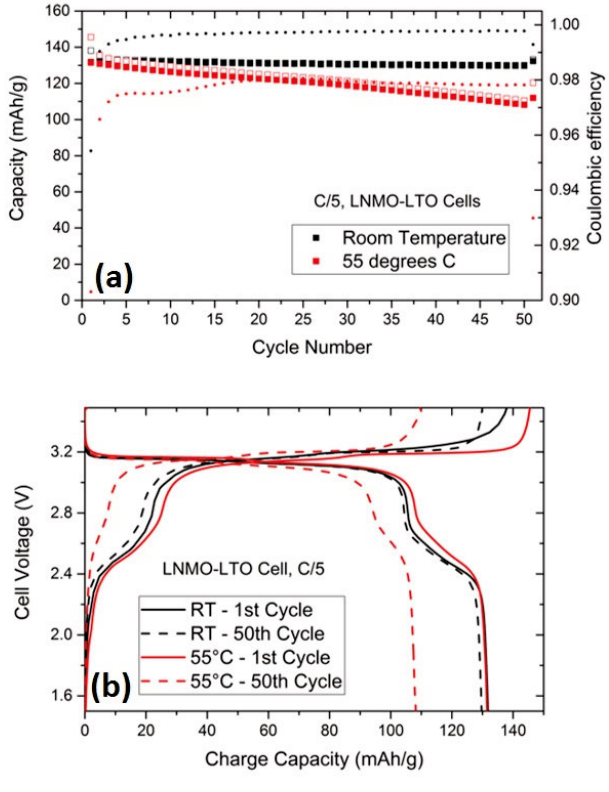

Figure 10. (a) Cycling of LNMO-LTO cells at RT and 55 °C. Small symbols are used for coulombic efficiency (right axis). (b) Selected voltage curves from the same cell. From *Paper II*.

4.2.2. Back-to-Back Cells vs. 3-Electrode Cells

Pseudo full cells, or back-to-back cells, were constructed by connecting one LNMO half cell to an LTO half cell through the negative poles, as suggested in reference [67]. This renders cross-talk impossible. Cycling was performed with short-duration intermittent current interruption technique to follow individual cell resistances. The cycling at room temperature, 40 and 55 ºC are shown in *Figure 11a*. When compared to *Figure 10*, the capacity fading is much faster. However, the effect of temperature on fading rate is not as large as in regular cells.

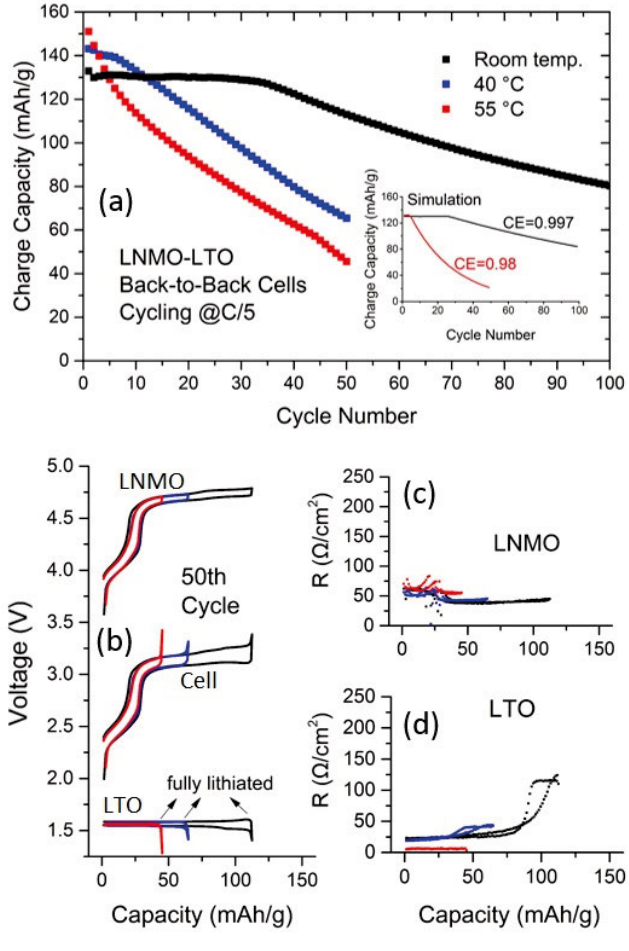

Figure 11. (a) Cycling in back-to-back cells at different temperatures. (b) Individual voltage curves in the 50th cycle together with resistance measurements for the same cycle for LNMO (c) and LTO (d). From *Paper II*.

Individual voltage curves and internal resistances for both electrodes are shown in *Figure 11b-d.* It is clear from these voltage curves that the cycling window of the LNMO electrode becomes limited to the higher lithiation states, and that this is more severe at higher temperature. From the voltage jumps observed for LTO at the end of charging, it is seen that LTO limits the capacity. This is expected if there is an increase in lithium inventory. Stable cycling at the beginning is due to excess capacity of LTO, which can compensate the increase in lithium inventory for a limited amount of time.

The internal resistance of LNMO and LTO sides show that neither resistances reach any high levels. Also, the effect of temperature on the resistance increase is limited. As a comparison to those cells, 3-electrode cells were prepared and cycled in a similar way. In this configuration, cross-talk is allowed between the electrodes. The results from these cells are shown in *Figure 12*. One clear difference is that the fading is slower compared to back-to-back cells, especially at room temperature it is seen that the 3-electrode cells perform very well.

As the back-to-back cells showed, there are severe side reactions on LNMO as compared to LTO. At first sight, from *Figure 12a*, one could believe that the rate of side reactions is slower in those full cells. However, if the rate of side reactions on LNMO is independent of cell configuration, then cross-talk can explain the observed behaviour. If migration of reaction products to LTO cause additional side reactions there, this would help to maintain the overall lithium inventory and reduce the capacity fading rate. This is because reduction reactions on LTO would decrease the Li inventory, in contrast to oxidation reactions on LNMO which would result in an increase in Li inventory. Therefore, if reactions occur to similar degree in terms of number of electrons involved, the overall change in Li inventory would be minimal due to counterbalancing effects. Therefore, a closer examination of voltage curves is necessary to determine which side is dominating the observed capacity fading.

In *Figure 12b*, voltage curves from the 50^{th} cycle is shown. Here, the cycling window is being limited to the lower LNMO lithiation states as the cycling proceeds. Moreover, the LTO voltage curve shows that the electrode returns to its fully de-lithiated state after discharging. This clearly shows that the capacity fading is due to a decrease in lithium inventory. This is only possible if more severe side reactions are occurring on the LTO electrode as a result of cross-talk of species originating from the LNMO electrode.

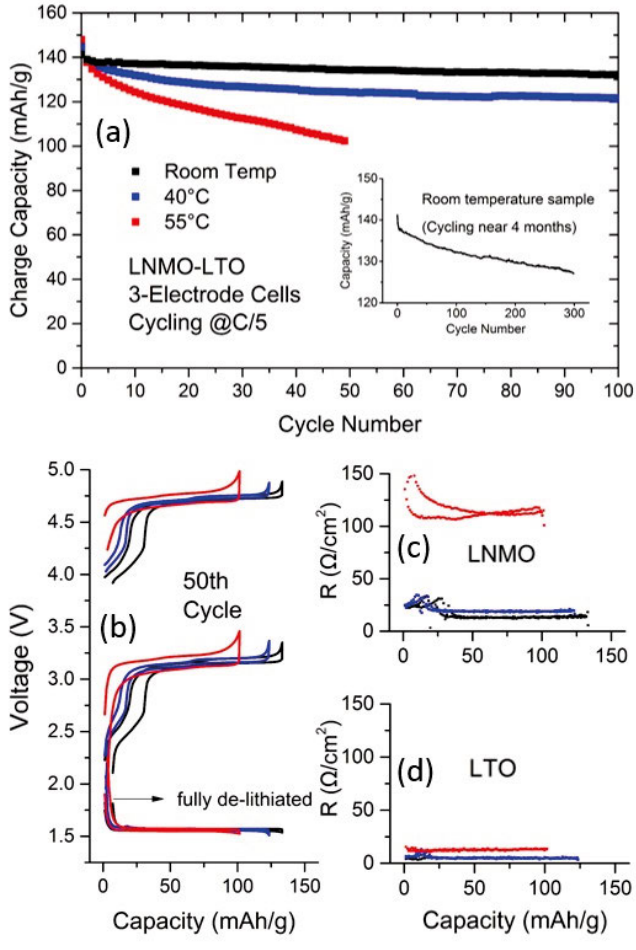

Figure 12. Cycling in 3-electrode cells at different temperatures (a). Individual voltage curves in 50th cycle (b) together with resistance measurements for the same cycle for LNMO (c) and LTO (d). From *Paper II*.

It is observed from resistance measurements (*Figure 12c-d*) that the contribution to overall cell resistance is smaller for LTO as compared to LNMO. At 55 ºC, this difference is higher, and most of the contribution comes from the LNMO electrode. In all cases, however, the resistances are not high enough to influence the cell behaviour significantly. Internal cell resistance might start to play a major role later in the cycling, near the cell break-down point, but it is seen that significant capacity losses occur earlier due to cyclable lithium loss. At elevated temperature, either new reactions (involving more electrons) on LTO become thermodynamically favorable, or the kinetics of cross-talk (e.g. migration of protic species or transition metals) is faster, or both. Testing of a modified back-to-back cell (allowing gas interactions but blocking electrolyte contact between two compartments) indicated that cross-talk affects

the capacity fading mainly due to migration of species soluble in the electrolyte (see *Paper II*). In either of these cases, it is clear that LTO's efficiency is more sensitive to temperature and this explains the unexpectedly large changes in the fading rate with increasing temperature.

4.2.3. Surface Characterization: RT vs. 55 ºC

For LNMO surfaces, no clear differences between pristine and cycled samples were observed in the SEM analysis (see *Paper II*). However, XPS analysis showed the presence of thin surface layers formed on LNMO (see *Figure 13*). The main difference after cycling is seen on C-O and C=O related surface species for both temperatures. When the surfaces are compared after cycling at two temperatures, the intensity of those peaks seem to be higher at 55 ºC. In the O 1s spectra, no considerable increase in the corresponding energy region for these species could be observed, indicating a possibly more favorable surface layer deposition on the carbon black and binder surfaces at 55 ºC (see also *Figure 13c* for atomic percentage changes) . The observation of intense metal oxide peaks indicate that there is no thick layers formed on the active material surface either at RT or at 55 ºC.

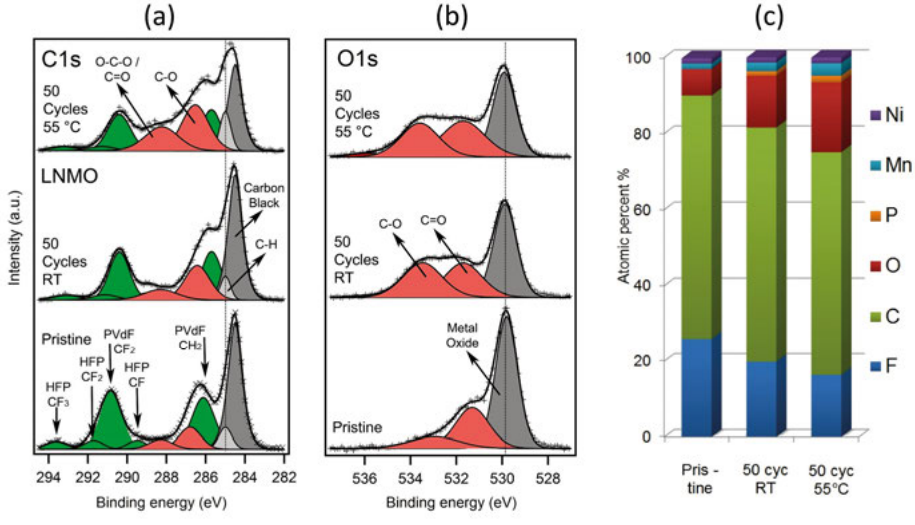

Figure 13. (a) C 1s and (b) O 1s XPS spectra of pristine and cycled LNMO electrodes. (c) Atomic percentages of elements in pristine and cycled electrodes. From *Paper II*.

In the case of LTO, the surface layers were surprisingly thicker as compared to LNMO surfaces (see *Figure 14)*. In fact, as seen in the O 1s spectra, it was not possible to see metal oxide peaks after cycling when in-house XPS was used for analysis (1486.6 eV), and therefore analysis with hard X-rays (2005

eV, 6015 eV) were performed on the same electrodes. In the C 1s spectra, an increase related to C-O species is observed after cycling while the intensity of the C-C peak decreases. Peaks related to C=O species also appear. If different photon energies are compared, it is seen that the organic components of the film decrease in intensity with increasing excitation energies. After room temperature cycling, a large contribution is still visible at 284 eV, but it rapidly decreases with lower excitation energies. This suggest that relatively thick surface layers are present. For the 55 ºC sample, even at 6015 eV, there is not a significant contribution from carbon additives which indicates that an even thicker SEI is formed after cycling at 55 ºC.

In the O 1s spectra, similar trends are observed. However, the main peak due to surface species becomes broader at 55 ºC, indicating compositional changes. Such changes can be due salt decomposition products (e.g. $Li_xPF_yO_z$) and C-O/C=O contributions from carboxylates. The relative intensities of the surface peaks to the metal-oxide peak can be used to estimate film thickness. For O 1s spectra, the probing depths can be estimated as 9, 14 and 40 nm for incoming photon energies of 1486.6, 2005 and 6015 eV, respectively. Therefore, it can be concluded that the film thickness is between 9-14 nm for RT and above 14 nm for the 55 ºC sample (see *Paper II* for further discussion).

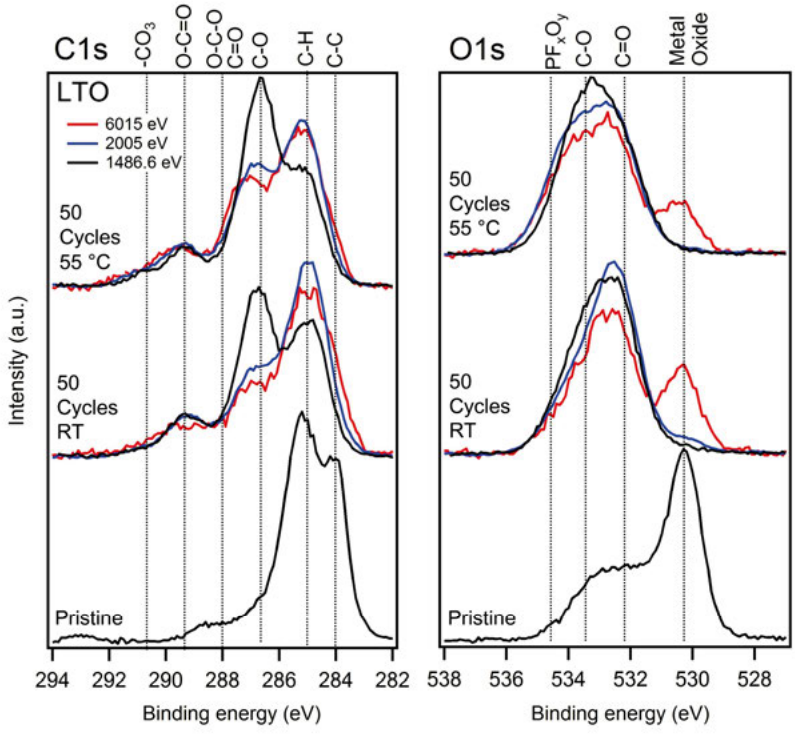

Figure 14. C 1s and O 1s spectra obtained at different photon energies (1486.6, 2005 and 6015 eV) for pristine and cycled (50 cycles at RT and 55 ºC) LTO samples. From *Paper II*.

These observations show that the layers formed on LNMO are relatively thin, while they are unexpectedly thick on LTO electrodes. If the internal resistance measurements are considered, one would expect thinner layers on LTO, as it did not show any major contribution to the cell resistance. This suggests that even if thicker layers are formed on the LTO electrode, these are ionically conductive and do not contribute significantly to the resistance. The increased SEI thickness on LTO at 55 ºC also supports the findings of 3-electrode measurements in the way that this is an indication of enhanced reactions occurring on LTO following cross-talk.

The deposition of transition metal ions on the anode (migrating from LNMO) was shown in *Paper I*, but it was then not possible to determine oxidation state of these metal ions through the XPS spectra. This is a well-known example of cross-talk, and it can also play a role in capacity fading. One possibility is that the metal cations are reduced on the anode to their metallic states, which would decrease the lithium inventory from anode. In order to determine the oxidation states of transition metal ions observed on LTO, XANES measurements have been performed. The results are shown in *Figure 15* and show the Mn oxidation state near to be +III and the Ni state near to be +II. This confirms that metal ion deposition on the LTO is not a direct cause for the capacity loss. However, the dissolved transition metal ions can still effect the capacity loss indirectly by being involved in the reduction reactions (e.g. by SEI film damage, catalytic effects, etc.) occurring on the LTO surface.

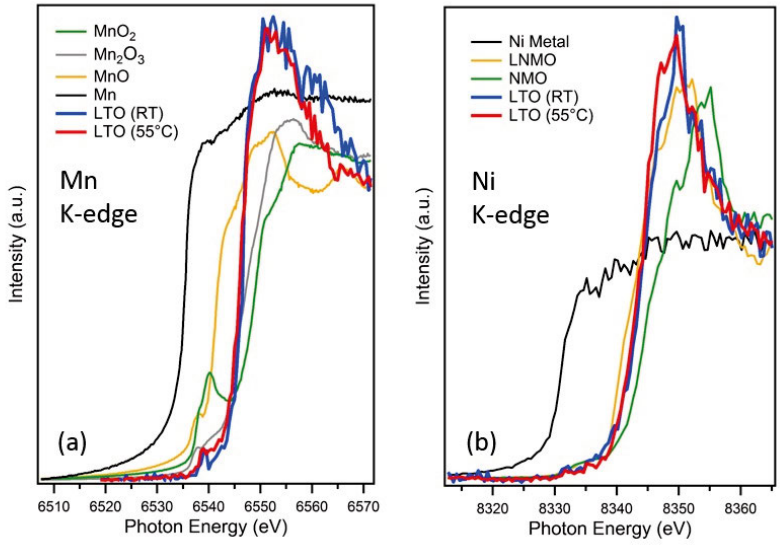

Figure 15. XANES measurements of cycled LTO samples (RT and 55 ˚C) together with reference samples. From *Paper II*.

4.3. In situ Studies of LNMO During Heating

The $LiNi_{0.5}Mn_{1.5}O_4$ spinel material adapts a $P4_332$ space group under ideal conditions, as this is the more thermodynamically stable structure at room temperature. During heating, oxygen release starts at temperatures about 700-730 ºC. A relationship between oxygen release and disordering has been suggested since the same temperature region yields cation disordering as observed from ex situ analyzed samples [29]. Apart from the cation disordering, heating to high temperatures—and accompanying oxygen release—are also known to effect oxygen stoichiometry [20,31], phase transformations from spinel to the rock-salt phases [31,33] and particle morphology [43,131,132]. Therefore, it is important to study this spinel material via in situ techniques as more insights can be gained on mechanisms and dynamics of material property changes. In situ ND and TEM studies were used for this purpose.

4.3.1. In situ Neutron Diffraction During Heating

As mentioned above, a direct relation between disordering and the oxygen release is believed to exist. If this is true, it would make it harder to determine the individual role of disordering on the electrochemical performance since it will not be possible to obtain suitable samples allowing to de-couple these two properties. In *Paper III*, in situ ND was used to follow ordering transitions during the heating/cooling of LNMO powders. Despite the large number of studies on ordering–disordering on LNMO, there have previously been only two important studies which have investigated ordering in situ with ND: one heating powders under vacuum [30] and another under air [22]. In *Paper III*, in situ heating/cooling characterization of slightly Mn-rich LNMO under pure oxygen atmosphere was performed. Increasing oxygen partial pressure is expected to shift the onset of oxygen release to higher temperatures. Thus, it can be tested if there is a direct relation between oxygen release and cation disordering, because the ordering–disordering transition temperature (T_{O-D}) would then shift accordingly. Mn-rich LNMO (Mn/Ni = 3.5) was also chosen to ensure that there was always some Mn^{3+} present in the structure, since the Mn/Ni ratio can deviate from the starting ratio of 3. This would also reduce the tendency towards rock-salt phase formation [31] and render the experiment less complex against further Mn/Ni ratio changes. Before the neutron diffraction experiment, a TGA analysis was made under similar conditions in order to confirm the shift of the oxygen release temperature (see *Figure 16*). It is seen that switching from air to pure oxygen atmosphere shifts the oxygen release temperature about 40 ºC.

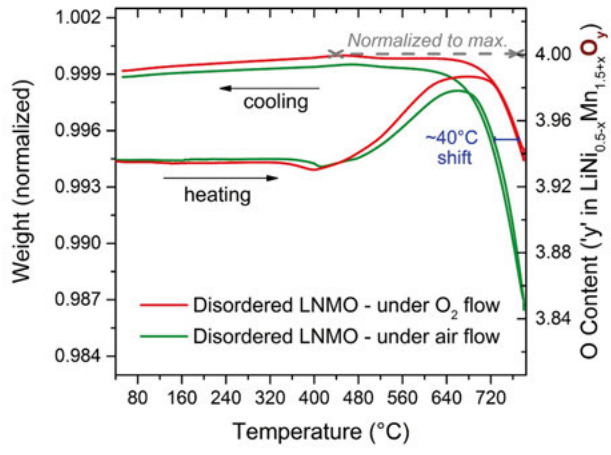

Figure 16. TGA analysis of disordered LNMO under oxygen or air. Right y-axis shows the corresponding oxygen stoichiometry with the assumption that the maximum point in the cooling curve is oxygen non-deficient. From *Paper III*.

In situ ND experiments were conducted under similar conditions. If there is a direct relationship between oxygen release and cation disordering, disordering would be expected to start around 725-730 ºC which is the temperature for oxygen release as observed in TGA analysis. Contour plot showing ND data is given in *Figure 17* together with the temperature profile given on the right-hand side of the plot.

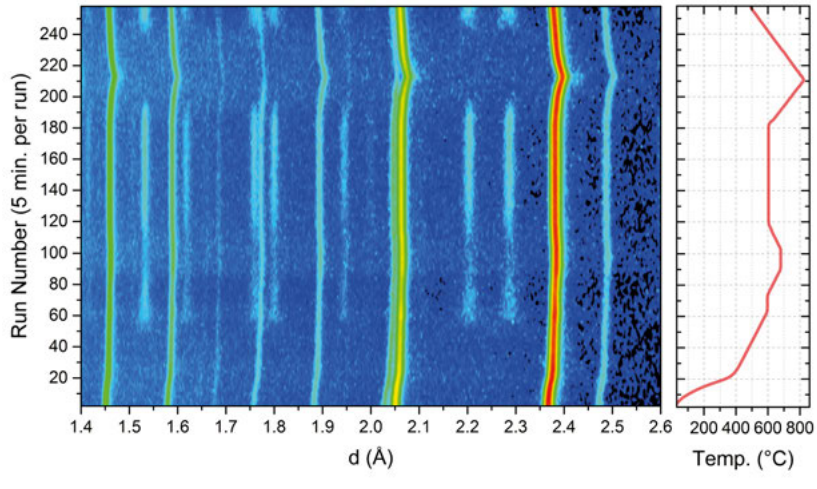

Figure 17. Neutron diffraction data of disordered LNMO powders under pure oxygen (atmospheric pressure). The intensity values are in arbitrary units. *From* Paper III.

As seen in *Figure 17*, additional peaks originating from ordering start to appear around run number 50. Later, at certain temperatures, these peaks disappear and re-appear again. Except for small peaks from the collimating mask at 1.76 Å and 2.03 Å, all other peaks belong to the spinel phase with no visible rock-salt phase formation. This shows that the pure oxygen atmosphere together with excess Mn in the structure delay the rock-salt phase formation temperature, since rock-salt phase formation was observed at lower temperatures (e.g. 750 ºC) for under air heating [22].

Sequential Rietveld refinement was performed on the neutron diffraction data (257 patterns in total). Here, the $P4_332$ model with a fixed Mn:Ni ratio of 0.78:0.22 (since no rock-salt phase was observed) was used and cation mixing was allowed to change. Li occupancy was fixed to 1. Attempts to refine the O occupancy were also made, however, these were not accurate enough to determine the small amount of changes that could be expected from the TGA measurement, and the O occupancy was therefore also fixed to 1. The Ni-4a site is the preferred site for Ni in the ordered phase, and its occupancy can thus be used to quantify the degree of ordering (i.e. Mn/Ni mixing). The results from the refinements are shown in *Figure 18*.

As seen in *Figure 18*, a sharp increase in Ni-4a occupancy starts around 530 ºC, and continues to increase until 630 ºC where the trend changes and disordering starts. However, no oxygen release was observed until 725-730 ºC. Therefore, it can be concluded that cation disordering is not initiated by oxygen release. During the experiment, isothermal steps were added. This shows that there is not a specific transition temperature for the ordering–disordering transition. Instead, the ordering degree changes gradually with temperature, indicating a second-order transformation (similar to the ordering transition observed in beta-brass; CuZn) [133,134].

An attempt to get information about the possible chemical changes was made by following the trends in lattice parameter changes (see *Figure 18b*). A deflection towards lower values are observed around 460 ºC with the oxygen recovery, as is expected from the reduction of the large Mn^{3+} ions. Above 730 ºC, a larger increase in the rate of cell expansion occurs, which is in accordance with the considerable oxygen release at these temperatures. While these trends are not highly conclusive, since no rock-salt phase was observed in temperatures below 800 ºC, it can still be speculated that oxygen vacancies cause the higher lattice constants.

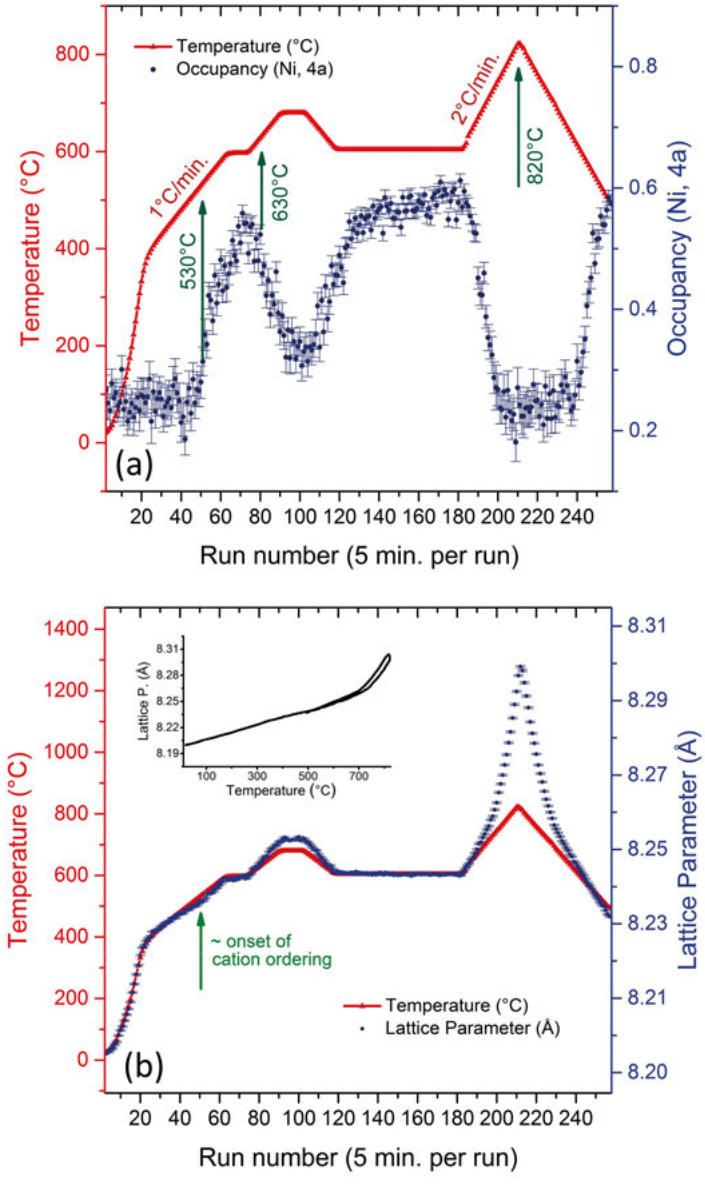

Figure 18. Results from Rietveld refinements. (a) Change of Ni-4a occupancy with temperature. (b) The change of lattice parameter with temperature. For easier evaluation, y-left and y-right axes are scaled so that the lines initially overlap completely. From *Paper III*.

In summary, this shows that oxygen release has no direct role in starting the cation disordering in LNMO. This shows that it is possible to obtain samples with varying degrees of ordering without changing the oxygen content under

suitable conditions. Also, when comparing with work by Cai et al. [22], a decrease in the ordering–disordering temperature is observed, which can be due to the excess Mn. The presence of Mn^{3+} can lower the tendency for ordering, but ordering is still possible to obtain [135]. Therefore, if the oxygen release and disordering temperatures are close to each other, oxygen release could initiate disordering as this also introduces Mn^{3+} into structure. Moreover, according to theoretical calculations [136], the formation of oxygen vacancies could lower the energy of the disordered phase and reduce the thermodynamical driving force for keeping ordering at high temperature. This would also initiate disordering. However, as results in *Paper III* show, if the disordering temperature is made lower than the oxygen release temperature (e.g. by increasing Mn/Ni ratio and oxygen partial pressure), a temperature zone is created in which cation ordering is possible without oxygen deficiency. This opens new possibilities to obtain a suitable set of samples to study the individual effects of ordering vs. oxygen release on the electrochemical performance, and thus allows to design electrode materials with optimum properties.

4.3.2. In situ TEM Analysis During Heating

While diffraction techniques give an average information on the structure, real time in situ microscopy techniques render it possible to obtain more local information on structural changes. In this part, in situ heating of ordered LNMO samples was studied with TEM. Using a FIB technique, a thin cross-section sample was prepared from micron sized LNMO particles and these particles were put onto a heater chip in a TEM chamber. In situ TEM images obtained at 250 and 400 ºC are shown in *Figure 19*.

As seen in *Figure 19a*, ordering in LNMO is well retained until 250 ºC. This is easily seen from the additional superlattice spots in the FFT image (given as inset). As the temperature increases to 400 ºC, disordering as well as structural transitions to rock-salt like phases occur (*Figure 19b*). These temperatures are significantly lower as compared to previous reports [30]. This can be explained by the ultra-high vacuum in the TEM chamber, effects of beam damage, and that small particles were selected, which would all increase the rate of oxygen release. It is seen that structural changes occur heterogeneously and small domains with ordering character remains while rock-salt like phases are formed in other regions. In *Figure 20*, EDS maps of the same region are shown after a short time annealing at different temperatures. It is seen that Ni and Mn become separated from each other over time and increasing temperature, forming Mn-rich and Ni-rich flake-like regions.

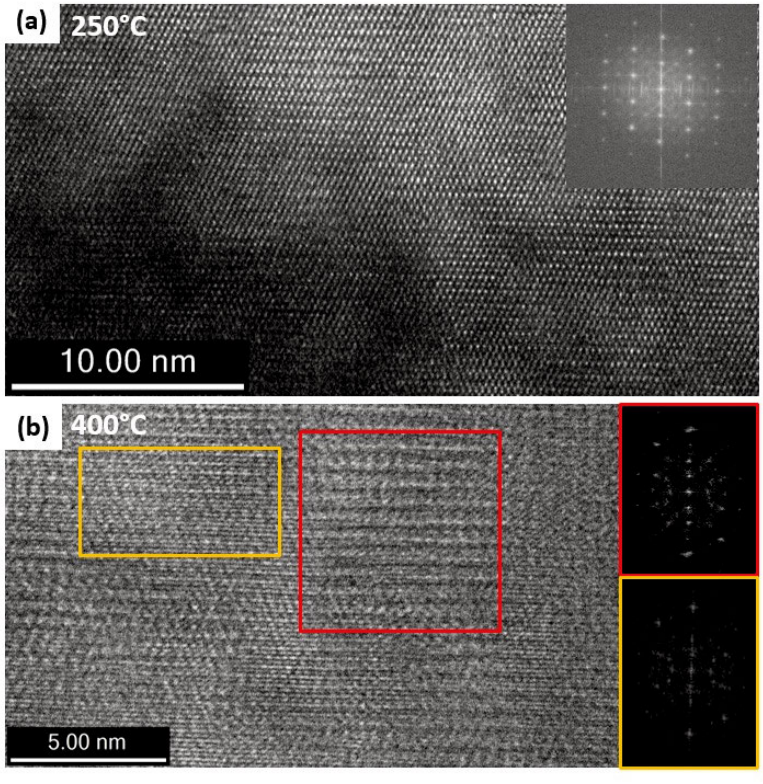

Figure 19. In situ TEM images from 250 ºC (a) and 400 ºC (b). As the temperature rises to 400 ºC, ordering disappears and rock-salt like phases start to form. Insets show the corresponding FFT images.

In *Figure 20*, as seen from the 500 ºC image, Ni first prefers to occupy high energy grain boundaries. A gradual increase of black regions also indicate that oxygen release occurs over particles and causes material erosion from the particle surface. Rock-salt impurities are usually Ni-rich phases, and thus likely the origin of the bright regions in the Ni maps. This shows how ordered domains co-exist with disordered and rock-salt like phases at specific temperatures. The microstructural evolution of Mn- and Ni-rich phases are observed dynamically in a LNMO particle following heating and oxygen release, which is likely useful when understanding the electrochemical performance of LNMO powders exposed to high temperatures and oxygen loss.

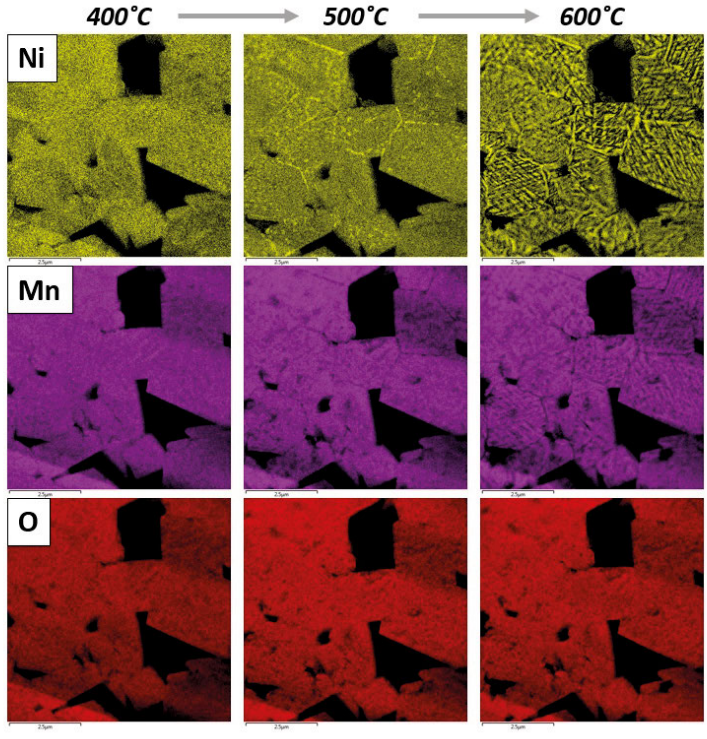

Figure 20. EDS results of LNMO samples heated to different temperatures for Ni, Mn and O. Measurements were done at RT after heating to desired temperature.

4.4. Understanding the Effect of Cation Ordering

In *Paper IV* and *V*, the focus was to understand individual effect of ordering on the electrochemical performance by isolating the effect of other material properties which inevitably appear from conventional sample preparation. The experimental approach relied on obtaining samples with different ordering degree but having other material properties, e.g. oxygen content, fixed. Preparation of such samples are possible with specific heat treatment conditions as seen in *Paper III*.

4.4.1. Preparation of Ordered and Disordered LNMO

LNMO powders were subjected to identical thermal treatments under pure oxygen atmosphere. The final step during heat treatment was an annealing period at 710 ºC. Under these conditions, as shown in the in situ ND experiment, the samples should be oxygen non-deficient but having disordered structures. Therefore, following the annealing at 710 ºC, quenching or slow-

cooling were performed to obtain disordered and ordered samples, respectively. The synthesized powders were analyzed using Raman spectroscopy to confirm if ordered and disordered phases were prepared successfully; the results are shown with reference samples with varying degrees of ordering (*Paper III)* in *Figure 21*a. A comparison shows that the preparation approach was successful since ordered and disordered samples were in good agreement with references.

It was also necessary to verify that no oxygen release occurred during sample preparation. This was done via TGA analysis under pure oxygen flow during a heating and cooling cycle. It is seen that both samples are oxygen non-deficient and have identical oxygen contents (see *Figure 21*b). For reference purposes, the same test was done for a disordered sample prepared conventionally (annealed at 800 ºC under air and then rapidly cooled). It was then verified that ordered and disordered samples were successfully prepared with the same oxygen content and with minimal differences in its preparation route.

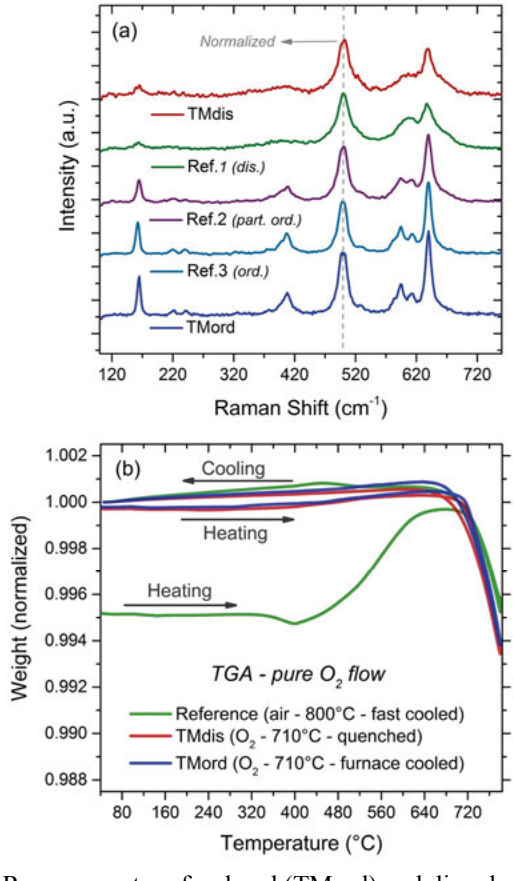

Figure 21. (a) Raman spectra of ordered (TMord) and disordered (TMdis) samples. (b) TGA analysis of ordered and disordered samples under oxygen atmosphere. From *Paper V*.

4.4.2 Electrochemical Performance

The electrochemical performance of ordered (TMord) and disordered (TMdis) LNMO samples were tested in full cells with LTO counter electrodes. Since the capacity fading is much faster at elevated temperature, testing was performed at 55 ºC. In the first part of the testing, cycling was started with galvanostatic cycling at C/2 charge and 10 C discharge rates (see *Figure 22*). Slow charging and fast discharging were chosen to investigate intrinsic rate capabilities of samples, because side reactions are expected to be more severe during charging. After 40 cycles, the cycling approach was changed. This time, both charge and discharge rates were C/2, however, a potentiostatic step was added for 2 hours at the end of charging (followed by additional 2 hours waiting step at OCV). The purpose was to observe how the stability varied between samples when they were kept in the delithiated state.

The results of electrochemical testing are shown in *Figure 22*. Initially, even at a discharge rate of 10 C, capacities around 110-120 mAh/g were obtained for all samples. In *Figure 22b*, individual voltage curves are shown for both samples. During charge (C/2), some differences are observed in the low voltage region and these can easily be seen as distinct peaks in the differential capacity plots (*Figure 22*c). The appearance of two distinct peaks in this region is due to cation ordering, since both samples have the same oxygen content.

It is important to note that both samples have similar capacities when discharged at 10 C rate (*Figure 22*b). Even though some extra overpotential is visible at the higher rate for the ordered sample, the similarity in capacity at such a rate indicates that the difference in rate capabilities are insignificant. However, with increasing cycle numbers, the ordered samples show a gradual decrease in rate performance. In the second part, lowering of rate to C/2 increases the capacities to the same level for all cells. As expected from the CV steps, cyclable lithium loss dominates the capacity fading in this region and is also accompanied by an impedance rise in the cells. This impedance rise occurs more significantly for the ordered sample, as can be concluded from *Figure 22f*. These results clearly show that cation (Mn/Ni) disordering in LNMO samples indeed mitigates the impedance growth during cycling without causing any considerable difference in terms of the side reactions, as the cyclable Li losses were similar and the samples had the same oxygen content and morphology.

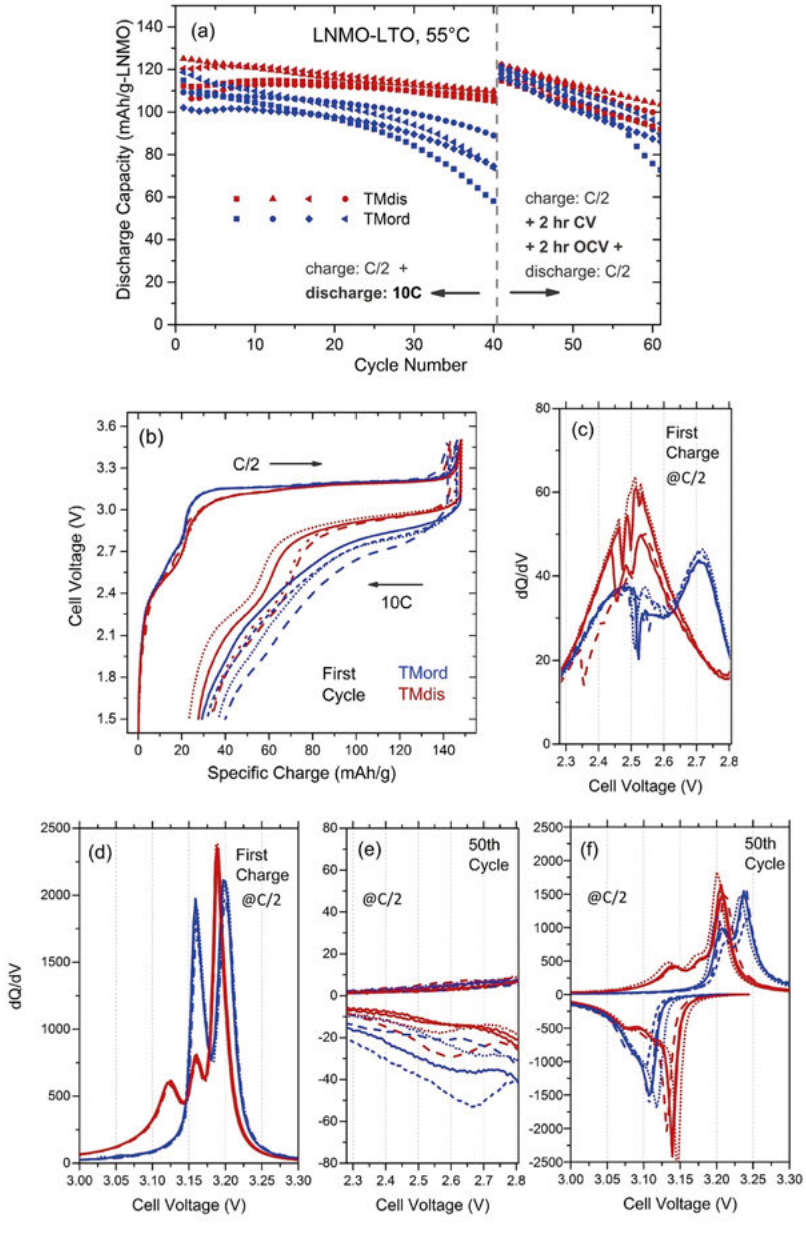

Figure 22. Electrochemical testing (at 55 ºC) of ordered (TMord; blue) and disordered (TMdis, red) samples in LNMO-LTO full cells. Each sample has been tested 4 times in order to assure reproducible results. These identical cells are shown with the same color, but with different symbols and line shapes. (a) Discharge capacity vs. cycle number; (b) voltage curves from the first cycle. In (c) and (d), differential capacity plots for the first charge (at C/2 rate) are shown for the low and high voltage region, respectively. In (e) and (f), similar plots are shown for the 50th cycle. From *Paper V*.

4.4.3. Unusual Anion Redox in Ordered and Disordered LNMO

In *Paper IV* it is shown that the high voltage plateau of LNMO is not due to a pure Ni redox activity, which is commonly accepted in literature, but rather that O also makes a considerable contribution to the charge distribution in this plateau. Therefore, both samples (at different state of charges) were investigated to see how the electronic structure of O and Ni differs depending on cation ordering. Ni L_3-edge XAS (PFY mode) and RIXS spectra of the samples are shown in *Figure 23* for the ordered and disordered samples. It is seen that pristine and charged samples at the end of charge (1-EoC) display both Ni^{2+} and Ni^{4+} character and that ordering does not seem to affect electronic structure. However, changes are observed during charging as ordered sample show a slightly increased Ni oxidation at 40% SOC at the beginning of plateau (1-BoP) while the disordered sample reaches higher oxidation states more abruptly when the SOC reaches 70% at near the end of plateau (1-EoP). After 11 cycles, the disordered sample also seems to reach higher oxidation levels for Ni at 100% SOC (11-EoC) while both samples had identical behaviour at the same SOC after the first delithiation (1-EoC). Ni L_3-RIXS spectra are also compared in *Figure 23b* for the delithiated samples. The main differences are the decrease of a low energy elastic peak for the disordered sample and a broadening of the main peak for the ordered sample. The latter can be caused by the charge transfer states related to holes in the oxygen band [137,138].

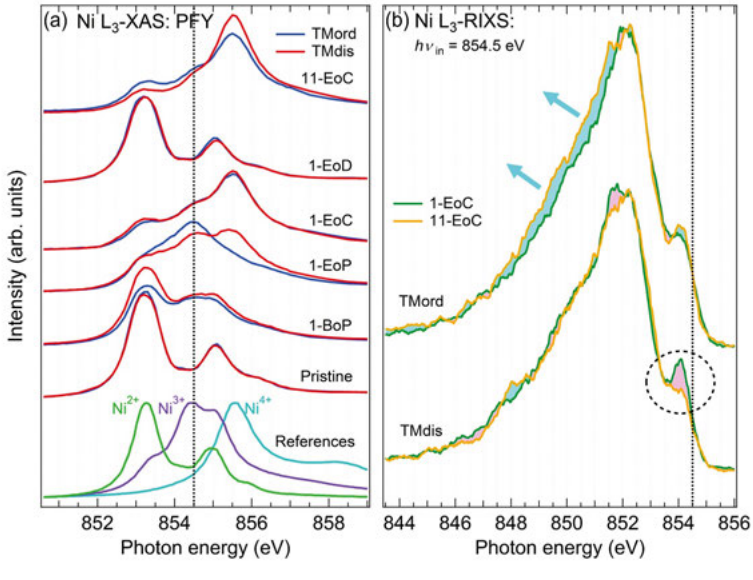

Figure 23. (a) Ni L_3-edge XAS LNMO electrodes at different SOC (reference spectra were reported by Qiao et al. [139]). (b) Ni L_3-edge RIXS spectra at an incident photon energy of 854.5 eV for delithiated LNMO samples. From *Paper V*.

In *Figure 24a*, O K-edge RIXS and XAS spectra are shown together (the excitation energy for RIXS is shown as a dashed line). During delithiation, both samples show a distinct pre-edge shoulder (around the dashed line) indicating the formation of holes in the Ni 3d – O 2p hybridized states. In the RIXS spectra, a distinct feature is formed around 526.5 eV and small changes are observed in the elastic peak. In the pristine state, there are also differences caused by ordering. As seen in *Figure 24b*, the sample at 70% SOC show differences in the elastic peak. The disordered material seems to retain its spectral shape between the 1st and 11th cycle while the ordered sample shows a slight decrease in peak area, as indicated by orange and green arrows. Those differences caused by the cation ordering are most likely related to faster degradation of the electrochemical performance. Therefore, XPS and TEM was done in order to achieve more information of surface and near-surface differences between ordered and disordered samples.

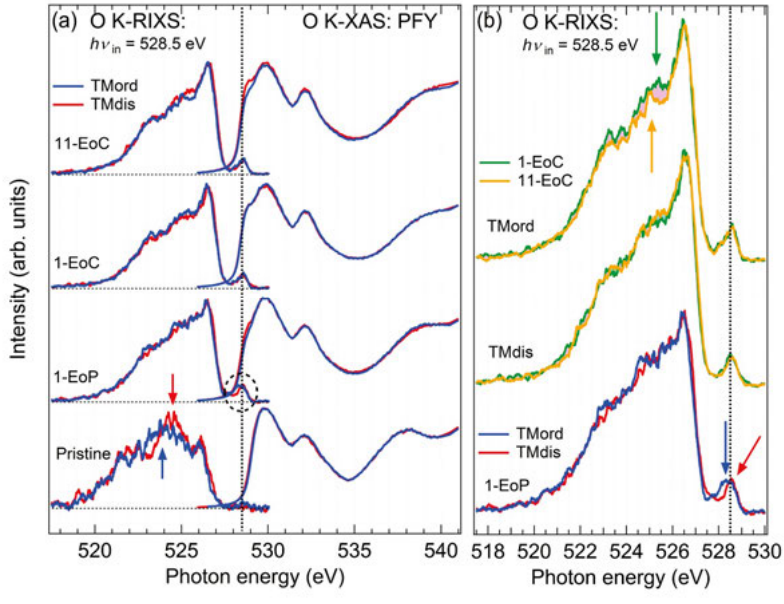

Figure 24. (a) O K-edge RIXS and XAS of selected SOC LNMO samples. (b) O K-edge RIXS spectra of selected samples showing the spectral differences. From *Paper V*.

4.4.4. XPS Analysis of Ordered and Disordered LNMO

C 1s, O 1s and Ni 2p XPS spectra are shown in *Figure 25* and the relative atomic percentages of the analyzed elements are also provided in the figure.

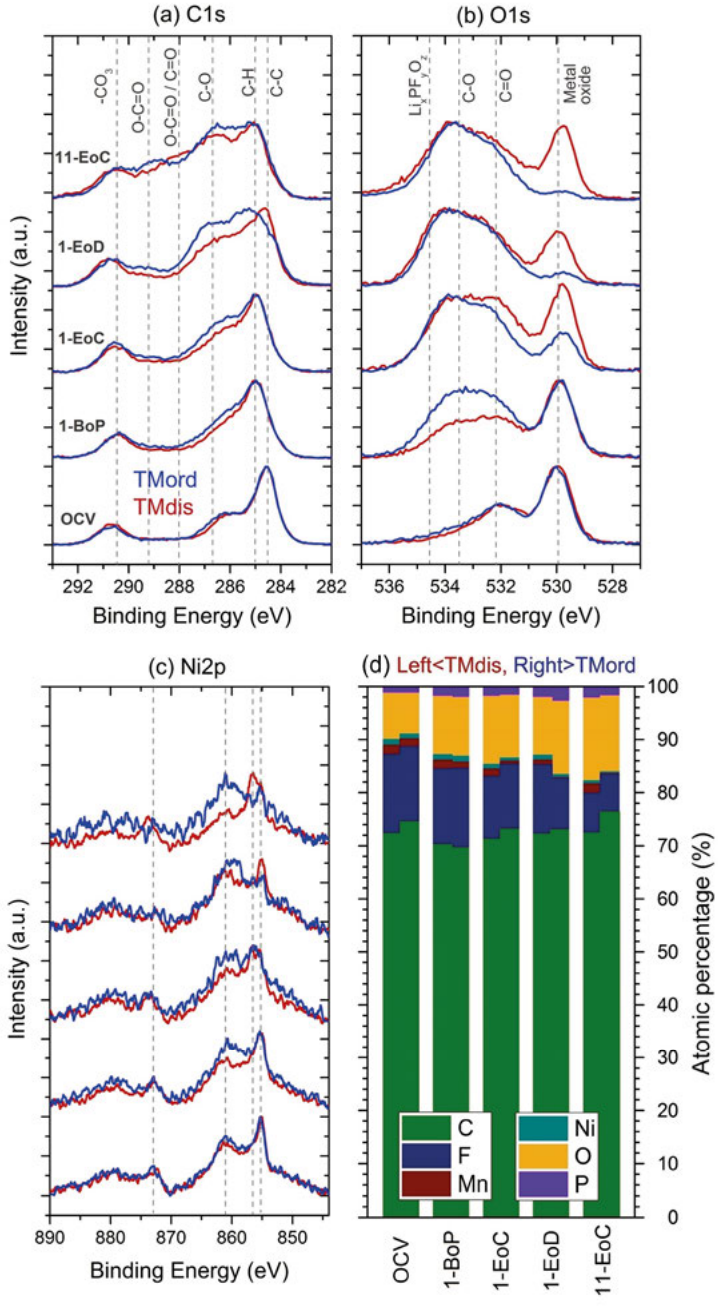

Figure 25. Normalized spectra for C 1s, O 1s and Ni 2p are shown in (a), (b), (c), respectively. (d) Relative atomic percentages of the analyzed elements (the left parts of the individual bars correspond to disordered samples and the right parts to ordered samples. From *Paper V*.

In the C 1s spectra (*Figure 25a*), organic species start to deposit with charging, seen from the intensity increase in regions where C-O and O−C−O/C=O related species are present. After 1 cycle (including CV and OCV steps), these effects are more significant and the ordered sample shows thicker film formation. In the O 1s spectra, it is observed that organic and inorganic species form to a larger degree on the active material of the ordered sample and the lattice metal oxide peak observed around 529.9 eV decreases. The trends clearly show that the film formation primarily occurs during the first cycle, while further growth proceeds to a limited extent in the following 10 cycles.

In the Ni 2p spectra (*Figure 25c*), the highest intensity feature of the Ni $2p_{3/2}$ multiplet peak (~855.2 eV) does not move in binding energy from OCV to 1-BoP, but shifts around 1.4 eV to higher energy (~ 856.6 eV) when charging is completed. It returns to its original position after discharge, which indicates that it is caused by Ni oxidation. Such a shift can be due to oxidation of Ni^{2+} to the Ni^{4+} state [140] or to the Ni^{3+} state [141] as reported for layered oxides. No shift was observed for the satellite peak (861 eV), which can be related to the ligands to which Ni is bonded [142]. With charging, also peak broadening is observed and the intensity of the main satellite peak increases, but irreversibly and continuously with further cycling. This increase in intensity occurs more pronouncedly for the ordered samples. It can be related to formation of defects such as oxygen vacancies [143] or changes in covalency [144,145] with the oxygen atoms.

4.4.5. TEM Analysis of Ordered and Disordered LNMO

To observe 'near-surface' structural changes, HRTEM images of ordered (a) and disordered (b) samples are shown in *Figure 26* (see *Paper V* for images of pristine samples). Significant structural changes obviously occurred during cycling, which are easily seen in FFT images obtained from different areas of the images (indicated by the colored rectangles). For the ordered sample, ordering is still visible as additional spots are present due to (110) planes, however, the brightness of additional spots decreases close to the surface which indicates a decrease in ordering. In the 'near-surface' regions just below the surface, domains of rock-salt like character are observed. Transition to rock-salt phase is clearly seen within the red rectangle as well as in the FFT image from the rock-salt like domain (blue rectangle). In this area, the increase in (440) spots are visible while the (110) spots disappear and the brightness of the (220) spots decreases.

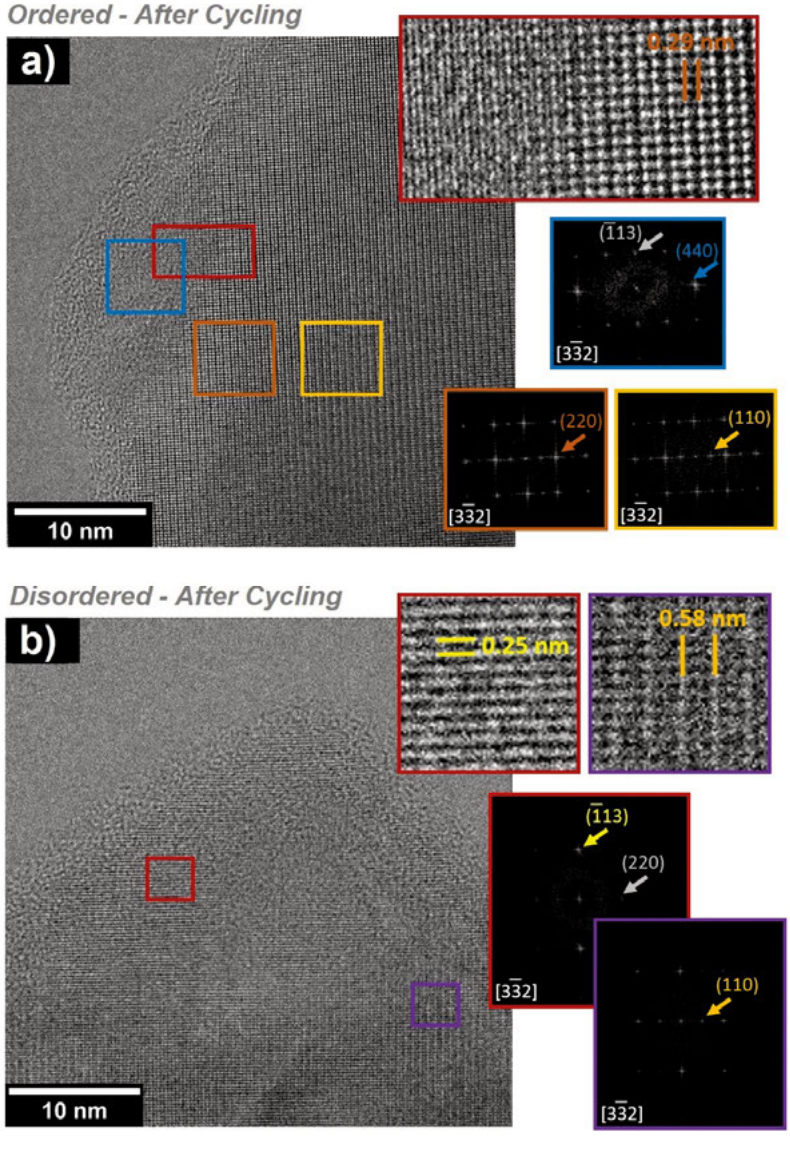

Figure 26. HRTEM images of ordered (a) and disordered (b) LNMO samples after cycling (10 cycles). HRTEM images of the pristine samples are shown in *Paper V*.

In the disordered samples (*Figure 26d*), no domains with rock-salt like character were observed. Unexpectedly, domains with some degree of ordering was on the other hand spotted in the inner regions of the particles. In this study, the disordered samples were prepared to be oxygen non-deficient. Therefore,

the driving force for ordering is predicted to be high and during lithiation/delithiation cycles at elevated temperature, it is possible that the inner regions could partially adapt cation ordering. In the near-surface regions, oxygen release and subsequent near-surface reconstruction would limit this effect.

Considering that the studies in *Paper V* comprise samples without changes in the oxygen content of samples, it can be concluded that disordering helps to delay degradation of electrochemical performance. While positive effects of disordering have been suggested in earlier studies, this thesis work shows this phenomenon experimentally for the first time by testing of two samples in which only cation ordering was different. The main reason for the performance difference is the rise of cell resistance. XPS analysis showed deposition of thicker films on the ordered sample, which might also accumulate on other cell components during prolonged cycling in different parts of the cell and prevent Li transport. More bulk sensitive XAS/RIXS technique showed that there were differences in electronic structure. These differences may affect the performance and trigger additional chemical reactions in the cell. The near surface changes observed with TEM shows a loss of ordering and formation of rock-salt like phase domains in the ordered sample after cycling, indicating that oxygen release might have taken place during cycling and caused near surface changes as well as chemical oxidation of electrolyte.

5. Conclusions

In this thesis, first the effectiveness of a well-known electrolyte additive, FEC, was tested in LNMO-LTO cells. Compared to alternatives, this cell chemistry can be considered a less complex full cell system in terms of anode surface reactions, and is therefore suitable for investigating the cathode's performance. Contrary to several other reports, this additive was found to have a limited effect when used in small amounts (1 wt%). Increased amounts, on the other hand, resulted in a *decrease* in charge capacity. Considerable side reactions occurred, but there was interestingly no considerable layer formation found on the LNMO electrodes. Moreover, the effect of temperature on capacity fading was dramatic and both Mn and Ni were detected on the surface of counter electrode already after one cycle.

Following these observations, a comprehensive study was conducted to identify different capacity-reducing mechanisms in this system and to understand the unusual effect of temperature. The results showed that the major contribution to capacity fading was due to a decrease in lithium inventory of the cell. It was seen that even though the side reactions originate from the cathode surface, reaction products migrate towards anode and cause further reductive reactions there, which reduce the lithium inventory. These reactions caused by electrochemical cross-talk is more sensitive to temperature and therefore explains the unusual increase in capacity fading rate at elevated temperature. It should be noted that the good capacity retention at room temperature is *also* due to cross-talk since reactions occur on both electrodes, but in a similar degree. Such deceptively 'stable' conditions can likewise be achieved at higher temperatures by applying some strategies aiming to increase the cell lifetime and can therefore give misleading results if extensive testing is not performed. It was also observed that the internal cell resistance increases during cycling, and it was seen that the main contribution originated from the LNMO side even though no thick surface films are formed on its surface. In contrast, thick films are observed on LTO surface but this layer does not cause any significant resistance.

In the third part of this thesis, the changes occurring in structure and microstructure were investigated in situ during heating and cooling of LNMO under different conditions. Observations from the neutron diffraction and TGA experiments showed that disordering starts around 630 ºC and oxygen release around 725-730 ºC when slightly Mn-rich samples are heated under pure oxygen flow. It was also observed that no specific temperature for the

order-disorder transition exists. These observations are noteworthy, as they show that there is not a direct relationship between oxygen release and cation disordering, and suggest that new sample preparation strategies which allow control of cation ordering in the samples without disrupting the oxygen content are possible. Observations from real time TEM analysis showed how ordered domains co-exist with disordered and rock-salt like phases at certain temperatures. It was also observed that further oxygen release caused formation of Mn- and Ni-rich phases on the microstructural level when the temperature was raised above 500 ºC under vacuum.

Following the insights gained from in situ studies, a suitable set of samples were prepared to study the effect of ordering on electrochemical performance. This was achieved by heating samples to 710 ºC (which is above disordering but below oxygen release temperature) and annealing for the same durations followed by either fast or slow cooling. This minimized changes in other material properties such as oxygen content when obtaining ordered and disordered samples. It was found that ordering in the structure causes faster electrochemical performance degradation. The results indicate that these differences are primarily dependent on the instability of the material in its delithiated state. Characterization of samples with XAS/RIXS showed that bulk related changes in the material might have a crucial role in performance failure of LNMO-based cells, and might also trigger further side reactions inside the cell via oxygen release. Participation of oxygen in the charge compensation during delithiation was shown, in contrast to the widely accepted pure cationic redox via transition metals in LNMO. With XPS, it was shown that ordering favors formation of thicker surface films on LNMO with more deposition of C-O, C=O and $Li_xPF_yO_z$ species. TEM analysis showed that cation ordering is partially lost in the particles after cycling and rock-salt like phases are formed near the surface. Thereby, a comprehensive picture of the interrelations between the structural chemistry, the surface chemistry and the electrochemistry of LNMO has been achieved.

This thesis illustrates the importance of acquiring a comprehensive understanding on degradation mechanisms in full and half cells. This way, more meaningful electrochemical testing of cells can be performed, generating new perspectives for future directions when solving degradation issues. The importance of performing advanced materials characterization is also clear, since vital property changes can be overlooked with more conventional techniques. The knowledge gained from this work will therefore hopefully provide insights for future studies and not least help designing more durable LNMO materials and LNMO-based batteries with longer lifetimes.

6. Sammanfattning på svenska

Användandet av Li-jon batterier i portabel elektronik, så som mobiltelefoner, laptops, surfplattor och så vidare, är idag mycket utbrett och ett intensivt pågående forskningsarbete sker för att förbättra prestandan i dessa batterier. Li-jon batterier kan som ersättare till fossila bränslen vara med och driva nästa generations elbilar på ett hållbart sätt genom användandet av el från förnyelsebara källor. En utbredd elektrifieringsprocess av fordonsparken i transportsektorn möjliggörs genom användandet av batterisystem med hög energidensitet, som samtidigt är säkra och långlivade. Det är viktigt att dessa batterisystem består av material som finns i stora mängder, är miljövänliga, och billiga. Det är även önskvärt att dessa batterisystem kan hantera höga strömmar så att de kan laddas snabbt.

I kommersiella batterier idag så kommer ungefär hälften av deras totala vikt ifrån katodmaterialet, och katoden har därför blivit ett viktigt mål för förbättring för utvecklingen av Li-jon batterier. Som ett alternativt katodmaterial har $LiNi_{0,5}Mn_{1,5}O_4$ (LNMO) flera fördelar mot nuvarande kommersiella standarder. Dessa fördelar inkluderar förmågan att hantera höga strömmar, hög energidensitet, låg produktionskostnad, och att materialet är miljövänligt. Den höga elektrokemiska potentialen detta material är behäftat med bidrar till en hög energidensitet, men introducerar även oönskade sidoreaktioner i batteriet. Dessa sidoreaktioner minskar batteriets livslängd och utgör därför hinder för storskalig implementeringen av LNMO som katodmaterial.

I denna doktorsavhandling har det undersöks det om en specifik metod, som är standard i många batteriter, kan användas för att öka livslängden i celler med LNMO. Denna metod går ut på att blanda in små mängder additiv i elektrolyten för att på så sätt skydda katoden ifrån oönskade sidoreaktioner. Resultaten från denna studie visar att ett av de vanligaste additiven för ändamålet inte gav någon positiv effekt alls. Vidare så visades det på vikten av att utveckla en god förståelse för vilka nedbrytningsmekanismer som sker vid användandet av detta nya katodmaterial. Till följd av dessa resultat gjordes en detaljerad uppföljningsstudie där användandet av avancerade karakteriseringstekniker identifierade effekten av olika nedbrytningsmekanismer. I denna studie användes ett anodmaterial som är känt för sin stabilitet som motelektrod, och det visade sig att en gradvis minskning av litiumförådet var huvudorsak till den observerade kapacitetsförlusten. Det anses generellt att en sådan kapacitetsförlust endast kan vara möjlig om sidoreaktionerna sker på anoden. Trots detta så visade det sig att med en ändrad celldesign så skedde i

stället sidoreaktionerna huvudsakligen på högvoltskatoden, vilket betyder att reaktionsprodukterna borde migrera från katoden till anoden där produkterna orsakar fler sidoreaktioner. Dessa sidoreaktioner är temperaturkänsliga, vilket förklarar varför kapacitetsförlusterna är större än förväntat vid höga temperaturer. Det visades också att mycket tjockare ytlagersprodukter bildas på anoden, men att däremot resistansen för transport av litiumjoner är mycket lägre i dessa ytlager. Denna studie visade att generella antaganden om kapacitetsförluster inte alltid stämmer för denna cellkemi.

Det är välkänt att förändringar av syntesförhållanden ändrar egenskaperna av katodmaterialet LNMO, vilket också påverkar den elektrokemiska prestandan. Vid exempelvis lågtemperaturssyntes följd av sakta nedkylning föredrar Mn och Ni specifika positioner i kristallstrukturen, vilket skapar ordnad LNMO (se *Figur 27*). Om syntestemperaturen i stället är hög så kommer inte Mn och Ni att ha specifika positioner i strukturen, och materialet får därför en oordnad kristallstruktur. Vid högtemperatursyntes förloras också syre från materialet och förändringar av partikelmikrostruktur och -morfologi sker. Dessa skillnader kan också påverka den elektrokemiska förmågan.

Inom ramarna för den här avhandlingen undersöktes sådana materialförändringar med avancerade karaktäriseringsmetoder såsom in situ neutrondiffraktion och in situ elektronmikroskopi. Tack vare dessa tekniker införskaffades viktig kunskap om LNMO. Exempelvis visade studierna att frigörelse av syre inte är direkt relaterat till katjonisk oordning i materialet. Det visades också att det finns ett temperaturintervall vid speciella förhållanden som tillåter bildning av katjonisk oordning, men utan syrefattighet varierade i LNMO-proven. I ett efterföljande projekt användes dessa insikter från in situ studierna, och anpassande provserier bereddes för att studera effekten av katjonordning på den elektrokemiska förmågan.

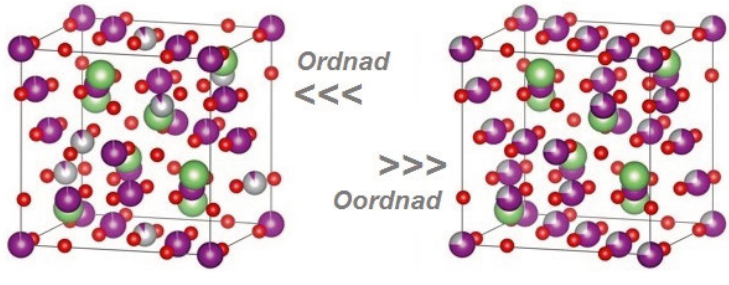

Figur 27. Kristallstrukturer av LNMO med ordnad Mn/Ni-distribution (vänster) och motsvarande oordnad struktur (höger). Atomer är: O (röd), Li (grön), Mn (lila) och Ni (grå).

Preparering av passande prov gjordes genom att upphetta av proven till 710 ºC (vilket är tillräckligt högt för oordning, men lägre än temperaturen för frisläppning av syre) där de glödgades lika lång tid, men med olika kylningshastigheter under den efterföljande kylningen. Ordnade och oordnade prov, vilka båda hade samma syrehalt, testades därefter i olika cellkonfigurationer och karaktäriserades med avancerade synkrotrontekniker, röntgenfotoelektronspektroskopi och transmissionselektronmikroskopi. Det visades att syre har ett betydande bidrag till energin som detta material levererar vid litiering och delitiering. Detta är skarp i kontrast till det vitt accepterade bilden av rena katjonsbidrag från övergångsmetaller. Därutöver visades att oordnad LNMO presterar bättre vid elektrokemisk testning. Detta förklaras av en mer stabil elektronstruktur, bildandet av en tunnare ytfilm och en mer stabil kristallstruktur.

Upptäckter från denna avhandling illustrerar betydelsen av att skapa en omfattande förståelse av degraderingsmekanismer för material i Li-jonbatterier. På detta vis kan mer meningsfull elektrokemisk celltestning utföras som skapar nya perspektiv för lösande av degraderingsproblem. Det är tydligt att avancerad materialkaraktärisering kan ge många insikter p.g.a. att vissa viktiga egenskapsförändringar kan missas med mer konventionella tekniker. Kunskapen som erhållits från detta arbete kommer därför förhoppningsvis att ge betydelsefulla insikter för fortsatta studier och design av mer hållbara LNMO-material och LNMO-baserade batterier med längre livstider.

7. Acknowledgements

Firstly, I would like to express my gratitude to my supervisors; Kristina Edström, Daniel Brandell, Wolfgang Zipprich, Carl Tengstedt and Fernanda Lodi Marzano for their guidance, help, understanding and motivating attitudes. Special thanks should go to Daniel Brandell who has been handling many of the practical, administrative and scientific matters throughout my PhD period (I should also thank on behalf of people whom I might supervise in the future). I would also like to acknowledge Reza Younesi for his guidance, support and valuable advices in all these years. Even though he was not a supervisor officially, he has been helpful as one.

As coming from a different field, Henrik Eriksson was very helpful when I was first trying to learn how to build batteries. I acknowledge him also for all other support he provided during these years. I highly appreciate Maria Hahlin and Julia Maibach for introducing me to the XPS world; as giving hands-on training to instruments in synchrotron and also in the lab, and helping with the theory and data analysis. I am grateful to Matthew Lacey for sharing his knowledge in electrochemistry as I learnt a lot from him. He has given feedback just to the point – in most clearest and effective way – during our collaboration in *Paper II*. Maria Hahlin and Roberto Felix Duarte are acknowledged for helping in BESSY, KMC-1 beamline with HAXPES and XANES measurements on LTO electrodes, and Tim Nordh for fruitful discussions and contribution on the analysis of HAXPES data. Also, many thanks to other colleagues who made the synchrotron beam times more enjoyable; Chao, Erik, Fredrik, Ida and Marco.

As being a nice officemate and also my collaborator in *Paper III*, I should thank William Brant for all his help and support, especially in preparation of long sheets of electrodes, running sequential Rietveld refinements and performing the in situ neutron diffraction experiment. I also owe a debt to Torbjörn Gustafsson for his help and advices. My co-authors; Mario Valvo, Ronald I. Smith and Magnus H. Sørby are acknowledged for their feedback and help with Raman spectrometer, Polaris neutron diffractometer at the ISIS spallation source and PUS neutron diffractometer at the JEEP II reactor, respectively. Edyta Nagrodzka is also acknowledged for ICP-OES measurements. In TEM experiments, Majid Ahmadi has performed a lot of meticulous measurements with TEM, which were all time consuming. I thank for his time, support and productive discussions.

Many thanks should go to my collaborators in Papers I*V*-*V*; Felix Massel, Laurent Duda for XAS/RIXS measurements, their interpretation and scientific discussions. I am thankful to Majid Ahmadi for performing TEM measurements, and Maria Hahlin and Mario Valvo for their valuable feedback. Even though not included in this thesis, I also owe to Jonas Mindemark for his help during the time I spent on preliminary studies on polymer electrolytes.

Technical support from Anders, and administrative help from Diana, Lina and Eva are highly appreciated. I would like to thank to Hilmi Buqa for providing LTO electrodes. Further, I thank to Mahsa for being a very nice officemate and wonderful conversations. Erik, we started to our PhDs around the same time and shared a lot, thanks for everything. 'High voltage' people, Girish and Alma, thanks for nice discussions and conversations. Many thanks to people in ÅABC and Chemistry-Ångström for their help and for just making this place a nice environment with their presence; Adam, Alina, Andoria, Andreas, Andy, Anti, Ashok, Charifa, Christofer, Charlotte, Chenjuan, David, Dickson, Edison, Erik, Fabian, Fredrik, Funeka, Gabi, Girma, Guiomar, Gustav, Habtom, Haidong, Hohyoun, Håkan, Ida, Isabell, Jiefang, Jonas, Julia, Kristina, Le Anh, Leif, Long, Mars, Martin, Mikaela, Ming, Murali, Nataliia, Nurul, Ocean, Olof, Pedro, Pushpaka, Rassmus, Robin, Ronnie, Ruijun, Sara, Sarmad, Sebastian, Siham, Simon, Solveig, Stefan, Stéven, Tatiana, Therese, Victor, Viktor, Yonas, Yu-Chuan, Yu-Kai, Yutaro, and others whom I might have forgotten.

I am thankful to people in other departments in Ångström; Umut, Serkan, İlknur, Esat and Seda. I should add that I am grateful to Umut and Serkan for joyful times spent in all these years both in Ångström and outside. Additionally, I am thankful to Arzu and Özge for nice times in rakı-table organizations. Especially for my first years in Sweden; support and friendship of people from utposten collective, Kerstin, Simon, and later Lars are appreciated. I am also grateful to Umut T and to my wonderful friends who came to Uppsala over a long distance to visit me; Can, Masumi, İrem, Didem, Aktöre, Aslı, Erkan and Sıla.

Finally, I would like to thank to my parents; Meliha and Arif, to my brother Yalçın and his family; Didem and Deniz for all their support and love.

/Burak

8. References

[1] B. Scrosati, J. Garche, Lithium batteries: Status, prospects and future, J. Power Sources. 195 (2010) 2419–2430. doi:10.1016/j.jpowsour.2009.11.048.

[2] A. Kraytsberg, Y. Ein-Eli, Higher, Stronger, Better… A Review of 5 Volt Cathode Materials for Advanced Lithium-Ion Batteries, Adv. Energy Mater. 2 (2012) 922–939. doi:10.1002/aenm.201200068.

[3] P.G. Bruce, B. Scrosati, J.-M. Tarascon, Nanomaterials for rechargeable lithium batteries., Angew. Chem. Int. Ed. Engl. 47 (2008) 2930–2946. doi:10.1002/anie.200702505.

[4] S. Brutti, G. Mulas, E. Piciollo, S. Panero, P. Reale, Magnesium hydride as a high capacity negative electrode for lithium ion batteries, J. Mater. Chem. 22 (2012) 14531. doi:10.1039/c2jm31827j.

[5] K. Xu, Nonaqueous liquid electrolytes for lithium-based rechargeable batteries, Chem. Rev. 104 (2004) 4303–4417. doi:10.1021/cr030203g.

[6] C.M. Julien, A. Mauger, Review of 5-V electrodes for Li-ion batteries: status and trends, Ionics (Kiel). 19 (2013) 951–988. doi:10.1007/s11581-013-0913-2.

[7] W. Li, B. Song, A. Manthiram, High-voltage positive electrode materials for lithium-ion batteries, Chem. Soc. Rev. 46 (2017) 3006–3059. doi:10.1039/C6CS00875E.

[8] J. Xu, F. Lin, M.M. Doeff, W. Tong, A review of Ni-based layered oxides for rechargeable Li-ion batteries, J. Mater. Chem. A. 5 (2017) 874–901. doi:10.1039/C6TA07991A.

[9] N. Yabuuchi, T. Ohzuku, Novel lithium insertion material of LiCo1/3Ni1/3Mn1/3O2 for advanced lithium-ion batteries, J. Power Sources. 119–121 (2003) 171–174. doi:10.1016/S0378-7753(03)00173-3.

[10] P. Rozier, J.M. Tarascon, Review—Li-Rich Layered Oxide Cathodes for Next-Generation Li-Ion Batteries: Chances and Challenges, J. Electrochem. Soc. 162 (2015) A2490–A2499. doi:10.1149/2.0111514jes.

[11] S. Hu, A.S. Pillai, G. Liang, W.K. Pang, H. Wang, Q. Li, Z. Guo, Li-Rich Layered Oxides and Their Practical Challenges: Recent Progress and Perspectives, Springer Singapore, 2019. doi:10.1007/s41918-019-00032-8.

[12] C. Sun, S. Rajasekhara, J.B. Goodenough, F. Zhou, Monodisperse porous LiFePO4 microspheres for a high power Li-ion battery cathode, J. Am. Chem. Soc. 133 (2011) 2132–2135. doi:10.1021/ja1110464.

[13] a. Manthiram, W. Choi, Suppression of Mn Dissolution in Spinel Cathodes by Trapping the Protons within Layered Oxide Cathodes, Electrochem. Solid-State Lett. 10 (2007) A228. doi:10.1149/1.2754387.

[14] O.K. Park, Y. Cho, S. Lee, H.-C. Yoo, H.-K. Song, J. Cho, Who will drive electric vehicles, olivine or spinel?, Energy Environ. Sci. 4 (2011) 1621. doi:10.1039/c0ee00559b.

[15] J.H. Kim, N.P.W. Pieczonka, L. Yang, Challenges and approaches for high-voltage spinel lithium-ion batteries, ChemPhysChem. 15 (2014) 1940–1954. doi:10.1002/cphc.201400052.
[16] G.Q. Liu, L. Wen, Y.M. Liu, Spinel LiNi0.5Mn1.5O4 and its derivatives as cathodes for high-voltage Li-ion batteries, J. Solid State Electrochem. 14 (2010) 2191–2202. doi:10.1007/s10008-010-1061-5.
[17] Y. Chen, Y. Cheng, J. Li, M. Feygenson, W.T. Heller, C. Liang, K. An, Lattice-Cell Orientation Disorder in Complex Spinel Oxides, Adv. Energy Mater. 7 (2017). doi:10.1002/aenm.201601950.
[18] A. Manthiram, K. Chemelewski, E.-S. Lee, A perspective on the high-voltage LiMn1.5Ni0.5O4 spinel cathode for lithium-ion batteries, Energy Environ. Sci. 7 (2014) 1339. doi:10.1039/c3ee42981d.
[19] J.-H. Kim, S.-T. Myung, C.S. Yoon, S.G. Kang, Y.-K. Sun, Comparative Study of LiNi0.5Mn1.5O4-δ and LiNi0.5Mn1.5O4 Cathodes Having Two Crystallographic Structures: Fd 3̄m and P 4332, Chem. Mater. 16 (2004) 906–914. doi:10.1021/cm035050s.
[20] J. Zheng, J. Xiao, X. Yu, L. Kovarik, M. Gu, F. Omenya, X. Chen, X.-Q. Yang, J. Liu, G.L. Graff, M.S. Whittingham, J.-G. Zhang, Enhanced Li+ ion transport in LiNi0.5Mn1.5O4 through control of site disorder, Phys. Chem. Chem. Phys. 14 (2012) 13515. doi:10.1039/c2cp43007j.
[21] M. Kunduraci, G.G. Amatucci, Synthesis and Characterization of Nanostructured 4.7 V LixMn1.5Ni0.5O4 Spinels for High-Power Lithium-Ion Batteries, J. Electrochem. Soc. 153 (2006) A1345. doi:10.1149/1.2198110.
[22] L. Cai, Z. Liu, K. An, C. Liang, Unraveling structural evolution of LiNi0.5Mn1.5O4 by in situ neutron diffraction, J. Mater. Chem. A. 1 (2013) 6908. doi:10.1039/c3ta00145h.
[23] J.H. Kim, A. Huq, M. Chi, N.P.W. Pieczonka, E. Lee, C.A. Bridges, M.M. Tessema, A. Manthiram, K.A. Persson, B.R. Powell, Integrated nano-domains of disordered and ordered spinel phases in LiNi0.5Mn1.5O4 for li-ion batteries, Chem. Mater. 26 (2014) 4377–4386. doi:10.1021/cm501203r.
[24] X. Ma, B. Kang, G. Ceder, High Rate Micron-Sized Ordered LiNi[sub 0.5]Mn[sub 1.5]O[sub 4], J. Electrochem. Soc. 157 (2010) A925. doi:10.1149/1.3439678.
[25] H. Duncan, B. Hai, M. Leskes, C.P. Grey, G. Chen, Relationships between Mn 3+ Content, Structural Ordering, Phase Transformation, and Kinetic Properties in LiNi x Mn 2– x O 4 Cathode Materials, Chem. Mater. 26 (2014) 5374–5382. doi:10.1021/cm502607v.
[26] Z. Moorhead-Rosenberg, A. Huq, J.B. Goodenough, A. Manthiram, Electronic and Electrochemical Properties of Li 1– x Mn 1.5 Ni 0.5 O 4 Spinel Cathodes As a Function of Lithium Content and Cation Ordering, Chem. Mater. 27 (2015) 6934–6945. doi:10.1021/acs.chemmater.5b01356.
[27] P.B. Samarasingha, J. Sottmann, S. Margadonna, H. Emerich, O. Nilsen, H. Fjellvåg, In situ synchrotron study of ordered and disordered LiMn 1.5 Ni 0.5 O 4 as lithium ion battery positive electrode, Acta Mater. 116 (2016) 290–297. doi:10.1016/j.actamat.2016.06.040.
[28] E. Lee, K.A. Persson, Solid-solution Li intercalation as a function of cation order/disorder in the high-voltage LixNi0.5Mn1.5O4 spinel, Chem. Mater. 25 (2013) 2885–2889. doi:10.1021/cm4014738.
[29] M. Kunduraci, G.G. Amatucci, Effect of oxygen non-stoichiometry and temperature on cation ordering in LiMn2-xNixO4 spinels, J. Power Sources. 165 (2007) 359–367. doi:10.1016/j.jpowsour.2006.11.051.

[30] D. Pasero, N. Reeves, V. Pralong, A.R. West, Oxygen Nonstoichiometry and Phase Transitions in LiMn 1.5Ni0.5O4−δ, J. Electrochem. Soc. 155 (2008) A282. doi:10.1149/1.2832650.
[31] J. Song, D.W. Shin, Y. Lu, C.D. Amos, A. Manthiram, J.B. Goodenough, Role of Oxygen Vacancies on the Performance of Li[Ni 0.5 −, 4 (2012).
[32] Q. Zhong, A. Bonakclarpour, M. Zhang, Y. Gao, J.R. Dahn, Synthesis and Electrochemistry of LiNiMn2 _ O4, J Electrochem Soc. 144 (1997) 205–213. doi:10.1149/1.1837386.
[33] J. Cabana, M. Casas-Cabanas, F.O. Omenya, N.A. Chernova, D. Zeng, M.S. Whittingham, C.P. Grey, Composition-Structure Relationships in the Li-Ion Battery Electrode Material LiNi 0.5 Mn 1.5 O 4, Chem. Mater. 24 (2012) 2952–2964. doi:10.1021/cm301148d.
[34] M. Kunduraci, J.F. Al-Sharab, G.G. Amatucci., High-Power Nanostructured LiMn2-xNixO4 High-Voltage Lithium-Ion Battery Electrode Materials:, Chem. Mater. 18 (2006) 3585–3592. doi:10.1021/cm060729s.
[35] X. Ma, B. Kang, G. Ceder, High Rate Micron-Sized Ordered LiNi0.5Mn1.5O4, J. Electrochem. Soc. 157 (2010) A925. doi:10.1149/1.3439678.
[36] R. Amin, I. Belharouk, Part I: Electronic and ionic transport properties of the ordered and disordered LiNi 0.5 Mn 1.5 O 4 spinel cathode, J. Power Sources. 348 (2017) 311–317. doi:10.1016/j.jpowsour.2017.02.071.
[37] M. Casas-Cabanas, C. Kim, J. Rodríguez-Carvajal, J. Cabana, Atomic defects during ordering transitions in LiNi $_{0.5}$ Mn $_{1.5}$ O $_{4}$ and their relationship with electrochemical properties, J. Mater. Chem. A. 4 (2016) 8255–8262. doi:10.1039/C6TA00424E.
[38] J. Cabana, H. Zheng, A.K. Shukla, C. Kim, V.S. Battaglia, M. Kunduraci, Comparison of the Performance of LiNi1/2Mn3/2O4 with Different Microstructures, J. Electrochem. Soc. 158 (2011) A997. doi:10.1149/1.3606570.
[39] K.M. Shaju, P.G. Bruce, A Stoichiometric Nano-LiMn2O4 Spinel Electrode Exhibiting High Power and Stable Cycling, Chem. Mater. 20 (2008) 5557–5562. doi:10.1021/cm8010925.
[40] X. Zhang, F. Cheng, J. Yang, J. Chen, Xiaolong Zhang, Fangyi Cheng, Jingang Yang, and Jun Chen *, (2013) 2–5. doi:0.1021/nl401072x.
[41] K.R. Chemelewski, E.S. Lee, W. Li, A. Manthiram, Factors influencing the electrochemical properties of high-voltage spinel cathodes: Relative impact of morphology and cation ordering, Chem. Mater. 25 (2013) 2890–2897. doi:10.1021/cm401496k.
[42] S. Kuppan, H. Duncan, G. Chen, Controlling Side Reactions and Self-discharge in High-voltage Spinel Cathodes: Critical Role of Surface Crystallographic Facets, Phys. Chem. Chem. Phys. 17 (2015) 26471–26481. doi:10.1039/C5CP04899K.
[43] H. Liu, J. Wang, X. Zhang, D. Zhou, X. Qi, B. Qiu, J. Fang, R. Kloepsch, G. Schumacher, Z. Liu, J. Li, Morphological Evolution of High-Voltage Spinel LiNi 0.5 Mn 1.5 O 4 Cathode Materials for Lithium-Ion Batteries: The Critical Effects of Surface Orientations and Particle Size, ACS Appl. Mater. Interfaces. 8 (2016) 4661–4675. doi:10.1021/acsami.5b11389.
[44] D. Aurbach, Review of selected electrode – solution interactions which determine the performance of Li and Li ion batteries, J. Power Sources. 89 (2000) 206–218. doi:http://dx.doi.org/10.1016/S0378-7753(00)00431-6.

[45] N.P.W. Pieczonka, Z. Liu, P. Lu, K.L. Olson, J. Moote, B.R. Powell, J. Kim, Understanding Transition-Metal Dissolution Behavior in LiNi0.5Mn1.5O4 High-Voltage Spinel for Lithium Ion Batteries, J. Phys. Chem. C 2013, 117, 15947−15957. (2013).

[46] S. Brutti, G. Greco, P. Reale, S. Panero, Insights about the irreversible capacity of LiNi0.5Mn1.5O4 cathode materials in lithium batteries, Electrochim. Acta. 106 (2013) 483–493. doi:10.1016/j.electacta.2013.05.111.

[47] L. Fransson, T. Eriksson, K. Edström, T. Gustafsson, J.. Thomas, Influence of carbon black and binder on Li-ion batteries, J. Power Sources. 101 (2001) 1–9. doi:10.1016/S0378-7753(01)00481-5.

[48] R. Younesi, A.S. Christiansen, R. Scipioni, D.-T. Ngo, S.B. Simonsen, K. Edstrom, J. Hjelm, P. Norby, Analysis of the Interphase on Carbon Black Formed in High Voltage Batteries, J. Electrochem. Soc. 162 (2015) A1289–A1296. doi:10.1149/2.0761507jes.

[49] M. Metzger, C. Marino, J. Sicklinger, D. Haering, H.A. Gasteiger, Anodic Oxidation of Conductive Carbon and Ethylene Carbonate in High-Voltage Li-Ion Batteries Quantified by On-Line Electrochemical Mass Spectrometry, J. Electrochem. Soc. 162 (2015) A1123–A1134. doi:10.1149/2.0951506jes.

[50] B. Streipert, S. Röser, J. Kasnatscheew, P. Janßen, X. Cao, R. Wagner, I. Cekic-Laskovic, M. Winter, Influence of $LiPF_6$ on the Aluminum Current Collector Dissolution in High Voltage Lithium Ion Batteries after Long-Term Charge/Discharge Experiments, J. Electrochem. Soc. 164 (2017) A1474–A1479. doi:10.1149/2.0671707jes.

[51] J.H. Kim, N.P.W. Pieczonka, Z. Li, Y. Wu, S. Harris, B.R. Powell, Understanding the capacity fading mechanism in LiNi0.5Mn 1.5O4/graphite Li-ion batteries, Electrochim. Acta. 90 (2013) 556–562. doi:10.1016/j.electacta.2012.12.069.

[52] M. Lin, L. Ben, Y. Sun, H. Wang, Z. Yang, L. Gu, X. Yu, X.-Q. Yang, H. Zhao, R. Yu, M. Armand, X. Huang, Insight into the Atomic Structure of High-Voltage Spinel LiNi 0.5 Mn 1.5 O 4 Cathode Material in the First Cycle, Chem. Mater. 27 (2015) 292–303. doi:10.1021/cm503972a.

[53] M. Ue, A. Murakami, S. Nakamura, Anodic Stability of Several Anions Examined by Ab Initio Molecular Orbital and Density Functional Theories, J. Electrochem. Soc. 149 (2002) A1572. doi:10.1149/1.1517579.

[54] E. Jónsson, P. Johansson, Electrochemical oxidation stability of anions for modern battery electrolytes: a CBS and DFT study, Phys. Chem. Chem. Phys. 17 (2015) 3697–3703. doi:10.1039/C4CP04592K.

[55] P. Johansson, Intrinsic anion oxidation potentials, J. Phys. Chem. A. 110 (2006) 12077–12080. doi:10.1021/jp0653297.

[56] M. He, L. Hu, Z. Xue, C.C. Su, P. Redfern, L.A. Curtiss, B. Polzin, A. von Cresce, K. Xu, Z. Zhang, Fluorinated Electrolytes for 5-V Li-Ion Chemistry: Probing Voltage Stability of Electrolytes with Electrochemical Floating Test, J. Electrochem. Soc. 162 (2015) A1725–A1729. doi:10.1149/2.0231509jes.

[57] O. Borodin, M. Olguin, C.E. Spear, K.W. Leiter, J. Knap, Towards high throughput screening of electrochemical stability of battery electrolytes., Nanotechnology. 26 (2015) 354003. doi:10.1088/0957-4484/26/35/354003.

[58] O. Borodin, W. Behl, T.R. Jow, Oxidative stability and initial decomposition reactions of carbonate, sulfone, and alkyl phosphate-based electrolytes, J. Phys. Chem. C. 117 (2013) 8661–8682. doi:10.1021/jp400527c.

[59] P. Arora, Capacity Fade Mechanisms and Side Reactions in Lithium-Ion Batteries, J. Electrochem. Soc. 145 (1998) 3647. doi:10.1149/1.1838857.

[60] D. Aurbach, B. Markovsky, Y. Talyossef, G. Salitra, H.-J. Kim, S. Choi, Studies of cycling behavior, ageing, and interfacial reactions of LiNi0.5Mn1.5O4 and carbon electrodes for lithium-ion 5-V cells, J. Power Sources. 162 (2006) 780–789. doi:10.1016/j.jpowsour.2005.07.009.

[61] L. Yang, B. Ravdel, B.L. Lucht, Electrolyte Reactions with the Surface of High Voltage LiNi[sub 0.5]Mn[sub 1.5]O[sub 4] Cathodes for Lithium-Ion Batteries, Electrochem. Solid-State Lett. 13 (2010) A95. doi:10.1149/1.3428515.

[62] L. Xing, W. Li, C. Wang, F. Gu, M. Xu, C. Tan, J. Yi, Theoretical investigations on oxidative stability of solvents and oxidative decomposition mechanism of ethylene carbonate for lithium ion battery use, J. Phys. Chem. B. 113 (2009) 16596–16602. doi:10.1021/jp9074064.

[63] M. Metzger, B. Strehle, S. Solchenbach, H.A. Gasteiger, Origin of H_2 Evolution in LIBs: H_2O Reduction vs. Electrolyte Oxidation, J. Electrochem. Soc. 163 (2016) A798–A809. doi:10.1149/2.1151605jes.

[64] A. Bhandari, J. Bhattacharya, Review — Manganese Dissolution from Spinel Cathode : Few unanswered questions, J. Electrochem. Soc. 164 (2017) A106–A127. doi:10.1149/2.0101614jes.

[65] D.H. Jang, S.M. Oh, Electrolyte Effects on Spinel Dissolution and Cathodic Capacity Losses in 4 V Li/LixMn2O4 Rechargeable Cells, J. Electrochem. Soc. 144 (1997) 3342. doi:10.1149/1.1838016.

[66] R. Dedryvère, D. Foix, S. Franger, S. Patoux, L. Daniel, D. Gonbeau, Electrode/Electrolyte Interface Reactivity in High-Voltage Spinel LiMn 1.6 Ni 0.4 O 4 /Li 4 Ti 5 O 12 Lithium-Ion Battery, J. Phys. Chem. C. 114 (2010) 10999–11008. doi:10.1021/jp1026509.

[67] S.R. Li, C.H. Chen, X. Xia, J.R. Dahn, The Impact of Electrolyte Oxidation Products in LiNi0.5Mn1.5O4/Li4Ti5O12 Cells, J. Electrochem. Soc. 160 (2013) A1524–A1528. doi:10.1149/2.051309jes.

[68] S.E. Sloop, J.B. Kerr, K. Kinoshita, The role of Li-ion battery electrolyte reactivity in performance decline and self-discharge, J. Power Sources. 119–121 (2003) 330–337. doi:10.1016/S0378-7753(03)00149-6.

[69] C. Delacourt, A. Kwong, X. Liu, R. Qiao, W.L. Yang, P. Lu, S.J. Harris, V. Srinivasan, Effect of Manganese Contamination on the Solid-Electrolyte-Interphase Properties in Li-Ion Batteries, J. Electrochem. Soc. 160 (2013) A1099–A1107. doi:10.1149/2.035308jes.

[70] D.R. Vissers, Z. Chen, Y. Shao, M. Engelhard, U. Das, P. Redfern, L.A. Curtiss, B. Pan, J. Liu, K. Amine, Role of Manganese Deposition on Graphite in the Capacity Fading of Lithium Ion Batteries, ACS Appl. Mater. Interfaces. 8 (2016) 14244–14251. doi:10.1021/acsami.6b02061.

[71] J.A. Gilbert, I.A. Shkrob, D.P. Abraham, Transition Metal Dissolution, Ion Migration, Electrocatalytic Reduction and Capacity Loss in Lithium-Ion Full Cells, J. Electrochem. Soc. 164 (2017) A389–A399. doi:10.1149/2.1111702jes.

[72] B. Michalak, H. Sommer, D. Mannes, A. Kaestner, T. Brezesinski, J. Janek, Gas Evolution in Operating Lithium-Ion Batteries Studied In Situ by Neutron Imaging, Sci. Rep. 5 (2015) 15627. doi:10.1038/srep15627.

[73] D.J. Xiong, L.D. Ellis, R. Petibon, T. Hynes, Q.Q. Liu, J.R. Dahn, Studies of Gas Generation, Gas Consumption and Impedance Growth in Li-Ion Cells with Carbonate or Fluorinated Electrolytes Using the Pouch Bag Method, J. Electrochem. Soc. 164 (2017) A340–A347. doi:10.1149/2.1091702jes.

[74] D.J. Xiong, R. Petibon, M. Nie, L. Ma, J. Xia, J.R. Dahn, Interactions between Positive and Negative Electrodes in Li-Ion Cells Operated at High Temperature and High Voltage, J. Electrochem. Soc. 163 (2016) A546–A551. doi:10.1149/2.0951603jes.

[75] B. Michalak, B.B. Berkes, H. Sommer, T. Bergfeldt, T. Brezesinski, J. Janek, Gas Evolution in LiNi0.5Mn1.5O4/Graphite Cells Studied In Operando by a Combination of Differential Electrochemical Mass Spectrometry, Neutron Imaging, and Pressure Measurements, Anal. Chem. 88 (2016) 2877–2883. doi:10.1021/acs.analchem.5b04696.

[76] E. Björklund, D. Brandell, M. Hahlin, K. Edström, R. Younesi, How the Negative Electrode Influences Interfacial and Electrochemical Properties of LiNi 1/3 Co 1/3 Mn 1/3 O 2 Cathodes in Li-Ion Batteries, J. Electrochem. Soc. 164 (2017) A3054–A3059. doi:10.1149/2.0711713jes.

[77] N.-S. Choi, J.-G. Han, S.-Y. Ha, I. Park, C.-K. Back, Recent advances in the electrolytes for interfacial stability of high-voltage cathodes in lithium-ion batteries, RSC Adv. 5 (2015) 2732–2748. doi:10.1039/C4RA11575A.

[78] D. Tang, Y. Sun, Z. Yang, L. Ben, L. Gu, X. Huang, Surface Structure Evolution of LiMn $_2$ O $_4$ Cathode Material upon Charge/Discharge, Chem. Mater. 26 (2014) 3535–3543. doi:10.1021/cm501125e.

[79] L. Ben, H. Yu, B. Chen, Y. Chen, Y. Gong, X. Yang, L. Gu, X. Huang, Unusual Spinel-to-Layered Transformation in LiMn2O4Cathode Explained by Electrochemical and Thermal Stability Investigation, ACS Appl. Mater. Interfaces. 9 (2017) 35463–35475. doi:10.1021/acsami.7b11303.

[80] Y.-S. Liu, D.M. Pickup, A. V. Chadwick, M.R. Roberts, P.G. Bruce, K. Edström, R. Hao, N. Guerrini, L.C. Duda, K. Luo, J. Guo, Charge-compensation in 3d-transition-metal-oxide intercalation cathodes through the generation of localized electron holes on oxygen, Nat. Chem. 8 (2016) 684–691. doi:10.1038/nchem.2471.

[81] M. Nádherná, J. Reiter, J. Moškon, R. Dominko, Lithium bis(fluorosulfonyl)imide–PYR14TFSI ionic liquid electrolyte compatible with graphite, J. Power Sources. 196 (2011) 7700–7706. doi:http://dx.doi.org/10.1016/j.jpowsour.2011.04.033.

[82] X. Cao, X. He, J. Wang, H. Liu, S. R??ser, B.R. Rad, M. Evertz, B. Streipert, J. Li, R. Wagner, M. Winter, I. Cekic-Laskovic, High Voltage LiNi0.5Mn1.5O4/Li4Ti5O12 Lithium Ion Cells at Elevated Temperatures: Carbonate- versus Ionic Liquid-Based Electrolytes, ACS Appl. Mater. Interfaces. 8 (2016) 25971–25978. doi:10.1021/acsami.6b07687.

[83] J. Li, C. Ma, M. Chi, C. Liang, N.J. Dudney, Solid electrolyte: The key for high-voltage lithium batteries, Adv. Energy Mater. 5 (2015) 1–6. doi:10.1002/aenm.201401408.

[84] J.P. Robinson, P.D. Kichambare, J.L. Deiner, R. Miller, M.A. Rottmayer, G.M. Koenig, High temperature electrode-electrolyte interface formation between LiMn1.5Ni0.5O4 and Li1.4Al0.4Ge1.6(PO4)3, J. Am. Ceram. Soc. 101 (2018) 1087–1094. doi:10.1111/jace.15294.

[85] L. Miara, A. Windm??ller, C.L. Tsai, W.D. Richards, Q. Ma, S. Uhlenbruck, O. Guillon, G. Ceder, About the Compatibility between High Voltage Spinel Cathode Materials and Solid Oxide Electrolytes as a Function of Temperature, ACS Appl. Mater. Interfaces. 8 (2016) 26842–26850. doi:10.1021/acsami.6b09059.

[86] J. Mindemark, M.J. Lacey, T. Bowden, D. Brandell, Beyond PEO—Alternative host materials for Li + -conducting solid polymer electrolytes, Prog. Polym. Sci. (2018). doi:10.1016/j.progpolymsci.2017.12.004.

[87] J. Ma, Z. Liu, B. Chen, L. Wang, L. Yue, H. Liu, J. Zhang, Z. Liu, G. Cui, A Strategy to Make High Voltage LiCoO 2 Compatible with Polyethylene Oxide Electrolyte in All-Solid-State Lithium Ion Batteries, J. Electrochem. Soc. 164 (2017) A3454–A3461. doi:10.1149/2.0221714jes.

[88] E. Markevich, G. Salitra, K. Fridman, R. Sharabi, G. Gershinsky, A. Garsuch, G. Semrau, M. a. Schmidt, D. Aurbach, Fluoroethylene carbonate as an important component in electrolyte solutions for high-voltage lithium batteries: Role of surface chemistry on the cathode, Langmuir. 30 (2014) 7414–7424. doi:10.1021/la501368y.

[89] et al. "Graphene-oxide-coated L. 0. . M. 1. . O. 4 as high voltage cathode for lithium ion batteries with high energy density and long cycle life. . J. of M.C.A. 1. 1. (2013): 4083-4088. Fang, Xin, Journal of Materials Chemistry A, (n.d.). doi:10.1039/c3ta01534c.

[90] J.-J. Shiu, W.K. Pang, S. Wu, Preparation and characterization of spinel LiNi0.5−xMgxMn1.5O4 cathode materials via spray pyrolysis method, J. Power Sources. 244 (2013) 35–42. doi:10.1016/j.jpowsour.2013.04.083.

[91] J. Liu, A. Manthiram, Kinetics Study of the 5 V Spinel Cathode LiMn1.5Ni0.5O4 Before and After Surface Modifications, J. Electrochem. Soc. 156 (2009) A833. doi:10.1149/1.3206590.

[92] J. Liu, A. Manthiram, Understanding the improvement in the electrochemical properties of surface modified 5 V LiMn1. 42Ni0. 42Co0. 16O4 spinel cathodes in lithium-ion cells, Chem. Mater. 21 (2009) 1695–1707.

[93] Y.-F. Deng, S.-X. Zhao, Y.-H. Xu, C.-W. Nan, Effect of temperature of Li 2 O–Al 2 O 3 –TiO 2 –P 2 O 5 solid-state electrolyte coating process on the performance of LiNi 0.5 Mn 1.5 O 4 cathode materials, J. Power Sources. 296 (2015) 261–267. doi:10.1016/j.jpowsour.2015.07.017.

[94] L. Li, R. Zhao, T. Xu, D. Wang, D. Pan, K. Zhang, C. Yu, X. Lu, G. He, Y. Bai, Stabilizing a high-voltage LiNi 0.5 Mn 1.5 O 4 cathode towards all solid state batteries: A Li-Al-Ti-P-O solid electrolyte nano-shell with a host material, Nanoscale. 11 (2019) 8967–8977. doi:10.1039/c9nr01655d.

[95] J. Chai, J. Zhang, P. Hu, J. Ma, H. Du, L. Yue, J. Zhao, H. Wen, Z. Liu, G. Cui, L. Chen, A high-voltage poly(methylethyl α-cyanoacrylate) composite polymer electrolyte for 5 v lithium batteries, J. Mater. Chem. A. 4 (2016) 5191–5197. doi:10.1039/c6ta00828c.

[96] J. Zhao, J. Zhang, P. Hu, J. Ma, X. Wang, L. Yue, G. Xu, B. Qin, Z. Liu, X. Zhou, G. Cui, A sustainable and rigid-flexible coupling cellulose-supported poly(propylene carbonate) polymer electrolyte towards 5 V high voltage lithium batteries, Electrochim. Acta. 188 (2016) 23–30. doi:10.1016/j.electacta.2015.11.088.

[97] Z. Liu, P. Hu, J. Ma, B. Qin, Z. Zhang, C. Mou, Y. Yao, G. Cui, Conformal poly(ethyl α-cyanoacrylate) nano-coating for improving the interface stability of LiNi 0.5 Mn 1.5 O 4, Electrochim. Acta. 236 (2017) 221–227. doi:10.1016/j.electacta.2017.03.168.

[98] T. Chen, Y. Liao, L. Yang, X. Li, W. Li, Improved performance of LiNi0.5Mn1.5O4 cathode for high-voltage lithium-ion battery at elevated temperature by using gel polymer electrolyte, Ionics (Kiel). 21 (2015) 2457–2463. doi:10.1007/s11581-015-1424-0.

[99] P. Sun, Y. Liao, H. Xie, T. Chen, M. Rao, W. Li, Poly(methyl methacrylate-acrylonitrile-ethyl acrylate) terpolymer based gel electrolyte for LiNi0.5Mn1.5O4 cathode of high voltage lithium ion battery, J. Power Sources. 269 (2014) 299–307. doi:10.1016/j.jpowsour.2014.07.014.

[100] X. Luo, Y. Liao, H. Xie, Y. Zhu, Q. Huang, W. Li, Enhancement of cyclic stability for high voltage lithium ion battery at elevated temperature by using polyethylene-supported poly(methyl methacrylate − butyl acrylate − acrylonitrile − styrene) based novel gel electrolyte, Electrochim. Acta. 220 (2016) 47–56. doi:10.1016/j.electacta.2016.09.147.
[101] S. Panero, D. Satolli, A. D'Epifano, B. Scrosati, High Voltage Lithium Polymer Cells Using a PAN-Based Composite Electrolyte, J. Electrochem. Soc. 149 (2002) A414. doi:10.1149/1.1454139.
[102] J.-H. Cho, J.-H. Park, M.-H. Lee, H.-K. Song, S.-Y. Lee, A polymer electrolyte-skinned active material strategy toward high-voltage lithium ion batteries: a polyimide-coated LiNi0.5Mn1.5O4 spinel cathode material case, Energy Environ. Sci. 5 (2012) 7124. doi:10.1039/c2ee03389e.
[103] S. Tanaka, T. Narutomi, S. Suzuki, A. Nakao, H. Oji, N. Yabuuchi, Acrylonitrile-grafted poly(vinyl alcohol) copolymer as effective binder for high-voltage spinel positive electrode, J. Power Sources. 358 (2017) 121–127. doi:10.1016/j.jpowsour.2017.05.032.
[104] P. Hu, J. Chai, Y. Duan, Z. Liu, G. Cui, L. Chen, Progress in nitrile-based polymer electrolytes for high performance lithium batteries, J. Mater. Chem. A. 4 (2016) 10070–10083. doi:10.1039/C6TA02907H.
[105] K. Xu, Electrolytes and interphases in Li-ion batteries and beyond, Chem. Rev. 114 (2014) 11503–11618. doi:10.1021/cr500003w.
[106] M. Xu, N. Tsiouvaras, A. Garsuch, H. a. Gasteiger, B.L. Lucht, Generation of cathode passivation films via oxidation of lithium bis(oxalato) borate on high voltage spinel (LiNi0.5Mn 1.5O4), J. Phys. Chem. C. 118 (2014) 7363–7368. doi:10.1021/jp501970j.
[107] V. Tarnopolskiy, J. Kalhoff, M. Nádherná, D. Bresser, L. Picard, F. Fabre, M. Rey, S. Passerini, Beneficial influence of succinic anhydride as electrolyte additive on the self-discharge of 5 v LiNi0.4Mn1.6O4 cathodes, J. Power Sources. 236 (2013) 39–46. doi:10.1016/j.jpowsour.2013.02.030.
[108] A. von Cresce, K. Xu, Electrolyte Additive in Support of 5 V Li Ion Chemistry, J. Electrochem. Soc. 158 (2011) A337. doi:10.1149/1.3532047.
[109] M. Xu, D. Lu, a. Garsuch, B.L. Lucht, Improved Performance of LiNi0.5Mn1.5O4 Cathodes with Electrolytes Containing Dimethylmethylphosphonate (DMMP), J. Electrochem. Soc. 159 (2012) A2130–A2134. doi:10.1149/2.077212jes.
[110] H. Rong, M. Xu, L. Xing, W. Li, Enhanced cyclability of LiNi0.5Mn1.5O4 cathode in carbonate based electrolyte with incorporation of tris(trimethylsilyl)phosphate (TMSP), J. Power Sources. 261 (2014) 148–155. doi:10.1016/j.jpowsour.2014.03.032.
[111] H.B. Lin, W.Z. Huang, H.B. Rong, S.W. Mai, J.N. Hu, L.D. Xing, M.Q. Xu, W.S. Li, Improving cyclic stability and rate capability of LiNi0.5Mn1.5O4 cathode via protective film and conductive polymer formed from thiophene, J. Solid State Electrochem. (2015). doi:10.1007/s10008-014-2717-3.
[112] P.T. Moseley, J.K. Park, H.S. Kim, W.S. Yoon, Y.J. Park, K.W. Leitner, H. Wolf, a. Garsuch, F. Chesneau, M. Schulz-Dobrick, Electroactive separator for high voltage graphite/LiNi0.5Mn1.5O4 lithium ion batteries, J. Power Sources. 244 (2013) 548–551. doi:10.1016/j.jpowsour.2013.01.187.
[113] J. Liu, A. Manthiram, Understanding the Improved Electrochemical Performances of Fe-Substituted 5V Spinel Cathode LiMn1.5 Ni0.5O4, J. Phys. Chem. C. 113 (2009) 15073–15079. doi:10.1021/jp904276t.

[114] T.-F. Yi, Y. Xie, M.-F. Ye, L.-J. Jiang, R.-S. Zhu, Y.-R. Zhu, Recent developments in the doping of LiNi0.5Mn1.5O4 cathode material for 5 V lithium-ion batteries, Ionics (Kiel). 17 (2011) 383–389. doi:10.1007/s11581-011-0550-6.
[115] F. Ulu Okudur, J. D'Haen, T. Vranken, D. De Sloovere, M. Verheijen, O.M. Karakulina, A.M. Abakumov, J. Hadermann, M.K. Van Bael, A. Hardy, Ti surface doping of LiNi0.5Mn1.5O4-: δ positive electrodes for lithium ion batteries, RSC Adv. 8 (2018) 7287–7300. doi:10.1039/c7ra12932g.
[116] H. Wang, L. Ben, H. Yu, Y. Chen, X. Yang, X. Huang, Understanding the Effects of Surface Reconstruction on Electrochemical Cycling Performance of Spinel LiNi0.5Mn1.5O4 Cathode Material at Elevated Temperatures, J. Mater. Chem. A. 00 (2016) 1–13. doi:10.1039/C6TA08636E.
[117] M.J. Lacey, Influence of the Electrolyte on the Internal Resistance of Lithium−Sulfur Batteries Studied with an Intermittent Current Interruption Method, ChemElectroChem. 4 (2017) 1997–2004. doi:10.1002/celc.201700129.
[118] X. Liu, T. Weng, Synchrotron-based x-ray absorption spectroscopy for energy materials, MRS Bull. 41 (2016) 466–472. doi:10.1557/mrs.2016.113.
[119] R. Qiao, Q. Li, Z. Zhuo, S. Sallis, O. Fuchs, M. Blum, L. Weinhardt, C. Heske, J. Pepper, M. Jones, A. Brown, A. Spucces, K. Chow, B. Smith, P.-A. Glans, Y. Chen, S. Yan, F. Pan, L.F.J. Piper, J. Denlinger, J. Guo, Z. Hussain, Y.-D. Chuang, W. Yang, High-efficiency in situ resonant inelastic x-ray scattering (iRIXS) endstation at the Advanced Light Source, Rev. Sci. Instrum. 88 (2017) 033106. doi:10.1063/1.4977592.
[120] S. Hull, R.I. Smith, W.I.F. David, A.C. Hannon, J. Mayers, R. Cywinski, The Polaris powder diffractometer at ISIS, Phys. B Phys. Condens. Matter. 180–181 (1992) 1000–1002. doi:10.1016/0921-4526(92)90533-X.
[121] A.C. Larson, R.B. Von Dreele, General Structure Analysis System (GSAS), Los Alamos Natl. Lab. Rep. LAUR 86-748. (2004).
[122] B.H. Toby, EXPGUI, a graphical user interface for GSAS, J. Appl. Crystallogr. 34 (2001) 210–213. doi:10.1107/S0021889801002242.
[123] N.S. Choi, K.H. Yew, K.Y. Lee, M. Sung, H. Kim, S.S. Kim, Effect of fluoroethylene carbonate additive on interfacial properties of silicon thin-film electrode, J. Power Sources. 161 (2006) 1254–1259. doi:10.1016/j.jpowsour.2006.05.049.
[124] F. Lindgren, C. Xu, L. Niedzicki, M. Marcinek, T. Gustafsson, F. Björefors, K. Edström, R. Younesi, SEI Formation and Interfacial Stability of a Si Electrode in a LiTDI-Salt Based Electrolyte with FEC and VC Additives for Li-Ion Batteries, ACS Appl. Mater. Interfaces. 8 (2016) 15758–15766. doi:10.1021/acsami.6b02650.
[125] H. Shin, J. Park, A.M. Sastry, W. Lu, Effects of Fluoroethylene Carbonate (FEC) on Anode and Cathode Interfaces at Elevated Temperatures, J. Electrochem. Soc. 162 (2015) A1683–A1692. doi:10.1149/2.0071509jes.
[126] M.H. Ryou, G.B. Han, Y.M. Lee, J.N. Lee, D.J. Lee, Y.O. Yoon, J.K. Park, Effect of fluoroethylene carbonate on high temperature capacity retention of LiMn2O4/graphite Li-ion cells, Electrochim. Acta. 55 (2010) 2073–2077. doi:10.1016/j.electacta.2009.11.036.
[127] Y. Xu, L. Wan, J. Liu, L. Zeng, Z. Yang, FEC as the additive of 5 V electrolyte and its electrochemical performance for LiNi0.5Mn1.5O4, J. Electroanal. Chem. 791 (2017) 109–116.

[128] D. Aurbach, E. Zinigrad, Y. Cohen, H. Teller, A short review of failure mechanisms of lithium metal and lithiated graphite anodes in liquid electrolyte solutions, Solid State Ionics. 148 (2002) 405–416. doi:10.1016/S0167-2738(02)00080-2.
[129] E. Markevich, G. Salitra, F. Chesneau, M. Schmidt, D. Aurbach, Very Stable Lithium Metal Stripping–Plating at a High Rate and High Areal Capacity in Fluoroethylene Carbonate-Based Organic Electrolyte Solution, ACS Energy Lett. 2 (2017) 1321–1326. doi:10.1021/acsenergylett.7b00300.
[130] C. Xu, G. Hernández, S. Abbrent, L. Kobera, R. Konefal, J. Brus, K. Edström, D. Brandell, J. Mindemark, Unraveling and Mitigating the Storage Instability of Fluoroethylene Carbonate-Containing LiPF 6 Electrolytes To Stabilize Lithium Metal Anodes for High-Temperature Rechargeable Batteries, ACS Appl. Energy Mater. (2019) acsaem.9b00607. doi:10.1021/acsaem.9b00607.
[131] K.R. Chemelewski, E.S. Lee, W. Li, A. Manthiram, Factors influencing the electrochemical properties of high-voltage spinel cathodes: Relative impact of morphology and cation ordering, Chem. Mater. 25 (2013) 2890–2897. doi:10.1021/cm401496k.
[132] M. Kunduraci, G.G. Amatucci, The effect of particle size and morphology on the rate capability of 4.7 V LiMn1.5Ni0.5O4 spinel lithium-ion battery cathodes, Electrochim. Acta. 53 (2008) 4193–4199. doi:10.1016/j.electacta.2007.12.057.
[133] J. Als-Nielsen, O.W. Dietrich, Long-range order and critical scattering of neutrons below the transition temperature in β-brass, Phys. Rev. 153 (1967) 717–721. doi:10.1103/PhysRev.153.717.
[134] D.T. Keating, B.E. Warren, Long-Range Order in Beta-Brass and Cu 3 Au, J. Appl. Phys. 22 (1951) 286–290. doi:10.1063/1.1699944.
[135] J. Xiao, X. Chen, P. V. Sushko, M.L. Sushko, L. Kovarik, J. Feng, Z. Deng, J. Zheng, G.L. Graff, Z. Nie, D. Choi, J. Liu, J.G. Zhang, M.S. Whittingham, High-performance LiNi 0.5Mn 1.5O 4 Spinel controlled by Mn 3+ concentration and site disorder, Adv. Mater. 24 (2012) 2109–2116. doi:10.1002/adma.201104767.
[136] Y. Chen, Y. Sun, X. Huang, Origin of the Ni/Mn ordering in high-voltage spinel LiNi 0.5 Mn 1.5 O 4 : The role of oxygen vacancies and cation doping, Comput. Mater. Sci. 115 (2016) 109–116. doi:10.1016/j.commatsci.2016.01.005.
[137] M. Matsubara, T. Uozumi, A. Kotani, J.C. Parlebas, Charge transfer excitation in resonant X-ray emission spectroscopy of NiO, J. Phys. Soc. Japan. 74 (2005) 2052–2060. doi:10.1143/JPSJ.74.2052.
[138] Y. Lu, D. Betto, K. Fürsich, H. Suzuki, H.H. Kim, G. Cristiani, G. Logvenov, N.B. Brookes, E. Benckiser, M.W. Haverkort, G. Khaliullin, M. Le Tacon, M. Minola, B. Keimer, Site-Selective Probe of Magnetic Excitations in Rare-Earth Nickelates Using Resonant Inelastic X-ray Scattering, Phys. Rev. X. 8 (2018) 1–9. doi:10.1103/PhysRevX.8.031014.
[139] R. Qiao, L.A. Wray, J.-H. Kim, N.P.W. Pieczonka, S.J. Harris, W. Yang, Direct Experimental Probe of the Ni(II)/Ni(III)/Ni(IV) Redox Evolution in LiNi 0.5 Mn 1.5 O 4 Electrodes, J. Phys. Chem. C. 119 (2015) 27228–27233. doi:10.1021/acs.jpcc.5b07479.
[140] G. Assat, D. Foix, C. Delacourt, A. Iadecola, R. Dedryvère, J.M. Tarascon, Fundamental interplay between anionic/cationic redox governing the kinetics and thermodynamics of lithium-rich cathodes, Nat. Commun. 8 (2017). doi:10.1038/s41467-017-02291-9.

[141] Z. Fu, J. Hu, W. Hu, S. Yang, Y. Luo, Quantitative analysis of Ni 2+ /Ni 3+ in Li[Ni x Mn y Co z]O 2 cathode materials: Non-linear least-squares fitting of XPS spectra, Appl. Surf. Sci. 441 (2018) 1048–1056. doi:10.1016/j.apsusc.2018.02.114.
[142] H.W. Nesbitt, D. Legrand, G.M. Bancroft, Interpretation of Ni2p XPS spectra of Ni conductors and Ni insulators, Phys. Chem. Miner. 27 (2000) 357–366. doi:10.1007/s002690050265.
[143] M.A. Van Veenendaal, G.A. Sawatzky, Nonlocal screening effects in 2p x-ray photoemission spectroscopy core-level line shapes of transition metal compounds, Phys. Rev. Lett. 70 (1993) 2459–2462. doi:10.1103/PhysRevLett.70.2459.
[144] A.P. Grosvenor, M.C. Biesinger, R.S.C. Smart, N.S. McIntyre, New interpretations of XPS spectra of nickel metal and oxides, Surf. Sci. 600 (2006) 1771–1779. doi:10.1016/j.susc.2006.01.041.
[145] M. Atanasov, D. Reinen, Non-local electronic effects in core-level photoemission, UV and optical electronic absorption spectra of nickel oxides, J. Electron Spectros. Relat. Phenomena. 86 (2002) 185–199. doi:10.1016/s0368-2048(97)00065-0.

Acta Universitatis Upsaliensis

Digital Comprehensive Summaries of Uppsala Dissertations from the Faculty of Science and Technology 1827

Editor: The Dean of the Faculty of Science and Technology

A doctoral dissertation from the Faculty of Science and Technology, Uppsala University, is usually a summary of a number of papers. A few copies of the complete dissertation are kept at major Swedish research libraries, while the summary alone is distributed internationally through the series Digital Comprehensive Summaries of Uppsala Dissertations from the Faculty of Science and Technology. (Prior to January, 2005, the series was published under the title "Comprehensive Summaries of Uppsala Dissertations from the Faculty of Science and Technology".)

Distribution: publications.uu.se
urn:nbn:se:uu:diva-389848

ACTA
UNIVERSITATIS
UPSALIENSIS
UPPSALA
2019